

Best
Available
Copy

AD-759 955

DEVELOPMENT OF A TECHNIQUE FOR REALISTIC
PREDICTION AND ELECTRONIC SYNTHESIS OF
HELICOPTER ROTOR NOISE

H. Kevin Johnson

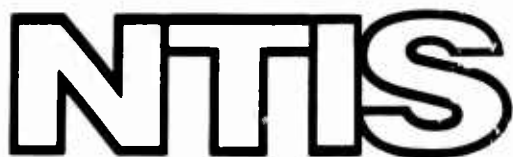
Rochester Applied Science Associates, Incorporated

Prepared for:

Army Air Mobility Research and Development
Laboratory

March 1973

DISTRIBUTED BY:



National Technical Information Service
U. S. DEPARTMENT OF COMMERCE
5285 Port Royal Road, Springfield Va. 22151

AD 759955

USAAMRDL TECHNICAL REPORT 73-8

DEVELOPMENT OF A TECHNIQUE FOR REALISTIC PREDICTION AND ELECTRONIC SYNTHESIS OF HELICOPTER ROTOR NOISE

By

H. Kevin Johnson

March 1973

D D C
RECEIVED
MAY 17 1973
RUCM-50
B

EUSTIS DIRECTORATE
U. S. ARMY AIR MOBILITY RESEARCH AND DEVELOPMENT LABORATORY
FORT EUSTIS, VIRGINIA

CONTRACT DAAJ02-71-C-0064
ROCHESTER APPLIED SCIENCE ASSOCIATES, INC.
ROCHESTER, NEW YORK

Approved for public release;
distribution unlimited.



Reproduced by
NATIONAL TECHNICAL
INFORMATION SERVICE
U S Department of Commerce
Springfield VA 22151

D D C
RECEIVED
MAY 17 1973
RUCM-50
B

1326

DISCLAIMERS

The findings in this report are not to be construed as an official Department of the Army position unless so designated by other authorized documents.

When Government drawings, specifications, or other data are used for any purpose other than in connection with a definitely related Government procurement operation, the United States Government thereby incurs no responsibility nor any obligation whatsoever; and the fact that the Government may have formulated, furnished, or in any way supplied the said drawings, specifications, or other data is not to be regarded by implication or otherwise as in any manner licensing the holder or any other person or corporation, or conveying any rights or permission, to manufacture, use, or sell any patented invention that may in any way be related thereto.

Trade names cited in this report do not constitute an official endorsement or approval of the use of such commercial hardware or software.

DISPOSITION INSTRUCTIONS

Destroy this report when no longer needed. Do not return it to the originator.

ACCESSION for	
NTIS	White Section
ORG	Buff Section <input checked="" type="checkbox"/>
CHARTERED	
NOTIFICATION	
BY	
DISTRIBUTION/AVAILABILITY CODES	
DATA	AVAIL. and/or SPECIAL
<i>A</i>	

UNCLASSIFIED

Security Classification

DOCUMENT CONTROL DATA - R & D

(Security classification of title, body of abstract and indexing annotation must be entered when the overall report is classified)

1. ORIGINATING ACTIVITY (Corporate author) Rochester Applied Science Associates, Inc. 140 Allens Creek Road Rochester, New York		2a. REPORT SECURITY CLASSIFICATION UNCLASSIFIED
3. REPORT TITLE DEVELOPMENT OF A TECHNIQUE FOR REALISTIC PREDICTION AND ELECTRONIC SYNTHESIS OF HELICOPTER ROTOR NOISE		2b. GROUP
4. DESCRIPTIVE NOTES (Type of report and inclusive dates) Final Report		
5. AUTHOR(S) (First name, middle initial, last name) H. Kevin Johnson		
6. REPORT DATE March 1973	7a. TOTAL NO. OF PAGES 117 138	7b. NO. OF REFS 11
8a. CONTRACT OR GRANT NO. DAAJ02-71-C-0064	9a. ORIGINATOR'S REPORT NUMBER(S) USAAMRDL Technical Report 73-8	
b. PROJECT NO. c. Task 1F162208AA8201	9b. OTHER REPORT NO(S) (Any other numbers that may be assigned this report) RASA Report 72-08	
10. DISTRIBUTION STATEMENT Approved for public release; distribution unlimited.		
11. SUPPLEMENTARY NOTES	12. SPONSORING MILITARY ACTIVITY Eustis Directorate, U.S. Army Air Mobility Research & Development Laboratory, Ft. Eustis, Virginia	
13. ABSTRACT A helicopter rotor noise prediction program has been developed so that the acoustic characteristics of new, untested rotor designs could be evaluated as well as the effects of basic rotor design changes on the acoustic signature of existing rotors. The prediction program is general enough to be able to consider future designs in hover and steady-state flight for any observer location. The program output is the digital pressure time history produced by the helicopter rotors at the observer location. This pressure time history corresponds to that which would be recorded by a microphone placed at the observer location. The program output can be Fourier analyzed so that the noise spectrum can be generated. The digital pressure time history can also be converted to an analog signal for subjective evaluation.		

DD FORM 1 NOV 64 1473
REPLACES DD FORM 1473, 1 JAN 64, WHICH IS
OBSOLETE FOR ARMY USE.

UNCLASSIFIED

Security Classification

UNCLASSIFIED

Security Classification

14 KEY WORDS	LINK A		LINK B		LINK C	
	ROLE	WT	ROLE	WT	ROLE	WT
Helicopter Noise						
Acoustics						
Rotor Noise						
Rotational Noise						
Vortex Noise						
Noise Prediction						

UNCLASSIFIED

Security Classification



DEPARTMENT OF THE ARMY
U. S. ARMY AIR MOBILITY RESEARCH & DEVELOPMENT LABORATORY
EUSTIS DIRECTORATE
FORT EUSTIS, VIRGINIA 23604

This report has been reviewed by the Eustis Directorate, U.S. Army Air Mobility Research and Development Laboratory and is considered to be technically sound.

The information presented is the result of a study to analytically describe the main and tail rotor noise signature of helicopters of various configurations. Further, once an analytical representation of the noise has been described at an observer's location, the digitized signature can be converted to an analog signal for subjective evaluation.

As part of this effort, a computer program that permits rapid prediction of a helicopter's noise signature was developed. Therefore, this tool can be exploited in the design of quieter helicopters.

The technical monitor for this contract was Mr. William T. Alexander Jr., Technology Applications Division.

11a

Task 1F162208AA8201
Contract DAAJ02-71-C-0064
USAAMRDL Technical Report 73-8
March 1973

DEVELOPMENT OF A TECHNIQUE FOR
REALISTIC PREDICTION AND ELECTRONIC
SYNTHESIS OF HELICOPTER ROTOR NOISE

Final Report

RASA Report 72-08

By
H. Kevin Johnson

Prepared by

Rochester Applied Science Associates, Inc.
Rochester, New York

for

FUSTIS DIRECTORATE
U. S. ARMY AIR MOBILITY RESEARCH AND DEVELOPMENT LABORATORY
FORT FUSTIS, VIRGINIA

Approved for public release;
distribution unlimited.

ii b

FOREWORD

This program was conducted by Rochester Applied Science Associates, Inc., under Contract DAAJ02-71-C-0064, Task 1F162208AA8201, and was carried out under the technical cognizance of Mr. William T. Alexander, Eustis Directorate, U. S. Army Air Mobility Research and Development Laboratory, Fort Eustis, Virginia.

The principal investigator at RASA was Dr. H. Kevin Johnson; Dr. Walter M. Katz and Mrs. Gay F. Moore conducted the numerical analysis. Boeing-Vertol and NASA/Langley supplied the data analyzed during the program.

TABLE OF CONTENTS

	<u>Page</u>
ABSTRACT	iii
FOREWORD	v
LIST OF ILLUSTRATIONS	viii
LIST OF TABLES	xiv
LIST OF SYMBOLS	xv
INTRODUCTION	1
DESCRIPTION OF ANALYTICAL TECHNIQUE	3
Theory	3
General Description of Program	14
DATA BANK OF OSCILLATORY FORCE CONSTANTS	15
Fitting for Oscillatory Force Constants	15
Data Analyzed	16
Sample Calculation	19
RESULTS - TEST CASES	23
CH-47B Whirl Tower	23
UH-1B in Hover and Forward Flight	30
Boeing-Vertol 347 in Hover and Forward Flight	40
HLH in Hover for Two Sets of Rotor Parameters	42
CONCLUSIONS AND RECOMMENDATIONS	44
LITERATURE CITED	111
DISTRIBUTION	113

LIST OF ILLUSTRATIONS

<u>Figure</u>		<u>Page</u>
1	Coordinate Systems Used in the Analysis.	46
2	Blade Element Forces and Velocities.	47
3	Boeing-Vertol Whirl Tower Microphone Array . .	48
4	Pressure Time History of Recorded Noise Generated From CH-47B Rotor on a Whirl Tower.	49
5	Spectrum of Recorded Noise Generated From CH-47B Rotor on a Whirl Tower (Reference Figure 4).	50
6	Pressure Time History of Predicted Noise Generated From a 1-Ft-Wide Station Centered at 15 Ft Radius Which Oscillates at 422 Hz With a Pressure of 1 Lb/Ft ²	51
7	Pressure Time History of Predicted Noise Generated From a 1-Ft-Wide Station Centered at 29.5 Ft Radius Which Oscillates at 827 Hz With a Pressure of 1 Lb/Ft ²	52
8	Spectrum of Predicted Noise Generated From a 1-Ft-Wide Station Centered at 15 Ft Radius Which Oscillates at 422 Hz With a Pressure of 1 Lb/Ft ² (Reference Figure 6)	53
9	Spectrum of Predicted Noise Generated From a 1-Ft-Wide Station Centered at 29.5 Ft Radius Which Oscillates at 827 Hz With a Pressure of 1 Lb/Ft ² (Reference Figure 7)	54
10	Pressure Time History of Recorded Noise Generated From CH-47B Rotor on a Whirl Tower.	55
11	Spectrum of Recorded Noise Generated From CH-47B Rotor on a Whirl Tower (Reference Figure 10)	56
12	Pressure Time History of Predicted Noise Generated From CH-47B Rotor on a Whirl Tower.	57

<u>Figure</u>		<u>Page</u>
13	Spectrum of Predicted Noise Generated From CH-47B Rotor on a Whirl Tower (Reference Figure 12)	58
14	Distribution of the Magnitude of Oscillatory Lift Over Ten Radial Stations for Four Cases.	59
15	Pressure Time History of Predicted Noise Generated From CH-47B Rotor on a Whirl Tower.	60
16	Spectrum of Predicted Noise Generated From CH-47B Rotor on a Whirl Tower (Reference Figure 15)	61
17	Pressure Time History of Recorded Noise Generated From CH-47B Rotor on a Whirl Tower.	62
18	Spectrum of Recorded Noise Generated From CH-47B Rotor on a Whirl Tower (Reference Figure 17)	63
19	Pressure Time History of Predicted Noise Generated From CH-47B Rotor on a Whirl Tower.	64
20	Spectrum of Predicted Noise Generated From CH-47B Rotor on a Whirl Tower (Reference Figure 19)	65
21	Spectrum of Predicted Rotational Noise Generated From CH-47B Rotor on a Whirl Tower.	66
22	Pressure Time History of Recorded Noise Generated From CH-47B Rotor on a Whirl Tower.	67
23	Pressure Time History of Recorded Noise Generated From CH-47B Rotor on a Whirl Tower.	68
24	Spectrum of Recorded Noise Generated From CH-47B Rotor on a Whirl Tower (Reference Figure 22)	69

<u>Figure</u>		<u>Page</u>
25	Spectrum of Recorded Noise Generated From CH-47B Rotor on a Whirl Tower (Reference Figure 23)	70
26	Pressure Time History of Predicted Noise Generated From CH-47B Rotor on a Whirl Tower.	71
27	Pressure Time History of Predicted Noise Generated From CH-47B Rotor on a Whirl Tower.	72
28	Spectrum of Predicted Noise Generated From CH-47B Rotor on a Whirl Tower (Reference Figure 26)	73
29	Spectrum of Predicted Noise Generated From CH-47B Rotor on a Whirl Tower (Reference Figure 27)	74
30	Spectrum of Predicted Rotational Noise Generated From CH-47B Rotor on a Whirl Tower.	75
31	Spectrum of Predicted Rotational Noise Generated From CH-47B Rotor on a Whirl Tower.	76
32	Relative Positions of Microphones at Wallops Island Air Station	77
33	Noise Spectrum by Ubiquitous Analyzer for UH-1B Helicopter in 100-Ft Hover, Recorded 200 Ft to the Right (Microphone 4)	78
34	Noise Spectrum by Ubiquitous Analyzer for UH-1B Helicopter in 100-Ft Hover, Recorded 200 Ft to the Left (Microphone 10)	79
35	Pressure Time History of Predicted Noise Generated From a UH-1B in 100-Ft Hover, Recorded 200 Ft to the Left (Microphone 10)	80
36	Spectrum of Predicted Noise Generated From a UH-1B in 100-Ft Hover, Recorded 200 Ft to the Left (Microphone 10) (Reference Figure 35)	81

<u>Figure</u>		<u>Page</u>
37	Pressure Time History of Predicted Tail Rotor Rotational Noise Generated From a UH-1B in 100-Ft Hover.	82
38	Spectrum of Predicted Tail Rotor Rotational Noise Generated From a UH-1B in 100-Ft Hover (Reference Figure 37)	83
39	Pressure Time History of Predicted Tail Rotor Rotational Noise Generated From a UH-1B in 100-Ft Hover	84
40	Spectrum of Predicted Tail Rotor Rotational Noise Generated From a UH-1B in 100-Ft Hover (Reference Figure 39)	85
41	Spectrum of Recorded Noise Generated From a UH-1B in Level Flight.	86
42	Spectrum of Predicted Noise Generated From a UH-1B in Level Flight.	87
43	Pressure Time History of Recorded Noise Generated From a UH-1B in Level Flight	88
44	Pressure Time History of Predicted Noise Generated From a UH-1B in Level Flight	89
45	Pressure Time History of Recorded Noise Generated From a UH-1B in Level Flight	90
46	Pressure Time History of Predicted Noise Generated From a UH-1B in Level Flight	91
47	Pressure Time History of Recorded Noise Generated From a UH-1B in Level Flight	92
48	Pressure Time History of Predicted Noise Generated From a UH-1B in Level Flight	93
49	Pressure Time History of Predicted Noise Generated From a UH-1B Main Rotor in Level Flight	94
50	Pressure Time History of Predicted Vortex Noise Generated From a UH-1B Main Rotor in Level Flight	95

<u>Figure</u>		<u>Page</u>
51	Pressure Time History of Predicted Vortex Noise Generated From a UH-1B Main Rotor in Level Flight	96
52	Pressure Time History of Recorded Noise Generated From a Boeing-Vertol Model 347 Helicopter Hovering in Ground Effect, Microphone 200 Ft to the Right	97
53	Spectrum of Recorded Noise Generated From a Boeing-Vertol Model 347 Helicopter Hovering in Ground Effect, Microphone 200 Ft to the Right (Reference Figure 52)	98
54	Pressure Time History of Predicted Noise Generated From a Boeing-Vertol Model 347 Helicopter Hovering in Ground Effect, Microphone 200 Ft to the Right	99
55	Spectrum of Predicted Noise Generated From a Boeing-Vertol Model 347 Helicopter Hovering in Ground Effect, Microphone 200 Ft to the Right (Reference Figure 54)	100
56	Pressure Time History of Predicted Single- Rotor Rotational Noise Generated From a Boeing-Vertol Model 347 Hovering in Ground Effect	101
57	Spectrum of Predicted Single-Rotor Rotational Noise Generated From a Boeing-Vertol Model 347 Hovering in Ground Effect (Reference Figure 56)	102
58	Pressure Time History of Predicted Single- Rotor Rotational Noise Generated From a Boeing-Vertol Model 347 Hovering in Ground Effect	103
59	Spectrum of Predicted Single-Rotor Rotational Noise Generated From a Boeing-Vertol Model 347 Hovering in Ground Effect (Reference Figure 58)	104
60	Spectrum of Recorded Noise Generated From a Boeing-Vertol Model 347 Helicopter in Level Flight	105

<u>Figure</u>		<u>Page</u>
61	Spectrum of Predicted Noise Generated From a Boeing-Vertol Model 347 Helicopter in Level Flight	106
62	Pressure Time History of Predicted Noise Generated From a Proposed HLH Configuration in 100-Ft Hover, Microphone 200 Ft to the Right.	107
63	Spectrum of Predicted Noise Generated From the Proposed HLH Configuration in 100-Ft Hover, Microphone 200 Ft to the Right (Reference Figure 62)	108
64	Pressure Time History of Predicted Noise Generated From the Proposed HLH Configuration in 100-Ft Hover, Microphone 200 Ft to the Right.	109
65	Spectrum of Predicted Noise Generated From the Proposed HLH Configuration in 100-Ft Hover, Microphone 200 Ft to the Right (Reference Figure 64)	110

LIST OF TABLES

<u>Table</u>		<u>Page</u>
I	Whirl Tower Test Conditions Used in Creating the Data Bank	17
II	Thrust Calculation for CH-47B Rotor (Tip Speed, Nominally 750 Ft/Sec; Thrust, 21,511 Lb)	20
III	Thrust Calculation for CH-47B Rotor (Tip Speed, Nominally 750 Ft/Sec; Thrust, 12,167 Lb)	24
IV	Thrust Calculation for CH-47B Rotor (Tip Speed, Nominally 804 Ft/Sec; Thrust, 12,167 Lb)	29
V	Thrust Calculation for CH-47B Rotor (Tip Speed, Nominally 900 Ft/Sec; Thrust, 7,023 Lb)	31
VI	Thrust Calculation for CH-47B Rotor (Tip Speed, Nominally 900 Ft/Sec; Thrust, 33,279 Lb)	32
VII	Thrust Calculation for CH-47B Rotor (Tip Speed, Nominally 980 Ft/Sec; Thrust, 7,023 Lb)	33
VIII	Thrust Calculation for CH-47B Rotor (Tip Speed, Nominally 933 Ft/Sec; Thrust, 33,279 Lb)	34
IX	Thrust Calculation for UH-1B Main Rotor (Tip Speed, Nominally 746 Ft/Sec; Thrust, 5,200 Lb)	36
X	Thrust Calculation for UH-1B Tail Rotor (Tip Speed, Nominally 746 Ft/Sec; Thrust, 330 Lb)	37

LIST OF SYMBOLS

a	area of blade station (ft ²)
c	speed of sound (ft/sec)
(ch)	blade chord (ft)
c_D	coefficient of blade station drag due to steady and oscillatory forces
c_d	coefficient of blade station steady drag
c_L	coefficient of blade station lift due to steady and oscillatory forces
c_l	coefficient of blade station steady lift
d	distance of microphone from source along the ground (ft)
\hat{d}	unit vector for drag in tip-path-plane coordinates
$\dot{\hat{d}} = \frac{d}{dt} (\hat{d})$	(sec ⁻¹)
\vec{F}	force on blade element (lb)
$\dot{\vec{F}} = \frac{d}{dt} (\vec{F})$	(lb/sec)
$\dot{\vec{F}}_D = \dot{c}_d + \frac{2\dot{u}}{u} c_d$	(sec ⁻¹)
FKD	oscillatory drag per square foot at the blade station (lb/ft ²)
f_a	frequencies at which the ground reflected signal is in phase with the direct signal (Hz)
f_c	frequencies at which the ground reflected signal is 180° out of phase with the direct signal (Hz)
\hat{f}_D	unit vector for drag in G-2 coordinate
$\dot{\hat{f}}_D = \frac{d}{dt} (\hat{f}_D)$	(sec ⁻¹)
FKL	oscillatory lift per square foot at the blade station (lb/ft ²)

$\dot{\mathbf{F}}_L = \dot{\mathbf{C}}_L + \frac{2\dot{\mathbf{u}}}{u} \mathbf{C}_L$	(sec ⁻¹)
$\hat{\mathbf{f}}_L$	unit vector for lift in G-2 coordinates
$\dot{\hat{\mathbf{f}}}_L = \frac{d}{dt} (\hat{\mathbf{f}}_L)$	(sec ⁻¹)
[H]	rotational transformation from the helicopter coordinate system to the G-2 coordinate system
\underline{h}	altitude of noise source (ft)
$\underline{\lambda}$	microphone height (ft)
$\hat{\lambda}$	unit vector for lift in tip-path-plane coordinates
$\dot{\lambda} = \frac{d}{dt} (\hat{\lambda})$	(sec ⁻¹)
λ_m	length of mast (ft)
\dot{M}	velocity of the blade station divided by the speed of sound
$\dot{\hat{M}} = \frac{d}{dt} (\hat{M})$	(sec ⁻¹)
M_R	component of the station velocity in the direction of the observer divided by the speed of sound
\dot{M}_R	component of the station acceleration in the direction of the observer divided by the speed of sound
n	non-negative integer
$\vec{P}(\vec{x}_0, t)$	acoustic pressure time history at observer's location (lb/ft ²)
P_{max}	maximum predicted pressure (lb/ft ²)
P_{min}	minimum predicted pressure (lb/ft ²)
P_{osc}	oscillatory lift per square foot at the blade station (lb/ft ²)
ϕ_{has}	phase of blade station shedding frequency initially random
q	dynamic pressure (lb/ft ²)

R	distance between the blade station and the observer (ft)
[R]	rotational transformation from tip-path-plane coordinate to G-2 coordinates
r	radius of blade station (ft)
S _t	Strouhal number
[T]	rotational transformation from tip-path-plane coordinates to coordinates parallel to the helicopter coordinates
t	real time (sec)
t'	retarded time (sec)
th	blade section thickness as seen by the flow (ft)
u	flow velocity (ft/sec)
$\dot{u} = \frac{d}{dt} (u)$	(ft/sec ²)
\vec{v}	total velocity of the blade station in the ground coordinate system (ft/sec)
\vec{v}_H	velocity of the helicopter (ft/sec)
\vec{v}	velocity of the blade station in the G-2 coordinate system due to rotation about the shaft (ft/sec)
\vec{v}	velocity of the blade station in the tip-path-plane coordinate system due to rotation about the shaft (ft/sec)
$\vec{x} = (x, y, z)$	location of the blade station in the ground coordinate system (ft)
\vec{x}_{H_0}	location of the helicopter in the ground coordinate system at time $t = 0$ (ft)
$\vec{x}_o = (x_o, y_o, z_o)$	location of the observer in the ground coordinate system (ft)
$\vec{x} = (x, y, z)$	location of the blade station in the G-2 coordinate system (ft)

\dot{x}_{hub}	location of the hub in coordinates parallel to G-2 coordinates but with the origin in the helicopter coordinate system (ft)
$\dot{\mathbf{x}} = (x, y, z)$	location of blade station in the tip-path-plane coordinate system (ft)
\dot{x}'_{hub}	location of the hub in the helicopter coordinate system (ft)
$\dot{x}'_m = (x'_m, y'_m, z'_m)$	location of the mast hinge in the helicopter coordinate system (ft)
α	angle of attack (rad)
$\dot{\alpha} = \frac{d}{dt} (\alpha)$	(rad/sec))
α_{FA}	forward-aft flapping angle relative to the shaft, defined positive for forward tilt of rotor (rad)
α_h	pitch, defined positive nose up (rad)
α_{LA}	lateral flapping angle relative to the shaft, defined positive for left tilt of rotor (rad)
β_h	yaw, defined positive nose to the right (rad)
β_o	coning angle (rad)
Δr	width of blade station (ft)
Δt	travel time of acoustic signal from blade station to observer (sec)
θ_m	shaft angle, defined positive for forward tilt of shaft (rad)
$\pi = 3.14159$	
ρ	density of air (lb sec ² /ft ⁴)
\sum	sum over the blade stations
γ	inflow angle at the blade station (rad)
$\dot{\gamma} = \frac{d}{dt} (\gamma)$	(rad/sec))
ψ	roll, defined positive right side up (rad)
$\dot{\psi}$	azimuthal position of blade (rad)

ψ_h heading, defined positive nose to the right
(rad)
 Ω rotor rotational speed (rad/sec)
 ω vortex shedding frequency (rad/sec)

INTRODUCTION

Rotor noise is the primary contributor to the external noise of modern gas-turbine-powered helicopters. Results of several research programs (References 1, 2, and 3) have shown that the acoustic pressure time history at an observer's location is due almost entirely to the noise output of main and tail rotor systems. This means that the helicopter's detectability and to a large extent its effectiveness as a weapons system is determined by the noise signature of its rotor system.

In the past, rotor systems were designed only on the basis of performance requirements since no reliable method of noise prediction existed; therefore, the noise signature of the rotor system was unknown until the design was complete and the rotor system had been built and tested. At this point in the development cycle, little change could be made in the design of the rotor system without seriously compromising both performance and cost.

It is known through studies that have been conducted in recent years that substantial gains in rotor noise reduction can be achieved. This was markedly demonstrated by the Army in its recent quiet helicopter program (References 4 and 5), in which several manufacturers were supported to investigate what improvements could be made in the noise characteristics of one of their existing aircraft. Considerable flexibility in compromising performance was allowed if improvements in noise could be achieved. Results of the program showed that attention to the aerodynamic sources of rotor noise could yield significant reductions in noise and significantly decrease the distance at which the helicopter could be detected.

The drawback to the quiet helicopter program was that noise reduction had to be achieved by modifying existing designs - designs which had been developed without initial attention to noise. Because of this, while quieting was achieved, significant penalties were noted in the performance of the helicopter as a consequence.

To avoid these problems, it has been desired for many years to have some means of predicting the noise of a given rotor system during the design stage. If this were realizable, design studies could be carried out and tradeoffs between noise and performance clearly delineated. Further, for a rotor system designed to meet given performance requirements, the optimum acoustic design could be determined. It is believed that the key to the optimum design of a rotor as regards noise is a thorough understanding of the noise generating mechanisms so that noise reduction methods can be evaluated without undertaking an experimental

program of rotor design and test. Several studies (References 1, 2, and 3) have concentrated on the aerodynamic mechanisms of rotor noise. The reports of these studies have shown what are the important aerodynamic mechanisms of noise generation for helicopter rotors. In order to use these results, however, an acoustic prediction program must be devised that will allow subjective as well as scientific evaluation of helicopter rotor noise during the design stage.

There have been efforts to provide such a prediction method in the past. Attempts were first made by empirical relations and scaling to forecast the overall noise level for a rotor design. Following this, empirical approaches have been tried that will foretell the octave-band noise signature. But even if overall and octave-band forecast techniques are entirely accurate, they reveal extremely limited information about a rotor system which is yet to be built.

What is required instead is an analytical tool that can be applied to a given rotor system including main and tail rotors, or a tandem configuration, and that will provide for either hover or forward flight:

1. A plot of the predicted acoustic pressure time history for any observer's location relative to the aircraft.
2. A plot of the predicted SPL or spectrum.
3. A tape recording of the predicted rotor noise that can be played for subjective evaluation.

The advantages of such a tool are many. As noted, it can be used for rotor design in which an acoustic evaluation can be made of the effects of blade chord, twist, planform, and rotational speed. Rotor parameters such as solidity, thrust, and number of blades could also be varied and the resulting noise signatures studied. Such a predictive tool would be of great value to both the manufacturers of helicopters and the users.

To provide such a predictive method was the object of the program reported herein. This was accomplished by extending and modifying an existing method already developed by RASA for the Army and reported in Reference 3.

DESCRIPTION OF ANALYTICAL TECHNIQUE

The prediction program discussed herein is an extension of the fundamental work conducted previously and reported in Reference 3. The previous research effort was an investigation of the fundamental characteristics of vortex noise produced by a helicopter rotor and the development of a technique by which the acoustic signature created by vortex shedding could be predicted at an observer's location for any single-rotor helicopter system in hover or forward flight. In order to predict the total noise signature from multiple-rotor systems in hover or forward flight, the program was expanded to include two rotors at arbitrary locations and the steady and harmonic aerodynamic forces that create rotational noise. The basic theoretical formulation of the technique is presented in Reference 3, and the description of the theoretical technique presented herein is associated with the inclusion of two rotors and the effects of rotational noise.

THEORY

Rotor noise is produced by aerodynamic forces acting on the blades (Reference 2). The forces on the blades can be modeled by dipoles (Reference 6) located at individual blade sections of a sectionalized blade. Using this model, the noise produced by the forces acting on the rotor can be determined by evaluating (Reference 2):

$$P(\vec{x}_0, t) = \left[\frac{1}{4\pi c R^2 (1-M_R)^2} \left\{ \vec{F} \cdot \vec{\nabla} \right. \right. \\ \left. \left. + (\vec{x} - \vec{x}_0) \cdot \left[\dot{\vec{F}} + \frac{\vec{F}}{(1-M_R)} \left(\dot{M}_R + \frac{c}{R} (1-M^2) \right) \right] \right\} \right]_t \quad (1)$$

where $\left[\right] =$ sum over the blade stations

$\left[\right]_t =$ evaluation of those quantities inside the brackets are at a "retarded time" t' corresponding to the real time t

$c =$ speed of sound (ft/sec)

$\vec{x}_0 =$ location of observer in ground coordinates (ft)

$R =$ distance between blade station and observer

$$= [(\vec{x} - \vec{x}_0) \cdot (\vec{x} - \vec{x}_0)]^{1/2} \quad (\text{ft})$$

Reproduced from
best available copy.

\vec{x} = location of blade station in ground coordinates (ft)

$$M_R = \frac{(\vec{x}_0 - \vec{x}) \cdot \vec{M}}{R}$$

= component of the station velocity in the direction of the observer divided by the speed of sound

$$\dot{M}_R = \frac{(\vec{x}_0 - \vec{x}) \cdot \vec{M}}{R}$$

= component of the station acceleration in the direction of the observer divided by the speed of sound

$$\vec{M} = \frac{\vec{V}}{c}$$

\vec{F} = force on blade element (lb)

$$\vec{V} = \vec{V}_H + \vec{v}$$
 (ft/sec)

= velocity of blade element in ground coordinates

\vec{V}_H = velocity of rotor hub in ground coordinates (ft/sec)

\vec{v} = velocity of blade element due to rotation in ground coordinates (ft/sec)

$$\dot{\vec{F}} = \frac{d}{dt} (\vec{F})$$

$$\dot{\vec{M}} = \frac{d}{dt} (\vec{M})$$

The quantities in Equation (1) inside the brackets are evaluated at a time prior to t since the signal was actually emitted at an earlier time due to the finite speed of sound. That is, a signal received at an observer's location that was emitted from a source at time t' required time $\Delta t = R/c$ to reach an observer (where R is the distance from source to observer, c is the speed of sound); $t' + \Delta t = t$, the real time at which the signal is received by the observer.

With terms comprising Equation (1) formulated, the pressure time history at an observer location may be specified once the forces at the blade have been specified. Since the forces are represented by dipoles, the acoustic signature of the rotor is generated by a series of moving dipoles located at a number of blade stations along the span. The total aerodynamic force at each blade station is composed of two different types of forces. The first force classification includes all forces that produce rotational noise, which is defined as that portion of a noise spectrum which has a number of narrow spikes occurring at integral multiples of blade passage frequency. While the magnitude and direction of the forces can vary with time, the time dependence must be harmonic with blade passage. The rotational noise forces are the lift and drag forces which are developed by the blade section. The second force classification includes forces that produce broadband or vortex noise. The forces that generate broadband noise have been assumed to be those induced by discrete vortex shedding at the blade sections (Reference 3). These forces are, therefore, represented by oscillatory forces with frequency equal to the vortex shedding frequency based on a Strouhal formulation. The vortex shedding frequency is not related to the blade passage frequency. These oscillatory forces from vortex shedding have both a lift and a drag component. As discussed more fully in the next section, the oscillatory lift component of the vortex shedding force has been determined from experimental data and can be represented by the following expression:

$$FKL = p_{osc} = 2(1 - M)(1 + (\frac{\alpha}{4})^2) \quad (2)$$

where p_{osc} = the oscillatory lift per square foot at the blade station (lb/ft^2)

M = the blade station Mach number > 0

α = the blade station angle of attack (deg)

The oscillatory drag component has been assumed to be negligible and therefore

$$FKD = 0 \quad (3)$$

Equation (2) is valid for Mach numbers $0 \leq M \leq 1$ and angles of attack $|\alpha| < \text{stall}$. These bounds were determined by the following considerations. First of all, there must be blade motion in order to have vortex shedding and so $M > 0$. Also, the trend shown from analyzing experimental data (detailed discussion in the next section) is that the oscillatory lift decreases with Mach number. No data, however, were analyzed with a sonic blade velocity and so the behavior of the vortex shedding

phenomena at $M=1$ is not known. Given the fact that equation (1) is not valid at $M=1$, it is reasonable to have $p_{osc} = 0$ at $M=1$; or more precisely, equation (2) is valid only for $M < 1$. Equation (2) also indicates that the oscillatory lift increases with angle of attack. The angle of attack dependence in equation (2) is similar to the angle of attack dependence of the airfoil section drag coefficient up to stall. Therefore, equation (2) is assumed valid below stall, $|\alpha| < \text{stall}$.

The force at each of the blade stations is, therefore, represented by a lift dipole, a drag dipole, and an oscillatory lift dipole with frequency equal to the vortex shedding frequency. Motion of the blade element relative to the observer shifts the apparent frequency of the oscillatory lift dipole and alters the pressure magnitude at the observer location. The resulting noise is broadband but modulated by the blade passage frequency. The lift and drag forces for hover were determined from blade-element momentum theory (as outlined in Gessow and Myers (Reference 7)) in terms of radial distributions of angle of attack, inflow angle, and flow velocity. The radial and azimuthal distributions of angle of attack, inflow angle, and flow velocity for a rotor in level flight were determined from the formulation presented in Reference 8. The calculation is outlined as follows. The radial and azimuthal variation of the flow velocity is determined by the vector sum of the rotational velocity and the component of the flight velocity parallel to the rotational velocity. The wake-induced inflow is assumed uniform and is calculated from the thrust coefficient and the advance ratio. The uniform wake-induced inflow, the inflow due to forward flight, and the flow velocity determine the radial and azimuthal dependence of the inflow angle. Finally, the radial and azimuthal dependence of the angle of attack is determined by subtracting the inflow angle from the sum of the collective pitch, the cyclic pitch, and the blade twist angles.

In order to properly sum the force contributions from the individual blade stations at the observer location, retarded time effects must be included. To elaborate, sounds emitted at the same time from a distributed source arrive at the observer location at different times because the distributed source is generally not equidistant from the observer. The inclusion of retarded time effects is accomplished by having the rotor blades generate noise from an array of blade stations at regular time intervals. The noise from the individual blade stations arrives at the observer location at irregular time intervals which are calculated. The irregular time intervals are then converted to regular time intervals by an interpolation technique, thereby accounting for retarded time effects.

To sum the contributions from the individual blade stations at the observer location, the blade element quantities must also be transformed from the moving rotor coordinates to the observer coordinates. The transformation from the blade stations to the observer location is accomplished using the following four coordinate systems: modified tip-path-plane coordinate system, helicopter coordinate system, G-2 coordinate system, and ground coordinate system (see Figure 1).

The modified tip-path-plane coordinate system's origin is located at the rotor hub parallel to tip path plane coordinates. The positive x coordinate is toward the front of the helicopter. The positive z coordinate is directed parallel to the thrust vector, away from the rotor mast. The positive y coordinate is chosen so that the coordinate system is right handed.

The helicopter coordinate system's origin is determined by the helicopter location in the ground coordinate system. The positive x' coordinate is directed toward the helicopter nose, the positive z' coordinate is directed up relative to the helicopter, and the positive y' coordinate is chosen so that the coordinate system is right handed.

The G-2 coordinate system origin is located at the rotor hub. The G-2 coordinates are parallel to the coordinates of the ground system.

The ground coordinate system's origin is located on the ground at any specified point; the Z coordinate is up while the X and Y coordinates are in the ground plane chosen so that the coordinate system is right handed.

The following discussion specifies the transformations required from tip-path-plane coordinates to the ground coordinates. The first transformation (1) rotates from the modified tip-path-plane coordinates to coordinates parallel to the helicopter coordinate system. The second transformation (2) rotates from the coordinates parallel to the helicopter coordinate system to the G-2 coordinate system. Since the G-2 coordinate system is parallel to the ground coordinate system, only a translation is required going from the G-2 system to the ground coordinate system.

(1) Due to the fact that there are basically three types of rotor orientations (main rotor, tail rotor on left side of the helicopter, tail rotor on right side of the helicopter), three separate rotations are required to transform from tip-path-plane coordinate to coordinates parallel to the helicopter coordinates:

For the main rotors,

$$[T] = \begin{bmatrix} \cos(\alpha_{FA} + \theta_m) & 0 & \sin(\alpha_{FA} + \theta_m) \\ 0 & 1 & 0 \\ -\sin(\alpha_{FA} + \theta_m) & 0 & \cos(\alpha_{FA} + \theta_m) \end{bmatrix} \begin{bmatrix} 1 & 0 & 0 \\ 0 & \cos \alpha_{LA} & \sin \alpha_{LA} \\ 0 & -\sin \alpha_{LA} & \cos \alpha_{LA} \end{bmatrix}$$

$$[T] = \begin{bmatrix} \cos(\alpha_{FA} + \theta_m) & -\sin(\alpha_{FA} + \theta_m) \sin \alpha_{LA} & \sin(\alpha_{FA} + \theta_m) \cos \alpha_{LA} \\ 0 & \cos \alpha_{LA} & \sin \alpha_{LA} \\ -\sin(\alpha_{FA} + \theta_m) & -\cos(\alpha_{FA} + \theta_m) \sin \alpha_{LA} & \cos(\alpha_{FA} + \theta_m) \cos \alpha_{LA} \end{bmatrix}$$

(4)

where α_{FA} = the forward-aft flapping angle relative to the shaft, defined positive for forward tilt of rotor (rad)

α_{LA} = the lateral flapping angle relative to the shaft, defined positive for left tilt of rotor (rad)

θ_m = mast or shaft angle, defined positive for forward tilt of shaft (rad)

For a tail rotor on the left side of the helicopter,

$$[T] = \begin{bmatrix} \cos(\alpha_{FA} + \theta_m) & -\sin(\alpha_{FA} + \theta_m) \sin \alpha_{LA} & \sin(\alpha_{FA} + \theta_m) \cos \alpha_{LA} \\ -\sin(\alpha_{FA} + \theta_m) & -\cos(\alpha_{FA} + \theta_m) \sin \alpha_{LA} & \cos(\alpha_{FA} + \theta_m) \cos \alpha_{LA} \\ 0 & -\cos \alpha_{LA} & -\sin \alpha_{LA} \end{bmatrix}$$

(5)

For a tail rotor on the right side of the helicopter ,

$$[T] = \begin{bmatrix} \cos(\alpha_{FA} + \psi_m) & -\sin(\alpha_{FA} + \psi_m) \sin \alpha_{LA} & \sin(\alpha_{FA} + \psi_m) \cos \alpha_{LA} \\ \sin(\alpha_{FA} + \psi_m) & \cos(\alpha_{FA} + \psi_m) \sin \alpha_{LA} & -\cos(\alpha_{FA} + \psi_m) \cos \alpha_{LA} \\ 0 & \cos \alpha_{LA} & \sin \alpha_{LA} \end{bmatrix} \quad (6)$$

(2) The rotational transformation from the helicopter coordinate system to the G-2 coordinate system is

$$[H] = \begin{bmatrix} \cos(\beta_h + \psi_h) & \sin(\beta_h + \psi_h) & 0 \\ -\sin(\beta_h + \psi_h) & \cos(\beta_h + \psi_h) & 0 \\ 0 & 0 & 1 \end{bmatrix} \begin{bmatrix} \cos \alpha_h & 0 & -\sin \alpha_h \\ 0 & 1 & 0 \\ \sin \alpha_h & 0 & \cos \alpha_h \end{bmatrix} \begin{bmatrix} 1 & 0 & 0 \\ 0 & \cos \phi_h & \sin \phi_h \\ 0 & -\sin \phi_h & \cos \phi_h \end{bmatrix}$$

$$[H] = \begin{bmatrix} \cos(\beta_h + \psi_h) \cos \alpha_h & \sin(\beta_h + \psi_h) \sin \phi_h + \cos(\beta_h + \psi_h) \sin \alpha_h \sin \phi_h & \sin(\beta_h + \psi_h) \sin \phi_h - \cos(\beta_h + \psi_h) \sin \alpha_h \cos \phi_h \\ -\sin(\beta_h + \psi_h) \cos \alpha_h & \cos(\beta_h + \psi_h) \cos \phi_h - \sin(\beta_h + \psi_h) \sin \alpha_h \sin \phi_h & \cos(\beta_h + \psi_h) \sin \phi_h + \sin(\beta_h + \psi_h) \sin \alpha_h \cos \phi_h \\ \sin \alpha_h & -\cos \alpha_h \sin \phi_h & \cos \alpha_h \cos \phi_h \end{bmatrix} \quad (7)$$

where β_h = yaw, defined positive nose to the right (rad)

ψ_h = heading, defined positive nose to right (rad)

α_h = pitch, defined positive nose up (rad)

ϕ_h : roll, defined positive right side up (rad)

Therefore, the transformation from modified tip-path-plane to G-2 coordinates is (combining equations for [T] and [H]):

$$[R] = [H] [T] \quad (8)$$

Again, since there are three basic types of rotor orientation, there are three separate positions of the hub in helicopter coordinates:

For a main rotor,

$$\vec{x}_{\text{hub}}' = \begin{bmatrix} x_m' + l_m \sin \theta_m \\ y_m' \\ z_m' + l_m \cos \theta_m \end{bmatrix} \quad (9)$$

For a tail rotor on the left side of the helicopter,

$$\vec{x}_{\text{hub}}' = \begin{bmatrix} x_m' + l_m \sin \theta_m \\ y_m' + l_m \cos \theta_m \\ z_m' \end{bmatrix} \quad (10)$$

For a tail rotor on the right side of the helicopter,

$$\vec{x}_{\text{hub}}' = \begin{bmatrix} x_m' + l_m \sin \theta_m \\ y_m' - l_m \cos \theta_m \\ z_m' \end{bmatrix} \quad (11)$$

where x_m' , y_m' , z_m' = position of mast hinge in helicopter coordinates (ft)

l_m = length of mast (ft)

[] = column representation of x' , y' , z'

The position of the hub in coordinates parallel to G-2 coordinates but with the origin in the helicopter coordinate system is

$$\dot{\vec{x}}_{\text{hub}} = [H] \dot{\vec{x}}'_{\text{hub}} \quad (12)$$

The position of the blade station in tip-path-plane coordinates is

$$\dot{\vec{x}} = \begin{bmatrix} -r \cos \psi \cos \theta_0 \\ -r \sin \psi \cos \theta_0 \\ r \sin \theta_0 \end{bmatrix} \quad (13)$$

where r = location of blade station (ft)

ψ = azimuthal position of blade (rad)

θ_0 = coning angle (rad)

The position of the blade in G-2 coordinates is

$$\dot{\vec{x}} = [R] \dot{\vec{x}} \quad (14)$$

Therefore, taking into account the translation of the helicopter, the blade station location in the ground coordinate system is

$$\dot{\vec{x}} = \dot{\vec{x}}_{H_0} + \dot{\vec{v}}_H t + \dot{\vec{x}}_{\text{hub}} + \dot{\vec{x}} \quad (15)$$

where $\dot{\vec{x}}_{H_0}$ = position of helicopter with respect to ground coordinates at time $t = 0$ (ft)

$\dot{\vec{v}}_H$ = velocity of helicopter (ft/sec)

$\dot{\vec{x}}_{\text{hub}}$ = location of hub in coordinates parallel to the G-2 coordinates but with the origin in the helicopter coordinate system (equation (12)) (ft)

$\dot{\vec{x}}$ = position of blade station in G-2 coordinate system (equation (14)) (ft)

In tip-path-plane coordinates, the velocity of the blade station due to rotation about the shaft is

$$\dot{\vec{v}} = \frac{d\dot{\vec{x}}}{dt} = \begin{bmatrix} r \sin \psi \cos \theta_0 \\ -r \cos \psi \cos \theta_0 \\ 0 \end{bmatrix} \quad (16)$$

where Ω = rotational speed of the rotor (rad/sec)

The velocity of the blade station in G-2 coordinates is

$$\vec{v} = [R] \vec{v} \quad (17)$$

The total velocity of the blade station in the ground coordinate system is

$$\vec{V} = \vec{V}_H + \vec{v} \quad (18)$$

The force formulation required to transform from the tip-path-plane coordinates to ground coordinates are now discussed.

The unit vectors for lift and drag in the tip-path-plane coordinate systems are (see Figure 2)

$$\hat{i} = \begin{bmatrix} -\sin\psi \sin\phi + \cos\psi \sin\beta_0 \cos\phi \\ \cos\psi \sin\phi + \sin\psi \sin\beta_0 \cos\phi \\ \cos\beta_0 \cos\phi \end{bmatrix} \quad (19)$$

$$\hat{d} = \begin{bmatrix} -\sin\psi \cos\phi - \cos\psi \sin\beta_0 \sin\phi \\ \cos\psi \cos\phi - \sin\psi \sin\beta_0 \sin\phi \\ -\cos\beta_0 \sin\phi \end{bmatrix} \quad (20)$$

where ϕ = inflow angle at blade station (rad)

In G-2 coordinates, these vectors become

$$\hat{f}_L = [R] \hat{i} \quad (20)$$

$$\hat{f}_D = [R] \hat{d}$$

The rate of change of the unit vectors for lift and drag are denoted as \dot{i} and \dot{d} , and in G-2 coordinates

$$\dot{f}_L = [R] \dot{i} \quad (21)$$

$$\dot{f}_D = [R] \dot{d}$$

Therefore, the force and its derivative at the blade station specified in ground coordinates are (Reference 3)

$$\dot{F} = qa (C_L f_L + C_D f_D) \quad (22)$$

$$\dot{F} = qa (C_L \dot{f}_L + \dot{F}_L f_L + C_D \dot{f}_D + \dot{F}_D f_D)$$

$$+ (ch)\Delta r \sin(\omega t + \text{phas}) (FKL \dot{f}_L + FKD \dot{f}_D)$$

where $q = 1/2 \rho u^2$

ρ = dynamic pressure (lb/ft^2)

ρ = density of air ($\text{lb sec}^2/\text{ft}^4$)

u = flow velocity at the blade station (ft/sec)

$a = (ch)\Delta r$

= area of blade station (ft^2)

(ch) = blade chord at station (ft)

Δr = width of station (span) (ft)

$C_L = C_L - \frac{FKL}{1/2\rho u^2} \cos(\omega t + \text{phas})$

= coefficient of blade station lift due to steady and oscillatory forces

C_L = coefficient of blade station steady lift

FKL = oscillatory lift per square foot at blade station (see equation (2)) (lb/ft^2)

ω = vortex shedding frequency (rad/sec)

phas = phase of blade station shedding frequency initially random

$C_D = C_D - \frac{FKD}{1/2\rho u^2} \cos(\omega t + \text{phas})$

= coefficient of blade station drag due to steady and oscillatory forces

C_D = coefficient of blade station steady drag

FKD = oscillatory drag per square foot at the blade station (see equation (3)) (lb/ft^2)

$$\dot{F}_L = \dot{C}_L + \frac{2\dot{u}}{u} C_L = \frac{dC_L}{du} \dot{u} + \frac{dC_L}{du} \dot{u} + \frac{2\dot{u}}{u} C_L$$

$$\dot{F}_D = \dot{C}_d + \frac{2\dot{u}}{u} C_d = \frac{dC_d}{du} \dot{u} + \frac{dC_d}{du} \dot{u} + \frac{2\dot{u}}{u} C_d$$

GENERAL DESCRIPTION OF PROGRAM

The equations of the previous section were programmed for computer use. The resulting program is discussed in the supporting documentation (see Reference 9). The noise produced by helicopter rotors is predicted for hover or steady-state flight. The noise contributions from each of the stations distributed along the blades of each of the helicopter rotors are summed at the observer's location, taking proper account of retarded time effects. The forces acting on each blade element are represented by four moving dipoles, one each for the lift, the drag, the oscillatory lift, and the oscillatory drag. The program input consists of the helicopter rotor design parameters, the helicopter flight condition, the helicopter attitude, the helicopter location, the observer position, and the distribution of angle of attack, inflow angle, and flow velocity along the rotor blade as a function of azimuth. The output of the program consists of the digital pressure time history in lb/ft^2 at the observer location specified. The program output has been plotted and Fourier analyzed so that noise spectra can be generated. In addition, the digital signal was transformed to an analog signal for subjective evaluation using an IBM 7700 computer which can convert a digital to an analog signal. The analog output (a voltage level) therefore corresponds to the digital pressure time history that was supplied as input and hence is recorded directly on a tape recorder. Since the peak-to-peak value of the predicted pressure is known, the input of a sine wave with the same peak-to-peak voltage as that of the predicted pressure recorded on tape will permit the signal to be calibrated using a sound level meter. The rms level of the recorded sine wave is just 0.707 times the peak value of the sine wave. The peak value of the sine wave is one-half the peak-to-peak value of the predicted pressure in lb/ft^2 . Therefore, the predicted pressure time history is properly calibrated by playing the recorded sine wave and adjusting the volume so the sound level meter reads

$$SLM = 20 \log_{10} \left| \frac{0.707 (P_{max} - P_{min})}{2 (4.184 \times 10^{-7})} \right|$$

where 4.184×10^{-7} is the reference pressure in lb/ft^2 .

DATA BANK OF OSCILLATORY FORCE CONSTANTS

It has been assumed that the nonperiodic broadband noise is that produced by the airfoil shedding vortices at frequencies determined by a Strouhal calculation. As explained previously, an array of dipoles oscillating at individual frequencies moving with the rotor blade produces a broadband signature at the observer location, but this random signature is modulated by the rotor passage frequency. With the frequency of the oscillatory forces known from the Strouhal calculation, the magnitude of the oscillatory forces can be determined as functions of the section Mach number and angle of attack from controlled rotor acoustic tests conducted on a whirl tower. The magnitudes can then be parameterized as functions of the section variables. This procedure defines a "data bank": a relation containing information concerning vortex noise that was reduced from 30 experimentally recorded acoustic records.

FITTING FOR OSCILLATORY FORCE CONSTANTS

The basic procedure used to determine the magnitudes of the oscillatory force constants was as follows:

1. Blade-element momentum theory was used to determine the distribution of angles of attack and flow velocity across the whirl tower rotor blade for a thrust value equal to that attained for the recorded acoustic data.
2. These angles of attack and flow velocities were used to determine the vortex shedding frequency by

$$\omega = \frac{S_t u}{th} \quad (23)$$

where ω = vortex shedding frequency

th = blade section thickness as seen by the flow (for most helicopter blades, th equals blade thickness since the aerodynamic angle of attack rarely exceeds 7 degrees)

u = flow velocity

S_t = Strouhal number

The Strouhal number was set equal to 0.235, held independent of section variables. This Strouhal number was determined as the "best fit" during the research investigation reported on in Reference 3.

3. A 1-ft spanwise station at mid-span and one at the blade tip were given an oscillatory pressure of 1 lb/ft² in the lift direction. (The oscillatory drag was set equal to zero since acoustic data taken in the plane of the rotor indicated that very little noise is produced by vortex shedding in that direction.) For each of the 1-ft-wide stations, a pressure time history was predicted at an observer location appropriate to the recorded data.
4. The predicted pressure time histories were then Fourier analyzed and compared to the spectrum of the experimental data in the appropriate frequency range. The oscillatory force magnitude at each of the blade stations was adjusted so that the predicted spectrum and experimental spectrum had the same magnitude in the appropriate frequency range.

This process resulted in obtaining two oscillatory pressures in the lift direction for different angles of attack and Mach numbers. Repetition of this process for 30 different rotor configurations yielded an array of oscillatory pressures which were then parameterized as functions of angle of attack and Mach number. The result of this parameterization was shown previously in equation (2).

DATA ANALYZED

The acoustic signatures used to create the data bank were recorded by Boeing-Vertol during their recent whirl tower tests (Reference 10) and by NASA/Langley. The UH-1B data analyzed previously (Reference 3) was not included in the data bank. The recordings taken from Boeing's whirl tower data were the most extensively documented available. A detailed discussion of the data is included in Reference 10. The test conditions included tip speeds that ranged from 600 to 900 ft/sec and thrusts that ranged from 6300 to 32,000 lb. The rotor tested was that for the CH-47B helicopter. This rotor has three blades, a 30-ft radius, and a chord of 25.25 inches. The airfoil section is the Vertol 23010-1.58. The twist is -9.13°, linear from the center of rotation. The cutout is 19.2% of the blade radius.

The NASA/Langley whirl tower acoustic recordings were made using a modified H-19 rotor. The rotor has two blades, a radius of 26.67 ft, a chord of 16.5 in. and a twist of -8°. The tip speeds recorded were 564, 628, 711, and 737 ft/sec. The thrusts ranged from 2000 lb and 8000 lb.

Certain records from the H-19 data and the CH-47B data were copied and analyzed for use in creating the data bank (see Table I). In order to study the effects of rotor noise

TABLE I. WHIRL TOWER TEST CONDITIONS USED IN
CREATING THE DATA BANK

Record source	Rotor Height (ft)	Microphone Distance From Rotor Axis (ft)	Microphone Height (ft)	Thrust (lb)	Tip Speed (ft/sec)	Number of Blades	Blade Radius/Chord (ft) / (in.)
NASA (H-19)	45	150	0	1965	564	2	26.67/16.5
	45	150	0	6385	564	2	26.67/16.5
	45	150	0	2735	628	2	26.67/16.5
	45	150	0	8150	628	2	26.67/16.5
	45	150	45	1965	564	2	26.67/16.5
	45	150	45	6385	564	2	26.67/16.5
	45	150	45	2735	628	2	26.67/16.5
	45	150	45	8150	628	2	26.67/16.5
	45	150	45	1965	564	2	26.67/16.5
	45	150	45	6385	564	2	26.67/16.5
APO-D (CH-47B)	47	100	4.3	8845	600	3	30/25.25
	47	284	3.9	8845	600	3	30/25.25
	47	100	4.3	15400	596	3	30/25.25
	47	284	3.9	15400	596	3	30/25.25
	47	100	4.3	24581	600	3	30/25.25
	47	284	3.9	24581	600	3	30/25.25
	47	100	4.3	11632	650	3	30/25.25
	47	284	3.9	11632	650	3	30/25.25
	47	100	4.3	18139	650	3	30/25.25
	47	284	3.9	18139	650	3	30/25.25
47	47	284	3.9	20430	703	3	30/25.25
	47	100	4.3	12167	750	3	30/25.25
	47	100	4.3	21511	753	3	30/25.25
	47	284	3.9	21511	753	3	30/25.25
	47	100	4.3	31363	753	3	30/25.25
	47	284	3.9	31363	753	3	30/25.25
	47	100	4.3	11458	850	3	30/25.25
	47	284	3.9	11458	850	3	30/25.25
	47	284	3.9	11458	850	3	30/25.25

TABLE I - Continued

Record Source	Rotor Height (ft)	Microphone Distance From Rotor Axis (ft)	Microphone Height (ft)	Thrust (lb)	Tip Speed (ft/sec)	Number of Blades	Blade Radius/Chord (ft), (in.)
	47	100	4.3	16863	847	3	30/25.25
	47	284	3.9	16863	847	3	30/25.25
	47	100	4.3	31849	850	3	30/25.25
	47	284	3.9	31849	850	3	30/25.25
	47						30/25.25

directivity, data from two different microphone positions were analyzed for each of the rotors. Table I lists the rotor/microphone locations, the rotor operating conditions, and the rotor geometric parameters. For the CH-47B data, the microphone located 100 ft from the rotor axis is called the "ground" microphone while the microphone located 284 ft from the rotor axis is called the "5D" microphone (see Figure 3 taken from Reference 10).

SAMPLE CALCULATION

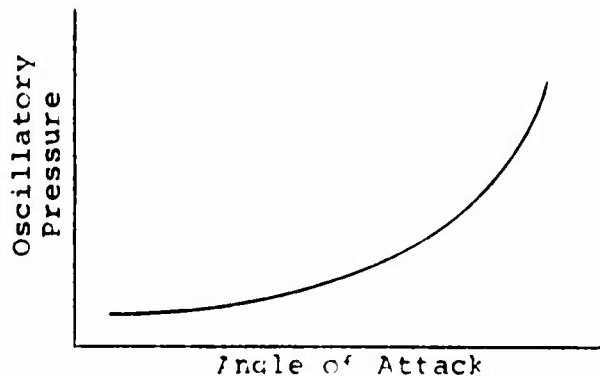
A sample calculation of the previously described procedure for determining the oscillatory force magnitude is presented so that a detailed understanding of the process that was used to generate the data bank can be obtained. The acoustic data that is used in the sample calculation was recorded at the "ground" microphone for the CH-47B rotor operating at a tip speed of 750 ft/sec and a thrust of 21,511 lb. The "ground" is 100 ft from the axis of rotation. The rotor is 47 ft high and the microphone is 4.3 ft high. The pressure time history and spectrum are shown in Figures 4 and 5. The spectrum has a 1-Hz bandwidth over a frequency range of 0 to 6750 Hz. Only the lower frequency portion (0-1700 Hz) is shown, as the higher frequency portion contains no distinctive features. It is noted that the pressure time history does not have a strong signal that repeats with rotor blade passage, which indicates that the signal that contributes to rotational noise is weak. In addition, it is noted that a broadband or random signal is very prominent in the recorded noise. The spectrum reflects the nature of the recorded pressure time history in that the rotor rotational noise is discernible only in the first few harmonics.

In order to determine the vortex shedding frequencies, the distribution of angles of attack and flow velocities must be determined. The output of the blade-element momentum theory for the operating conditions appropriate to the recorded data is presented in Table II. Using this information, a 1-ft-wide station centered about a 15-ft radius has a flow velocity of 377 ft/sec and an angle of attack of 5.4 deg, while a 1-ft-wide station in the tip region has a flow velocity of 740 ft/sec and an angle of attack of 3.2 deg. The vortex shedding frequencies in the rotating coordinate system for these two stations are 422 and 827 Hz, respectively (Strouhal number = 0.235, blade thickness = 0.21 ft). An oscillatory pressure of 1 lb/ft² is specified for each of these 1-ft-wide stations, and individual pressure time histories are predicted at the microphone location; see Figures 6 and 7.

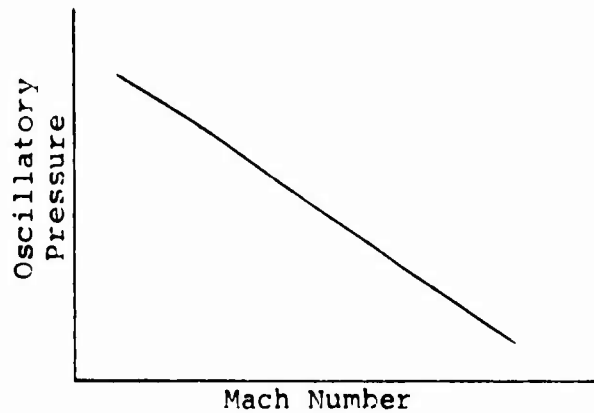
TABLE II. THRUST CALCULATION FOR CH-47B
ROTOR (TIP SPEED, NOMINALLY
750 FT/SEC; THRUST, 21,511 LB)

Radial Station (ft)	Angle of Attack (rad)	Inflow Angle (rad)	Flow Velocity (ft/sec)
5.75	0.092	0.151	145.5
8.44	0.099	0.130	213.1
11.14	0.100	0.114	280.6
13.83	0.097	0.102	348.0
16.53	0.091	0.094	415.5
19.22	0.085	0.086	482.9
21.92	0.078	0.078	550.2
24.61	0.070	0.072	617.5
27.31	0.063	0.065	684.9

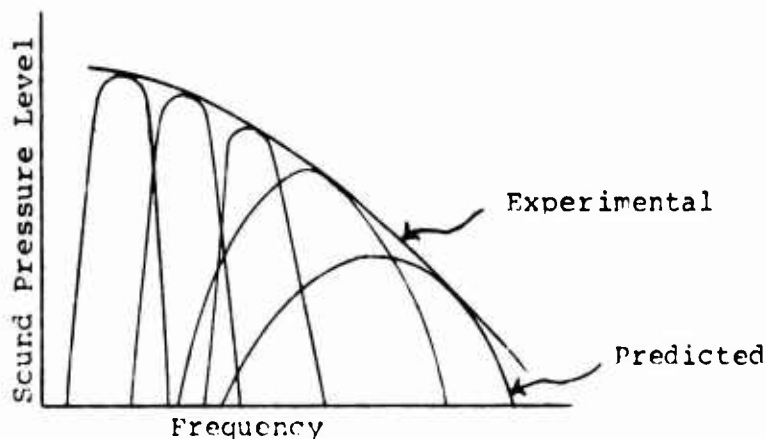
As these plots indicate, the individual vortex shedding frequencies are shifted by the motion of the blade relative to the observer. The relative Mach number of the blade with respect to the observer also alters the magnitude of the pressure time history received by the observer. The motion of the blade toward the observer increases the frequency and magnitude of the oscillatory pressure received by the observer and conversely as the blade moves away from the observer. This effect is present in both plots, but it is more pronounced in Figure 7 because of the higher station velocity. The pressure time histories are Fourier analyzed to obtain the spectra shown in Figure 8 and 9, respectively. Note that each station's contribution is a band of noise. The width in frequency is related to the Doppler shift of the shedding frequency due to the relative motion of the blade element with respect to the observer. Therefore, the frequency band for the station at the tip is wider than at mid-span. These frequency bands are compared to the experimental spectrum, and the magnitude differences in decibels are converted to magnitude differences in pressure. The pressure differences may be regarded as correction factors that are applied to the control pressure of 1 lb/ft². These two correction factors are functions of angle of attack and Mach number. A repetition of this process for other rotor conditions and configurations yields an array of oscillatory pressures as functions of angle of attack and Mach number. For constant Mach number, the observed angle-of-attack dependence of the oscillatory pressures is depicted below:



For constant angle of attack, the observed Mach number dependence of the oscillatory pressures is depicted below:



The effect of individual blade stations having an overlap of their noise signals due to the Doppler shift has not been included since the two control stations were picked so that very little noise energy overlap would exist. To account for the noise energy overlap, a distribution of oscillatory pressures was located across the blade so that the entire spectrum of vortex noise could be represented by the unit oscillatory pressures. The magnitudes of the unit control oscillatory pressures were then adjusted so that the predicted spectrum matches the experimental spectrum over the entire frequency range.



The oscillatory pressures that are determined by these means are then parameterized so that one expression can represent the oscillatory forces generated by vortex shedding as functions of Mach number and angle of attack (see equation (2)).

RESULTS - TEST CASES

In order to evaluate the accuracy of the noise prediction program, a number of comprehensive test cases were devised. The first test of the prediction technique was to determine its capability of reproducing the broadband noise for the rotor systems from which the data bank was created. In addition to the broadband noise, the rotational noise prediction technique was also tested for these same rotor systems. These first two checks were accomplished by predicting the acoustic data measured for the CH-47B at the "ground" microphone 100 ft from the rotor axis. The next three test cases were conducted to determine whether the prediction program could successfully predict the whirl tower data not included in the data bank. These three check cases were conducted for the CH-47B data at the "5D" microphone. After the successful prediction of the check cases, the UH-1B helicopter noise was predicted for a hover and steady-state flight configuration. In addition, the Boeing-Vertol 347 helicopter noise was predicted for hover and steady-state flight. Finally, the noise produced by a heavy-lift helicopter configuration was predicted in hover for two different thrust values. A discussion of the results obtained from these predictions is presented on the following pages.

CH-47B WHIRL TOWER

The first test of the program was to determine the accuracy of the rotational noise prediction and to determine whether the parameterization of the oscillatory force magnitudes accurately reproduced the broadband noise from which they were derived. This first test of the predictive program was carried out for the acoustic data measured by the microphone placed 100 ft from the rotor axis (Figure 3) and for the rotor operating at tip speed of 750 ft/sec and a thrust of 12,167 lb. The measured pressure time history is shown in Figure 10, while the spectrum is shown in Figure 11. As noted previously for Figures 4 and 5, the pressure time history recorded at the ground microphone does not have a strong signal that repeats with rotor blade passage. Therefore, the signal that contributes to rotational noise is weak. Conversely, the broadband or random signal is dominating the recorded noise. The spectrum shows a weak rotational noise signal in that only the first few harmonics are discernible from the strong broadband signal.

The prediction was carried out for the same microphone location, thrust, and tip speed. The distributions of angles of attack, inflow angles, and flow velocities calculated for this configuration are presented in Table III. The predicted pressure time history and spectrum are shown, respectively, in Figures 12 and 13. The predicted spectrum has a 1-Hz bandwidth, the same as

TABLE III. THRUST CALCULATION FOR CH-47B
ROTOR (TIP SPEED, NOMINALLY
750 FT/SEC; THRUST, 12,157 LB)

Radial Station (ft)	Angle of Attack (rad)	Inflow Angle (rad)	Flow Velocity (ft/sec)
5.75	0.066	0.127	145.1
8.44	0.071	0.108	212.6
11.14	0.070	0.094	280.0
13.83	0.067	0.083	347.4
16.53	0.060	0.076	414.8
19.22	0.053	0.068	482.2
21.92	0.047	0.061	549.5
27.31	0.033	0.046	684.1
30.00	0.026	0.038	751.4

the experimental spectrum.

In comparing the experimental and predicted pressure time histories (Figures 10 and 12), note the difference in the plotting scales. It is noted that the predicted pressure time history has a weak rotational noise signal, and the peak-to-peak pressure magnitude of the predicted rotational noise signal is approximately equal to the peak-to-peak pressure magnitude of the experimental rotational noise signal. The high-frequency noise is broadband in nature, and as in the experimental records, the predicted broadband noise is modulated at the rotor blade passage frequency. The high-frequency, high-magnitude random noise is followed by low-frequency, low-magnitude noise (see previous discussion regarding the Doppler shift of discrete vortex shedding). The peak-to-peak pressure magnitude of the predicted vortex noise signal is equivalent to the peak-to-peak pressure magnitude of the experimental vortex noise.

In order to compare the experimental and predicted spectrums (Figures 11 and 13), the effects of ground reflection on the experimental record should be described. Reproducing the ground reflection calculation presented in Reference 3, the reflected and direct wave are in phase and add for the frequencies:

$$f_a = c \frac{\sqrt{h^2 + d^2}}{2lh} n \quad (24)$$

where f_a = frequencies at which the reflected signal is in phase with the direct signal (Hz)

c = speed of sound (ft/sec)

h = altitude of noise source (ft)

d = distance of microphone from source along the ground (ft)

l = microphone height (ft)

n = non-negative integer

The reflected and direct signals are 180° out of phase for the frequencies

$$f_c = c \frac{\sqrt{h^2 + d^2}}{2lh} (n + 1/2) \quad (25)$$

where f_c = frequencies at which the reflected signal is 180° out of phase with the direct signal.

For the frequency f_c , cancellation occurs. The whirl tower is 47 ft high; the microphone is 4.3 ft high and is 100 ft from the rotor axis. Therefore, equation (25) gives the first frequency of cancellation as $f_c = 150$ Hz ($c = 1100$ ft/sec, $n = 0$). Referring to Figure 11, the noise minimum in the spectrum at 150 Hz is clearly evident. The first frequency region of pressure reinforcement occurs from 0 to less than 150 Hz. The next region of pressure reinforcement occurs from approximately 150 to 450 Hz. If the ground surface effectively reflects the sound, then 6 dB should be added to those frequency regions where the reflected wave reinforces the direct wave. Effective reflection of sound from ground surfaces occurs primarily for low-frequency noise. Therefore, when comparing predicted rotational noise with the experimental rotational noise, 6 dB must be added to the predicted rotational noise in the frequency regions where the reflected wave reinforces the direct wave. Note the excellent comparison in the first few harmonics of rotational noise when these effects of ground reflection are included. The predicted level of the broadband noise also compares quite well with the experimental level, except in the low-frequency region. The low-frequency broadband noise observed in the experimental record masks out much of the rotational noise. This low-frequency broadband noise is not observed in the same record recorded at the "5D" microphone, which is 284 ft from the axis of rotation; see Figure 18. It is believed that this low-frequency broadband noise is pseudo-sound; the microphone may be recording flow variations in the downwash since the rotor diameter is 60 ft, the whirl tower height is 47 ft, and the microphone is only 100 ft from the axis of rotation.

The band of noise energy seen in the predicted spectrum centered about 125 Hz (Figure 13) is caused by one of the inboard stations used in the prediction being too wide. This particular station did not have sufficient velocity for the Doppler effect to overlap the frequency content of its signal with the signals of its neighbors. If two or more stations replaced this single station, the spectrum would become more continuous as it is in the experimental data. This effect will appear on some of the later predictions as well. The analog tapes generated from the predicted pressure time history sound like the experimental tapes except that the predicted tapes are more staccato. Analysis of this and other generated tapes for hover has indicated that variability in noise from blade passage to blade passage is an important effect when subjective evaluations are being conducted. The analysis done to date has assumed that quasi-stationary processes govern the rotor noise output so that the problem could be made tractable. These assumptions have not significantly limited the scientific content of the program results, but they have reduced the "realism" of the acoustic tapes generated for hover. This variability is most apparent in the broadband noise associated

with discrete vortex shedding from the airfoil when the helicopter is in hover. The variability is best described by referring to Figure 14, taken from Reference 3. As the title indicates, the figure shows the distribution of the magnitude of the oscillatory lift force calculated over the rotor blade. These oscillatory lift forces are those assumed to be induced by vortex shedding. The variation in the oscillatory pressures reflects the signal variation from blade passage to blade passage. The analysis was carried out for a UH-1B in hover. The first station is at the radius of 7 ft, while the tenth station is at the blade tip. Four hover cases, designated A, B, C, D, were analyzed. The oscillatory lift forces were found to be distributed about mean values which correspond to the oscillatory pressure parameterization of the previous section (equation (2)). Observe that the variation is significant and is therefore believed to be very important in the subjective evaluation of helicopter noise.

The next test case was also conducted for the CH-47B rotor system for data recorded at the "ground" microphone. The tip speed of the rotor was 750 ft/sec and the thrust was 21,511 lb. The recorded pressure time history and spectrum were those shown and discussed previously in Figures 4 and 5. The predicted pressure time history and spectrum are shown in Figures 15 and 16. The distribution of angles of attack, inflow angles, and flow velocities used in the prediction are shown in Table II. The predicted pressure time history has a weak rotational noise signal as does the experimental pressure time history (Figures 15 and 4; note the difference in scaling). The high-frequency noise is broadband in nature and is associated with vortex shedding. As before, the predicted and experimental broadband noise is modulated in frequency and magnitude by the rotor blade passage frequency. The predicted and experimental spectrums may be compared upon making the correction for ground reflection already outlined. The accuracy of the rotational noise prediction is significant in spite of the fact that much of the experimental rotational noise is obscured by the low-frequency broadband noise believed to be pseudo-sound (see Figures 16 and 5). The predicted broadband noise level induced by vortex shedding is the same as the experimental broadband noise level. The predicted tapes compare favorably with the experimentally recorded noise except for the staccato effect discussed previously.

The next series of tests was conducted for the whirl tower data but for a rotor and microphone configuration not used to develop the data bank. The first of these test conditions repeats one of the earlier rotor conditions but was recorded at the "5P" microphone. The rotor tip speed was 750 ft/sec and the thrust was 12,167 lb. The microphone was 284 ft from the rotor axis and is 3.9 ft off the ground. The recorded pressure time history is shown in Figure 17, while its spectrum is shown in Figure 18. The rotational noise signal is more evident in the pressure time history recorded at the "5D" microphone than that of the identical

conditions recorded at the "ground" microphone (see Figure 10). This difference is partly due to the directivity of the noise emanating from the rotor. The spectrum (Figure 18) shows a stronger rotational signal as well. It is noted that approximately 10 harmonics of rotor blade passage are distinguishable in this spectrum. The broadband noise is also clearly evident in both the pressure time history and the spectrum. Since the whirl tower is 47 ft high, cancellation of the noise due to ground reflection occurs at 430 Hz (see equation (25)). Reference to Figure 18 reveals that the ground reflection minimum does occur at 430 Hz. The prediction was carried out for the same microphone location, thrust, and tip speed. The distributions of angles of attack, inflow angles, and flow velocities developed by the rotor are shown in Table III. The predicted pressure time history and spectrum are shown in Figures 19 and 20 respectively. With the correction for ground reflection included, the vortex noise levels of the predicted spectrum are just slightly less than the levels of the experimental spectrum, but the rotational noise prediction is low by 6 to 8 dB. Examination of the experimental spectrum reveals that the harmonic spikes are separated by 12.8 Hz, which means that the rotor was really operating at 256 rpm instead of the reported rotational speed of 239 rpm. In an effort to resolve this discrepancy, another noise prediction was generated with the rotational speed equal to 256 rpm and for the same thrust of 12,167 lb. The distributions of angles of attack, inflow angles, and flow velocities are shown in Table IV for this configuration. For this prediction, the oscillatory lift (FKL) was set equal to zero so that only rotational noise would be predicted. The resulting spectrum is shown in Figure 21. Note that the higher rotational speed increases the magnitude of the predicted rotational noise spikes and reduces their drop-off rate with frequency so that the predicted rotational noise spectrum (Figure 21) compares more favorably with the experimental noise spectrum (Figure 18) when the ground reflection correction is included in the predicted spectrum. It is anticipated that the higher rotational speed will also increase the broadband noise level of the predicted signature, thereby improving the comparison between the predicted and experimental broadband signals.

The final two test cases for the CH-47B data were conducted for a nominal tip speed of 900 ft/sec and thrusts of 7023 and 33,279 lb. The microphone location is 284 ft from the rotor axis and 3.9 ft off the ground. The recorded pressure time histories are shown in Figures 22 and 23 while their spectrums are shown in Figures 24 and 25. The rotational noise signals displayed in these pressure time histories and spectrums are dominating the noise signature. The noise minimum at 430 Hz is caused by ground reflection, which also distorts significantly the shape of the analog rotational noise signals.

TABLE IV. THRUST CALCULATION FOR CH-47B
ROTOR (TIP SPEED, NOMINALLY
804 FT/SEC; THRUST, 12,167 LB)

Radial Station (ft)	Angle of Attack (rad)	Inflow Angle (rad)	Flow Velocity (ft/sec)
5.75	0.062	0.122	155.3
8.44	0.065	0.104	227.6
11.14	0.065	0.090	299.8
13.83	0.060	0.080	372.0
16.53	0.053	0.073	444.3
19.22	0.047	0.065	516.4
21.92	0.041	0.057	588.5
24.61	0.034	0.049	660.6
27.31	0.028	0.041	732.6
30.00	0.021	0.034	804.7

Predictions were carried out for the same microphone location, tip speed, and thrust values. The distributions of angles of attack, inflow angles, and flow velocities for these two predictions are listed in Tables V and VI. The predicted pressure time histories are shown in Figures 26 and 27, while their spectrums are shown in Figures 28 and 29. Note that the predicted pressure time histories are basically symmetrical about their mean lines, while the recorded pressure time histories are distorted by the effects of ground reflection (Figures 22 and 23). With the magnitude correction for ground reflection included, the vortex noise levels of the predicted spectrums for these two cases are lower than the levels of the appropriate two experimental spectrums by about 4 or 5 dB. The rotational noise predictions are low by approximately 10 dB. Examination of the experimental spectrums reveals that the harmonic spikes are separated by 15.6 Hz for the run with 7023 lb thrust and by 14.9 Hz for the run with 33,279 lb thrust. Therefore, the rotational speeds for these two runs were really 312 rpm and 297 rpm instead of the reported speed of 286 rpm. In order to determine the change in the noise generated, two rotational noise predictions were prepared; the distributions of angle of attack, inflow angle, and flow velocity are listed in Tables VII and VIII for the rotational speeds of 312 rpm and 297 rpm respectively. The resulting spectrums of the rotational noise are shown in Figures 30 and 31. Again, the higher rotational speeds induce higher levels of rotational noise and reduce the drop-off rates with frequency of the spikes. These spectrums now compare quite well with the experimental spectrums when the magnitude correction for ground reflection is included (compare Figure 30 with 24 and Figure 31 with 25). The rotational noise spikes in Figure 30 drop off more slowly than those of Figure 31, even though the latter plot was predicted for a much higher thrust. The thrust affects the magnitude level of the rotational noise spikes, but the tip speed affects both the magnitude level and the drop-off rate. The higher tip speed narrows the wave to a pulse-like structure, thereby creating higher harmonics and reducing the drop-off rate of the harmonics. The higher rotational speeds should also increase the broadband noise levels of the two predicted signatures so that they compare more favorably with the recorded broadband signatures.

UH-1B IN HOVER AND FORWARD FLIGHT

The next tests were conducted to evaluate the capability of the program to predict the rotor noise of a complete helicopter in hover and forward flight. The UH-1B helicopter was chosen for these predictions, as extensive, well documented noise data exists for this helicopter. These noise tests were reported in References 11 and 3 and are known as the Wallops Island Tests. Some of this data was analyzed previously in Reference 3. For the test conditions under this program, however, different

TABLE V. THRUST CALCULATION FOR CH-47B
ROTOR (TIP SPEED, NOMINALLY
900 FT/SEC; THRUST, 7,023 LB)

Radial Station (ft)	Angle of Attack (rad)	Inflow Angle (rad)	Flow Velocity (ft/sec)
5.75	0.045	0.102	173.1
8.44	0.047	0.086	253.8
11.14	0.045	0.073	334.5
13.83	0.038	0.066	415.2
16.53	0.032	0.057	495.8
19.22	0.027	0.049	576.4
21.92	0.021	0.040	656.9
24.61	0.016	0.030	737.4
27.31	0.011	0.022	818.0
30.00	0.007	0.011	898.5

TABLE VI. THRUST CALCULATION FOR CH-47B
ROTOR (TIP SPFED, NOMINALLY
900 FT/SEC; THRUST, 33,279 LB)

Radial Station (ft)	Angle of Attack (rad)	Inflow Angle (rad)	Flow Velocity (ft/sec)
5.75	0.095	0.154	174.2
8.44	0.102	0.132	255.1
11.14	0.103	0.117	335.9
13.83	0.099	0.107	416.7
16.53	0.093	0.098	497.4
19.22	0.087	0.089	578.0
21.92	0.080	0.082	658.6
24.61	0.073	0.075	739.2
27.31	0.065	0.069	819.7
30.00	0.060	0.059	900.1

TABLE VII. THRUST CALCULATION FOR CH-47B
ROTOR (TIP SPEED, NOMINALLY
980 FT/SEC; THRUST, 7,023 LB)

Radial Station (ft)	Angle of Attack (rad)	Inflow Angle (rad)	Flow Velocity (ft/sec)
5.75	0.043	0.098	188.8
8.44	0.044	0.082	276.8
11.14	0.041	0.071	364.9
13.83	0.034	0.064	452.9
16.53	0.029	0.055	540.8
19.22	0.024	0.045	628.7
21.92	0.019	0.036	716.5
24.61	0.013	0.027	804.4
27.31	0.009	0.017	892.3
30.00	0.011	0.001	980.2

TABLE VIII. THRUST CALCULATION FOR CH-47B
ROTOR (TIP SPEED, NOMINALLY
933 FT/SEC; THRUST, 33,279 LB)

Radial Station (ft)	Angle of Attack (rad)	Inflow Angle (rad)	Flow Velocity (ft/sec)
5.75	0.091	0.151	180.8
8.44	0.098	0.130	264.8
11.14	0.099	0.155	348.7
13.83	0.094	0.105	432.6
16.53	0.089	0.096	516.4
19.22	0.083	0.088	600.1
21.92	0.076	0.080	683.8
24.61	0.068	0.074	767.5
27.31	0.061	0.067	851.1
30.00	0.064	0.049	934.2

conditions were chosen than those analyzed previously. The array of microphone locations is shown in Figure 32, which is reproduced from Reference 3. The direction of flight is shown; the hover position is nominally over microphone 13. In Reference 3, the 100-ft-hover acoustic records of microphones 4 and 6 were analyzed. The acoustic predictions conducted herein are for the data recorded at microphone 10 for the 100-ft hover and the data recorded at microphone 4 for the 122-knot flyby at 100 ft.

Hover

Spectrums of the experimentally recorded noise for the 100 ft-hover at microphones 4 and 10 are shown in Figures 33 and 34. The spectral analysis was undertaken on a Ubiquitous Analyzer by Boeing-Vertol. The bandwidth is 2 Hz over the frequency range of 0 to 1000 Hz. Comparison of these two figures reveals that ground reflection was effective over a wide frequency range and that the ground reflection minimums do not occur at the same frequency in the two plots. Therefore, the two microphones are not equidistant from the helicopter as reported. For microphone 4, the first minimum occurs at 105 Hz; while for microphone 10, the first minimum occurs at 125 Hz. This information can be used together with equation (25) to determine the helicopter position; the helicopter was actually positioned 20 ft to the right of the desired location and only 95 ft high. Therefore, the helicopter hub of the main rotor is 220 ft from microphone 10 (180 ft from microphone 4) and 95 ft off the ground. Figure 34 shows that the main rotor dominates the frequency region of 0 to 100 Hz (the main rotor blade passage is 10.8 Hz). The tail rotor blade passage is 5.108 times that of the main rotor, or 55.2 Hz. The first harmonic of the tail rotor is not distinguishable from the fifth harmonic of the main rotor in Figure 34 since the bandwidth is only 2 Hz. The second harmonic of the tail rotor occurs in the frequency region of ground reflection cancellation and therefore cannot be seen. The third, fourth, fifth, and sixth harmonic of tail rotor are observed at 166, 221, 276, and 332 Hz respectively. Higher harmonics are not discernible. The tail rotor noise is less important at microphone 4 than at microphone 10; see Figures 33 and 34. The reason for this difference is that at microphone 10 the lift- and drag-induced rotational noise are additive, while at microphone 4 the lift- and drag-induced noise are subtractive.

Additional specifications supplied by the Army for the UH-1B are: the main rotor has two blades with a radius of 22 ft and a chord of 21 in., the rotational speed is 324 rpm, and the thrust is 5200 lb. The tail rotor also has two blades but with a radius of 4.3 ft and a chord of 8.4 in., the rotational speed is 1656.8 rpm, and the thrust is 330 lb in hover. The distributions of angles of attack, inflow angles, and flow velocities are listed in Tables IX and X. With the observer located at microphone 10,

TABLE IX. THRUST CALCULATION FOR UH-1B MAIN ROTOR (TIP SPEED, NOMINALLY 746 FT/SEC; THRUST, 5,200 LB)

Radial Station (ft)	Angle of Attack (rad)	Inflow Angle (rad)	Flow Velocity (ft/sec)
0.0	0.227	0.0	0.0
2.44	0.062	0.146	83.8
4.89	0.075	0.114	166.9
7.33	0.075	0.094	249.9
9.78	0.070	0.079	332.8
12.22	0.062	0.068	415.6
14.67	0.053	0.058	498.5
17.11	0.042	0.050	581.3
19.56	0.031	0.041	664.1
22.00	0.020	0.033	746.8

TABLE X. THRUST CALCULATION FOR UH-1B TAIL
ROTOR (TIP SPEED, NOMINALLY
746 FT/SEC; THRUST, 330 LB)

Radial Station (ft)	Angle of Attack (rad)	Inflow Angle (rad)	Flow Velocity (ft/sec)
0.0	0.108	0.0	0.0
0.47	0.015	0.094	82.3
0.94	0.023	0.085	164.5
1.42	0.029	0.079	246.6
1.89	0.034	0.074	328.6
2.36	0.038	0.070	410.7
2.83	0.041	0.068	492.7
3.31	0.042	0.066	574.8
3.78	0.044	0.065	656.8
4.25	0.044	0.064	738.9

the predicted pressure time history and spectrum were generated (Figures 35 and 36 respectively). With the 6-dB correction for ground reflection added to the predicted spectrum in the appropriate frequency ranges, the main rotor rotational noise spikes match the levels of the experimental main rotor spikes (see Figure 34). The vortex noise levels of the prediction also compare quite well with the experimental noise levels. The tail rotor rotational noise spikes of the prediction are much less than the levels shown in the experimental spectrum.

It was believed that a possible reason for this difference in the tail rotor noise was the orientation of the helicopter with respect to the microphone. Physically, if the helicopter is oriented parallel to the flight path, the plane of the tail rotor is inclined 68° to a line drawn from the observer to the tail rotor hub. If, however, the helicopter is yawed from the flight path, the inclination angle decreases and the change in angle results in an increase in number of harmonics and the level of each harmonic. To illustrate this effect, two tail rotor rotational noise predictions were generated. The rotational speed, thrust, and distribution of angle of attack, inflow angle, and flow velocity are the same as those used in the prediction shown in Figures 35 and 36. The only parameter changed during the prediction is the yaw of the helicopter, i.e., the orientation of the tail rotor with respect to the observer. The first prediction repeats the tail rotor position used in generating the prediction shown in Figures 35 and 36. That is, the tail rotor boom is over the flight path. The pressure time history is shown in Figure 37, and the spectrum is shown in Figure 38. Note that the pressure time history is almost a sine wave; hence, few high harmonics exist in the spectrum. The second prediction was generated with the tail rotor boom yawed 60° to the right of the flight path. The pressure time history is shown in Figure 39, while the spectrum is shown in Figure 40. Note that the magnitude of the pressure oscillation has increased by a factor of 4 and the wave form is distorted from that of a sine wave. The spectrum reflects these changes in that the harmonics content has increased as well as the magnitude of the spikes. Therefore, it is suspected that the difference in the measured and predicted spectrums is due to the helicopter's not holding position and orientation during the hover tests. It is noted, however, that the tail rotor also operates in the environment of the main rotor, which induces irregularities in the tail rotor pressure field, and this effect could also contribute to the difference in the measured and predicted tail rotor signatures.

Forward Flight

The UH-1B forward flight data was recorded under the same test program as the hover data. The microphone position was 200 ft to the right of the flight path (microphone 4 in Figure 32). The helicopter speed was 122 knots at a nominal altitude of 100 ft.

The spectrum of the experimental noise was generated when the helicopter was 1160 ft uprange ($X = -1160$ ft) and is shown in Figure 41. The positive X axis is in the direction of flight, the positive Z axis is directed up, and the positive Y axis is toward microphone 10 (see Figure 32).

It has been shown that a noise spectrum of a moving helicopter is meaningful if the helicopter-observer orientation does not change significantly (see Reference 3) for the time period required to generate the spectrum. Since the length of the data record used to generate the spectrum was only 1 second and the helicopter position was far uprange, the helicopter-observer orientation could not change significantly and the spectrum presented in Figure 41 is meaningful. In Figure 41, note that the ground reflection minimum occurs at 590 Hz, which confirms the reported position of the helicopter (see equation (25)). The main rotor rotational noise is significant to 300 Hz, and the tail rotor rotational noise is significant to 1400 Hz. The broadband noise becomes important beyond 1000 Hz. The noise prediction was carried out for the conditions appropriate to the experimental spectrum. The predicted spectrum is shown in Figure 42. With the 6-dB correction for ground reflection added in the appropriate frequency ranges, the predicted spectrum agrees with the experimental spectrum to within a few dB over the entire frequency range. Both spectrums are 1-Hz bandwidths. Particularly noticeable is the excellent agreement in the rotational noise levels of both main and tail rotors. The main and tail rotor rotational noise drop-off rates also are identical in the two plots.

In order to demonstrate the changes in the noise pressure time history during the flyby, the following comparisons of the experimental and predicted pressure time histories at three different helicopter locations during the flyby are shown. In addition, the main rotor noise is studied by separating the rotational noise from the vortex noise. Figures 43 and 44 are pressure time histories when the helicopter is at $X = -1000$ ft. Figure 43 is the experimental record taken from an oscilloscope trace. Note the double peaks of the tail rotor rotational noise pressure pulses. These double peaks are caused by ground reflection; the separation distance between the double peaks increases as the helicopter approaches. The predicted pressure time history is shown in Figure 44. It is noted that neither the experimental nor predicted results show much evidence of vortex noise and that periodically the main rotor rotational signature is distorted by the tail rotor due to the main rotor-tail rotor phasing caused by the nonintegral relationship in the rotational speeds.

The next two plots repeat the format of the previous two, but for the helicopter at $X = -500$ ft. Figure 45 is the experimental pressure time history. It can be seen that the separation in the double tail rotor peaks has increased from that which is evident at $X = -1000$ ft. The predicted pressure time history is shown in

Figure 46. The vortex noise is clearly evident in both the experimental and predicted results.

The next two plots are the pressure time histories when the helicopter is at $X = 0$ ft. Figures 47 and 48 are the experimental and predicted pressure time histories. Note that the tail rotor noise is no longer visible in either record and that the main rotor vortex noise has become much more prominent. The tail rotor noise disappears because the plane of the tail rotor has a large inclination angle with a line drawn from the observer to the tail rotor hub.

In order to study the main rotor noise, the tail rotor noise was removed from the acoustic signature plotted in Figure 46. The resulting plot shows the main rotor rotational and vortex noise at $X = -500$ ft; see Figure 49. The main rotor vortex noise at $X = -500$ ft is shown in Figure 50 with a pressure magnitude scale three times that of the previous plot. Note the essentially random signal modulated by the main rotor blade passage frequency. The main rotor vortex noise at $X = 0$ ft is plotted in Figure 51, to the same scale, and it can be seen that the broadband pressure magnitudes have increased significantly from those shown in Figure 50.

The predicted noise tapes for the UH-1B flyby are realistic when compared to the experimental tapes. The main rotor and tail rotor rotational noise levels and frequencies are accurately reproduced. The main rotor, tail rotor beating phenomenon is also evident (tail rotor rotational speed is 5.108 times the main rotor rotational speed). The Doppler shift as the helicopter flies past the observer is present in the predicted tapes, and the vortex noise sounds like the broadband noise heard in the experimental tapes. A subjective difference is observable, however, due to the fact that the ground reflection effects are not in the prediction program, thereby causing a difference in the main rotor and tail rotor rotational noise signals when compared to the recorded signals. The ground-reflected signal alters not only the pressure magnitude but also the frequency content of the perceived signal and thus is important in a subjective evaluation (see Figures 43, 44, 45, and 46).

BOEING-VERTOL 347 IN HOVER AND FORWARD FLIGHT

The next test series was conducted for the Boeing-Vertol 347 in hover and forward flight. The experimental data used in the following comparisons were generated by Boeing as a noise reduction demonstration. The tape records are AM, and consequently the low-frequency noise is not accurately reproduced. Since the recorded data were not intended for use in research, the documentation is not as complete as for the data collected by Boeing-Vertol on the whirl tower for the CH-47B rotor.

Hover

The Boeing-Vertol 347 helicopter has a tandem-rotor configuration. Each rotor develops 17,250 lb thrust, has a tip speed of 740 ft/sec, and has four blades with a radius of 30 ft. The chord is 25.25 in. and the twist is -9.13 deg. The helicopter is hovering in ground effect, and the microphone is located 200 ft to the right of the helicopter. The experimental pressure time history is shown in Figure 52, and its spectrum is shown in Figure 53. Analysis of these two plots indicates that the 347 helicopter has one rotor operating in the concentrated vortex wake of the other rotor because one of the rotors is generating more noise than the other rotor. The time separation of the main pressure pulses observable in the pressure time history shows a 4/rev signal, yet ideally the signal would be expected to be 8/rev since the microphone is located equidistant from counterrotating rotors. The spectrum (Figure 53) also shows the blade passage frequency to be 4/rev rather than 8/rev. Also, the high number of harmonics of rotational noise indicates that the main source of noise is generated by a blade wake interaction. The noise generated by blade wake interaction is aggravated by the microphone position, as the microphone is located such that the advancing blades of both rotors relative to the observer are in the blade overlap region where the blade wake interaction occurs. A microphone position on the left side of the helicopter would reduce the significance of the blade wake interaction in relation to the total signature recorded. Without detailed information concerning the distribution of angle of attack, inflow angle, and flow velocity, the noise prediction program cannot predict this type of noise accurately. The predicted pressure time history of the 347 in hover is shown in Figure 54, and its spectrum is shown in Figure 55. Note that the predicted vortex noise levels compare quite well with the experimental levels; the predicted rotational noise, however, has much less harmonic content than the experimental record because the predicted noise does not have the blade vortex interaction induced noise included. An 8/rev signal is observable in both the pressure time history and the spectrum.

The blade vortex interaction effect on the noise signature can be demonstrated graphically. Two rotational noise predictions of the 347 were generated for the forward rotor. The first prediction was carried out for the uniform azimuthal inflow used previously. The pressure time history is shown in Figure 56, and its spectrum is shown in Figure 57. The second prediction was carried out for the same inflow except that at one azimuthal position an inflow increase in the advancing blade region was artificially introduced. The resulting pressure time history and spectrum are shown in Figures 58 and 59. The radical change in the pressure time histories is clearly evident when Figures 56 and 58 are compared. The inflow variation created by a blade

wake interaction causes a variation in angle of attack and therefore a change in blade station lift and drag. The variation in lift and drag causes a significant pressure pulse at the observer location. The spectrum of this distorted pressure time history induced higher harmonic noise (see Figures 59 and 57) because of the narrow pulse-like structure. The spectrum shown in Figure 59 now may be compared to the experimental spectrum, Figure 53. Note the similarity in the fall-off rates even though the calculation performed has been only qualitative in nature.

Forward Flight

The Boeing-Vertol 347 noise data for forward flight was recorded 200 ft to the left of the flight path. The helicopter had a velocity of 203 ft/sec and an altitude of 200 ft. The rotor rotational speed was 214 rpm. The spectrum of the noise generated when the helicopter was 875 ft uprange is shown in Figure 60. The spectrum was valid as long as the helicopter observer orientation did not change significantly during the record analyzed (see Reference 3). The ground reflection minimums occur at 230 and 690 Hz. The experimental spectrum is dominated by broadband noise and the turbine noise around 1700 Hz. The rotational noise signal is not prevalent. The predicted flyby noise is shown in Figure 61. The predicted rotational and broadband noise levels compare quite well with the experimental levels (vortex noise was predicted only above 100 Hz). The predicted flyby acoustic tapes also compare favorably with the experimental tapes when the turbine noise in the experimental record is discounted. The shift in frequency of the vortex modulated noise is noticeable in the tapes as the helicopter flies past the observer.

HLH IN HOVER FOR TWO SETS OF ROTOR PARAMETERS

The final noise predictions were carried out for the proposed heavy-lift helicopter configuration. The predictions were generated for the helicopter in hover at two different thrusts. The first thrust was chosen to be 120,000 lb, while the second thrust was set equal to 60,000 lb. The rotor configuration is tandem; each rotor has four blades with a radius of 45 ft. The rotational speed is 160 rpm and the chord is 42 in. The microphone location is 200 ft to the right of the helicopter, equidistant from the two rotors. The helicopter rotors are 100 ft off the ground. The predicted pressure time history for 120,000 lb thrust is shown in Figure 62, and its spectrum is shown in Figure 63. The noise signature is dominated by vortex noise; rotational noise in this helicopter observer orientation is not significant. The broadband noise level is significant considering that the spectrum shown in Figure 63 has a 1-Hz

bandwidth. The noise prediction for 60,000 lb thrust is shown in Figure 64; its spectrum is shown in Figure 65. Note that the vortex noise level has dropped almost 6 dB, or a factor of two. Ground reflection effects would alter the nature of the predicted signal. In the predicted noise spectrum, the first frequency at which the reflected signal cancels the direct signal would be 123 Hz, the next frequency at which cancellation would occur is 369 Hz, etc. The frequency regions of the spectrum between these minimums would have noise energy magnitudes increased up to 6 dB depending on the reflection characteristics of the ground surface. Also, the blade vortex interaction problem of the 347 would apply to the HLH configuration and introduce high harmonics of rotational noise in the hover configuration, thereby adding significantly to the helicopter detectability.

CONCLUSIONS AND RECOMMENDATIONS

This program has resulted in the successful development of a design tool that realistically predicts helicopter rotor noise. The design tool has the capability of evaluating the acoustic characteristics of new untested rotor designs as well as evaluating the effects of basic rotor design changes on the acoustic signature of existing rotors. The computer design tool should find popular use in the Government as well as the helicopter industry because the predictions are accurate and the program inputs are just the geometric and aerodynamic parameters of the helicopter rotor system. One of the most important features of this tool is that only a digital-to-analog conversion is required in order to evaluate the helicopter noise prediction subjectively.

The following specific conclusions were drawn:

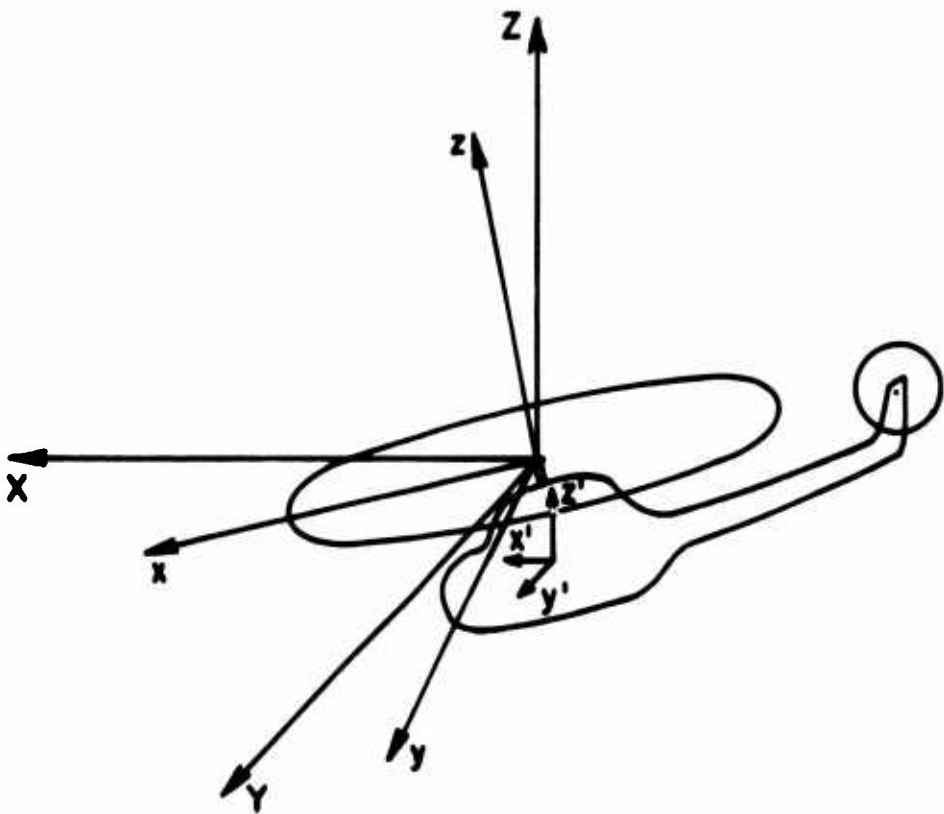
1. Ground reflection effects distort the radiated acoustic pressure-time history, and this distortion is particularly important subjectively.
2. The variability of broadband noise from blade passage to blade passage in a hover configuration is also important in subjective analysis.
3. The program can predict the noise resulting from blade vortex interactions provided the proper aerodynamic information is supplied as input to the program.
4. The parameterization of the oscillatory forces accurately represents the broadband noise over the range of parameters normally encountered in specifying helicopter rotor systems.

To improve the subjective application of this program the following recommendations are made:

1. Modify the prediction program to include the effects of ground reflection.
2. Modify the prediction program to introduce the variability in rotor vortex noise from blade passage to blade passage.

It is also recommended that an effective demonstration of the rotor noise prediction program's capabilities be conducted. The ideal vehicle for this demonstration is the recently conducted quiet helicopter program. The noise prediction program has the capability of predicting the results of the quiet helicopter program at a fraction of the cost. The acceptance of the noise prediction program would allow the scientific consideration and

subjective evaluation of rotor noise during the design stage instead of expensive "retro" type solutions to or investigations of rotor acoustic problems.



(x, y, z) : modified tip path plane coordinate system

(x', y', z') : helicopter coordinate system

(X, Y, Z) : G-2 coordinate system

$(\bar{X}, \bar{Y}, \bar{Z})$: ground coordinate system

α_{FA} = forward-aft flapping angle; rotation about y

α_{LA} = lateral flapping angle; rotation about x

θ_m = shaft angle; rotation about y

ϕ_h = roll; rotation about x'

α_h = pitch; rotation about y'

β_h = yaw; rotation about z'

ψ_h = heading; rotation about z'

Figure 1. Coordinate Systems Used in the Analysis.

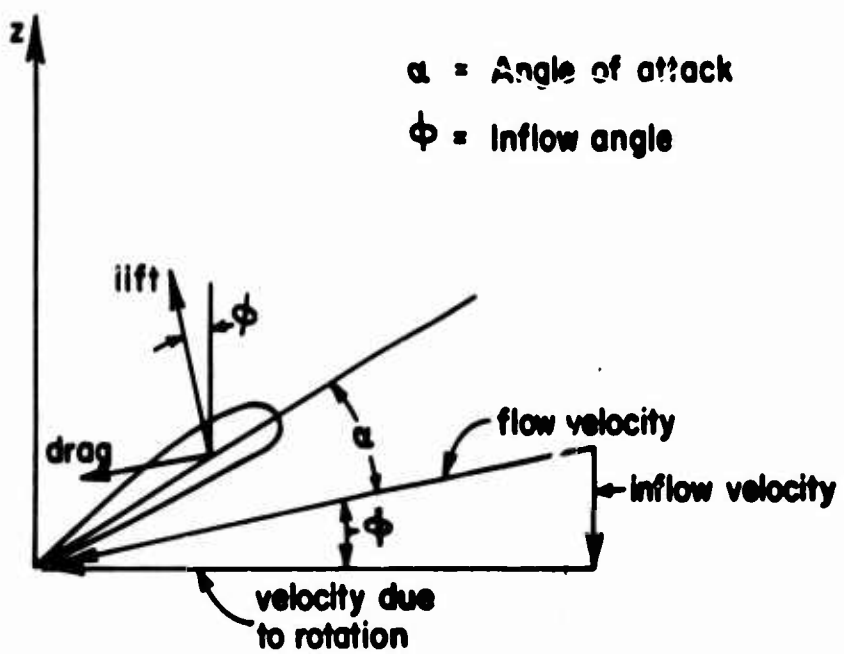


Figure 2. Blade Element Forces and Velocities.

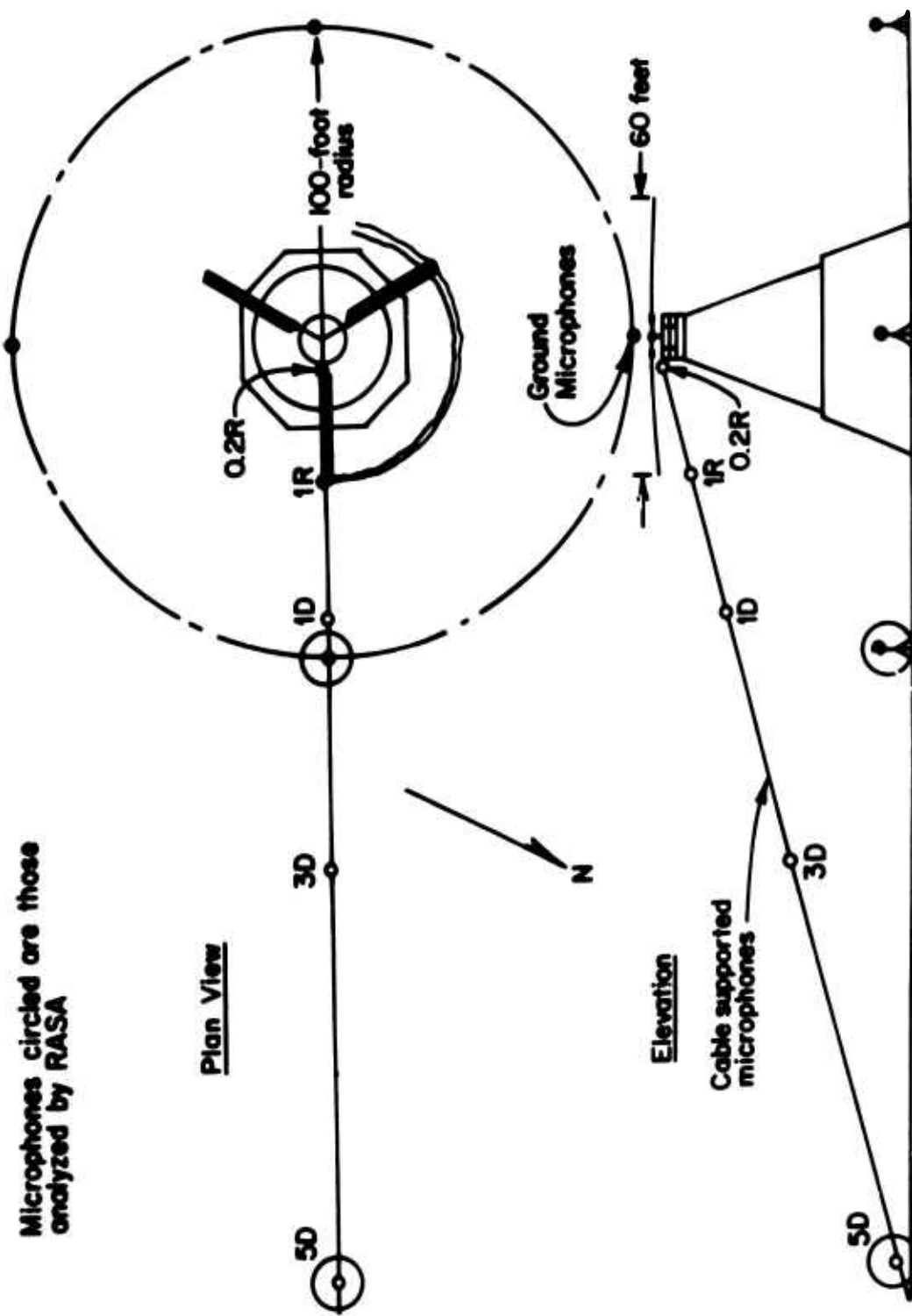


Figure 3. Boeing-Vertol Whirl Tower Microphone Array.

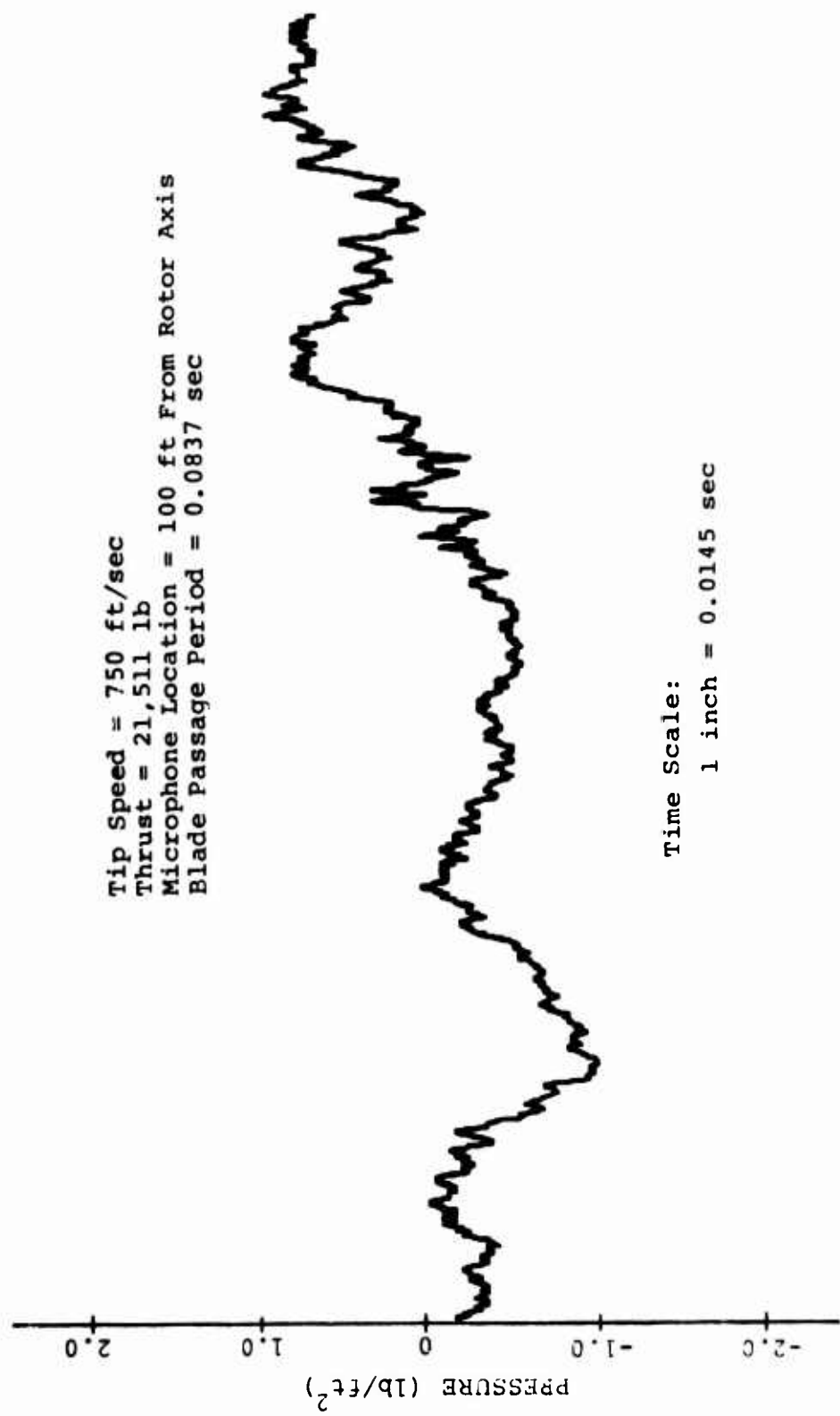


Figure 4. Pressure Time History of Recorded Noise Generated From CH-47B Rotor on a Whirl Tower.

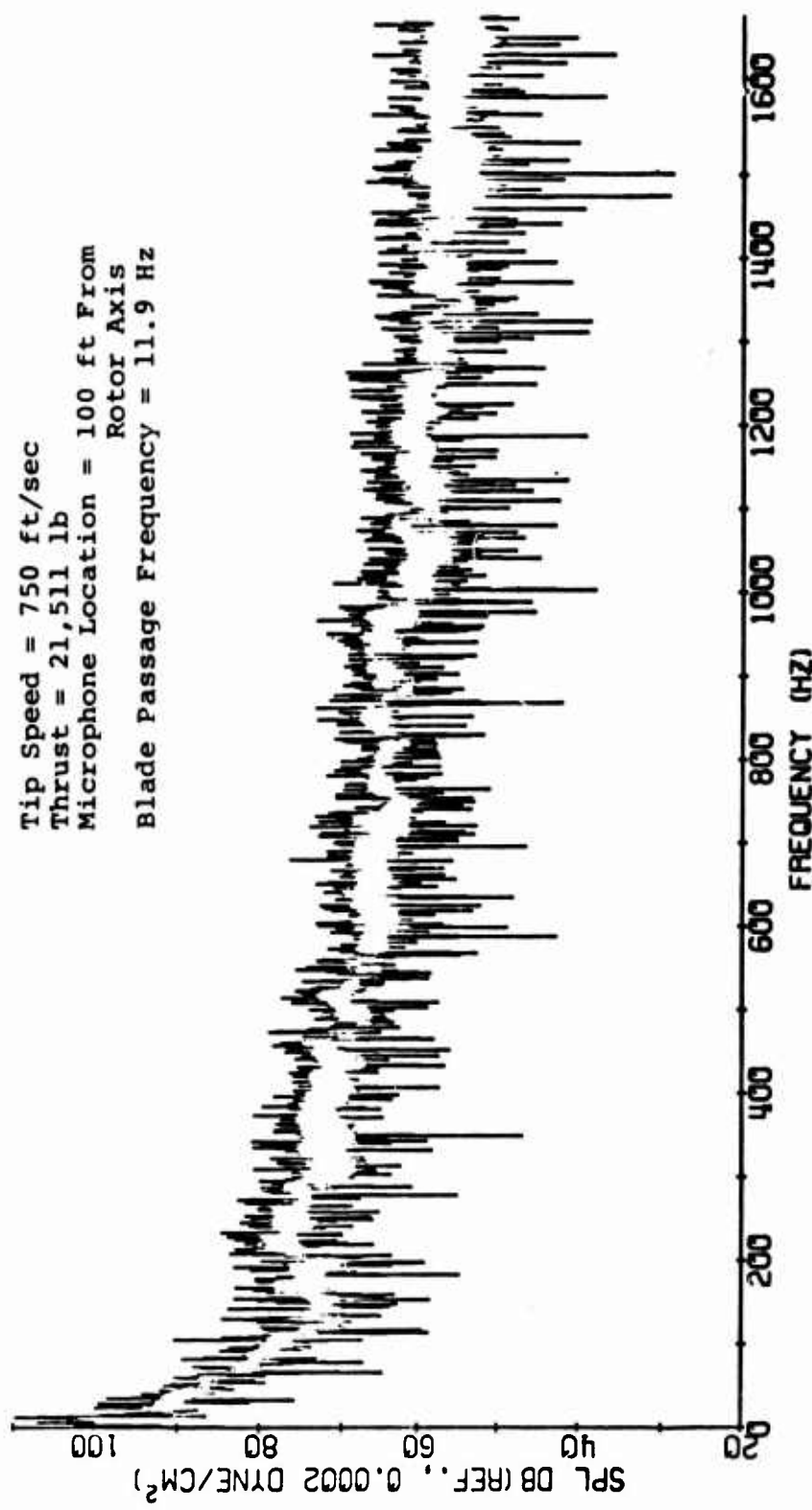


Figure 5. Spectrum of Recorded Noise Generated From CH-47B Rotor on a Whirl Tower (Reference Figure 4).

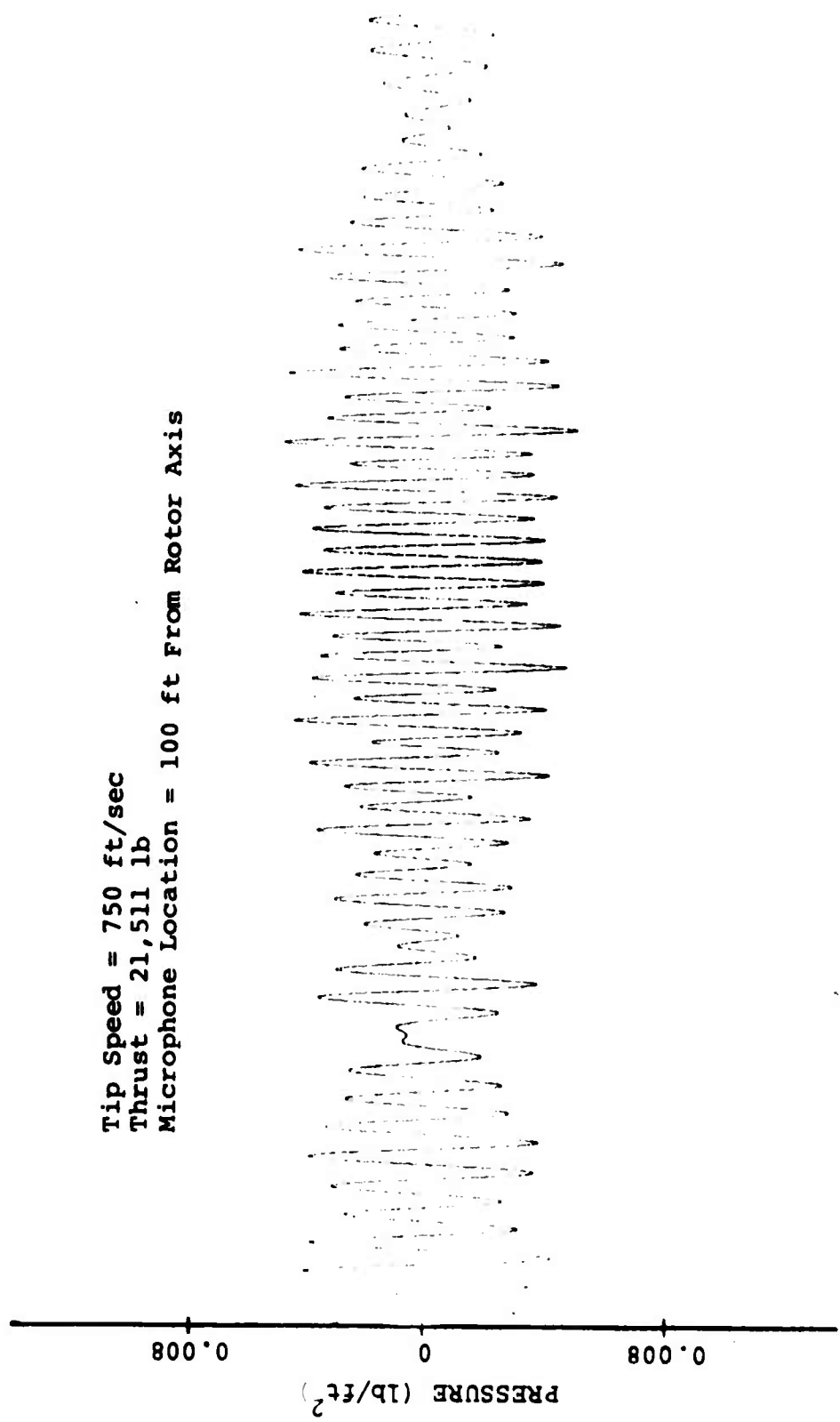


Figure 6. Pressure Time History of Predicted Noise Generated From a 1-Ft-Wide Station Centered at 15 Ft Radius Which Oscillates at 422 Hz With a Pressure of 1 lb/ft².

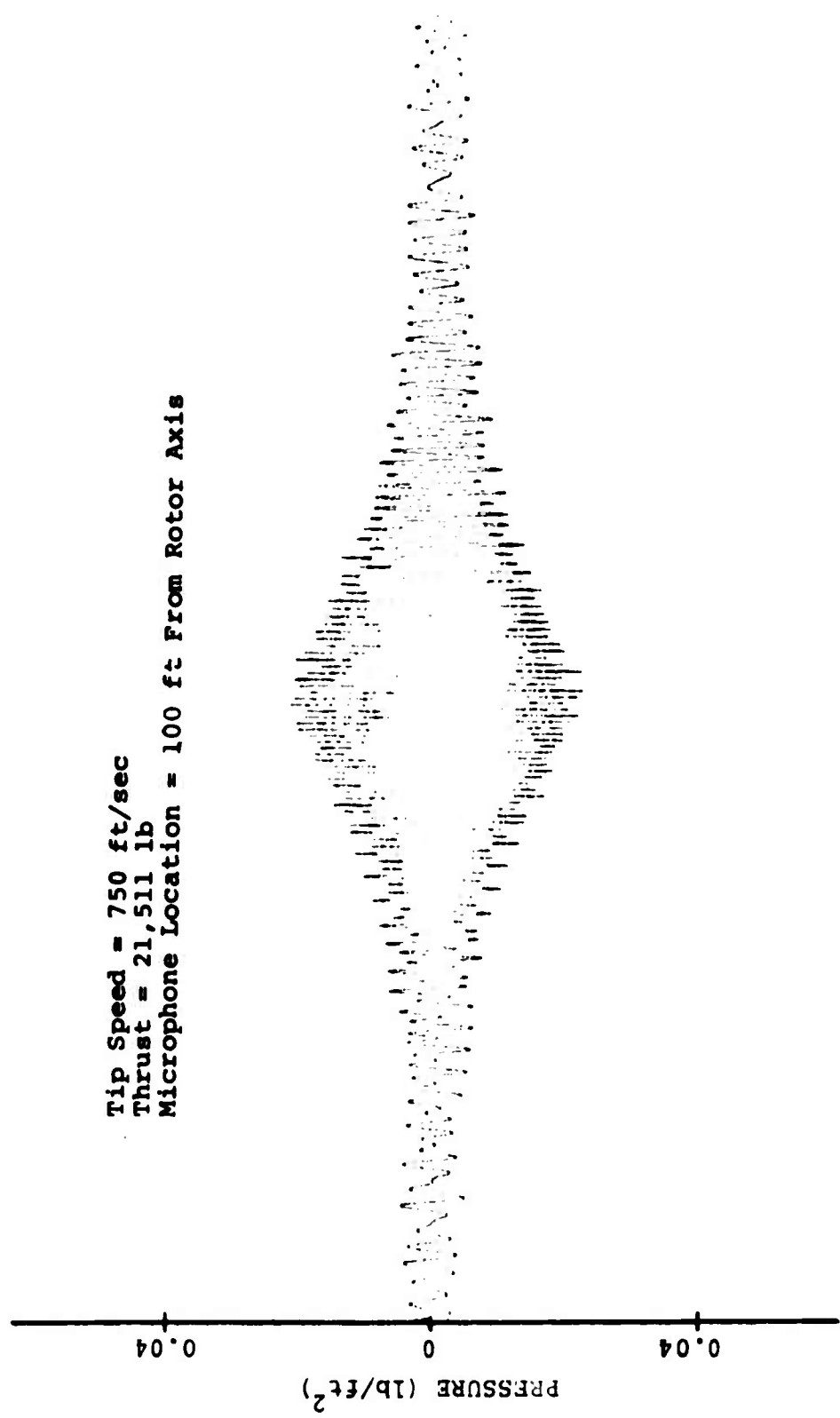


Figure 7. Pressure Time History of Predicted Noise Generated From a 1-Ft-Wide Station Centered at 29.5 Ft Radius Which Oscillates at 827 Hz With a Pressure of 1 lb/Ft².

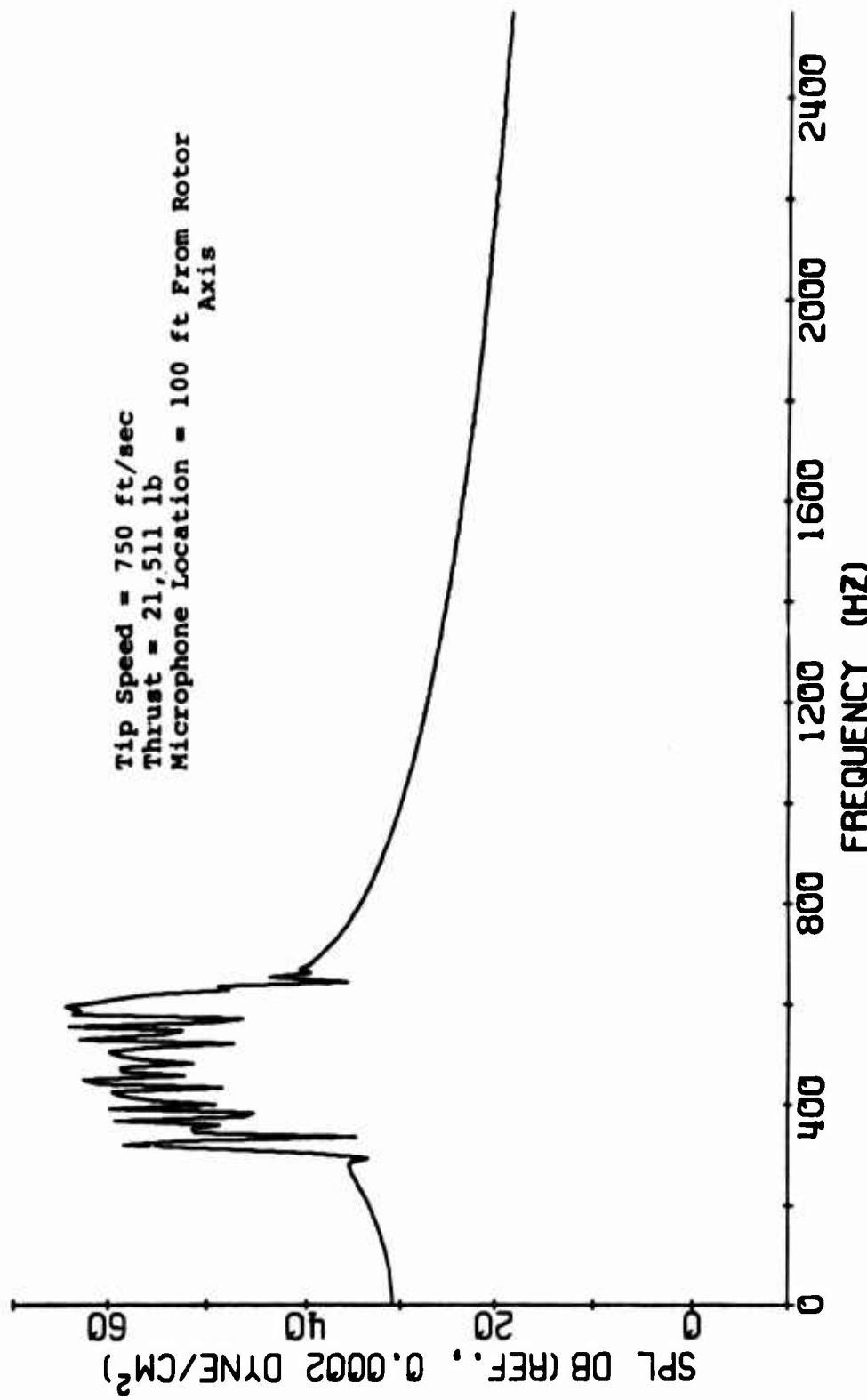


Figure 8. Spectrum of Predicted Noise Generated From a 1-Ft-Wide Station Centered at 15 ft Radius Which Oscillates at 422 Hz With a Pressure of 1 lb/ft² (Reference Figure 6).

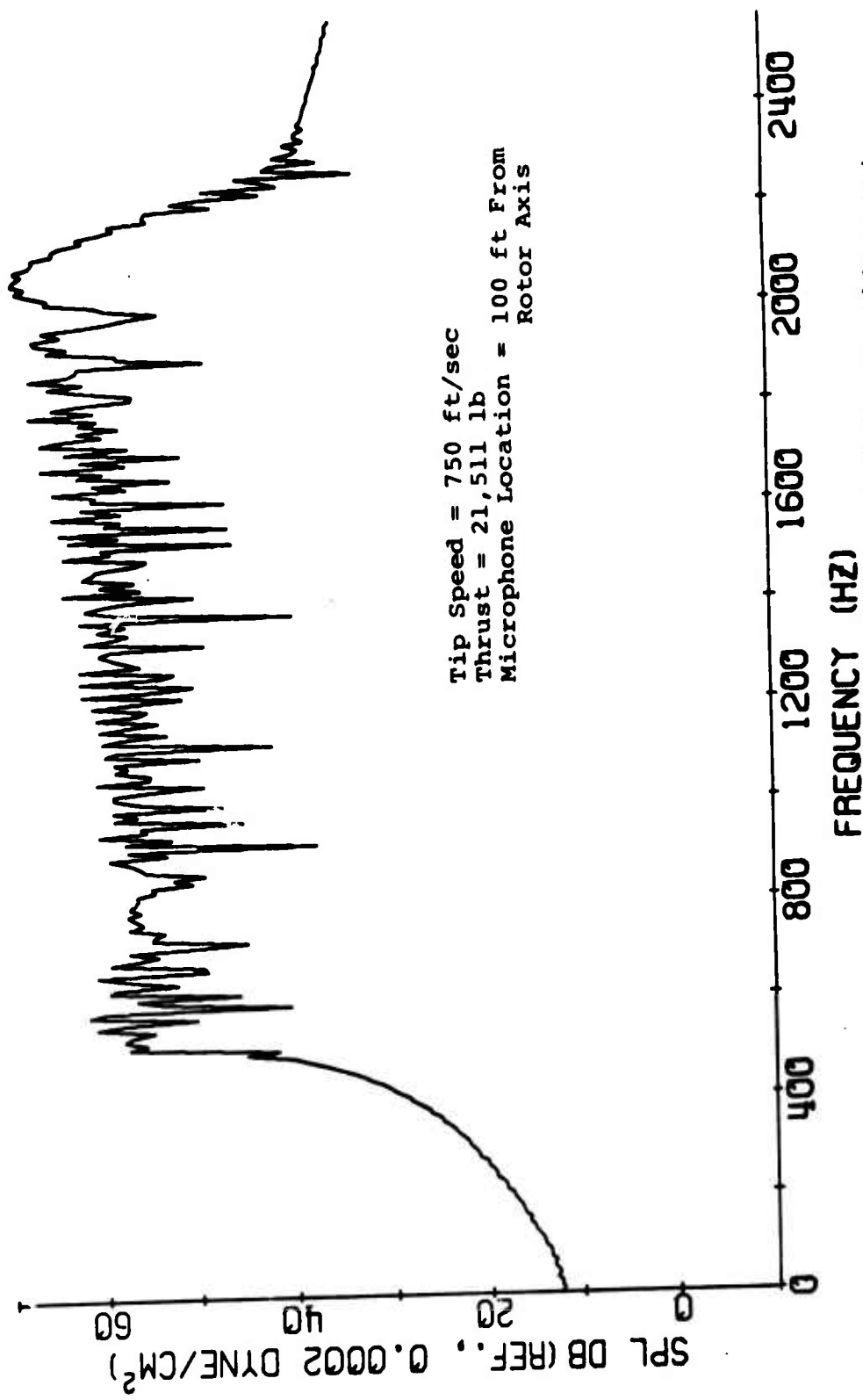


Figure 9. Spectrum of predicted noise generated from a 1-ft-wide station centered at 29.5 ft radius which oscillates at 827 Hz with a pressure of 1 lb/ft² (Reference Figure 7).

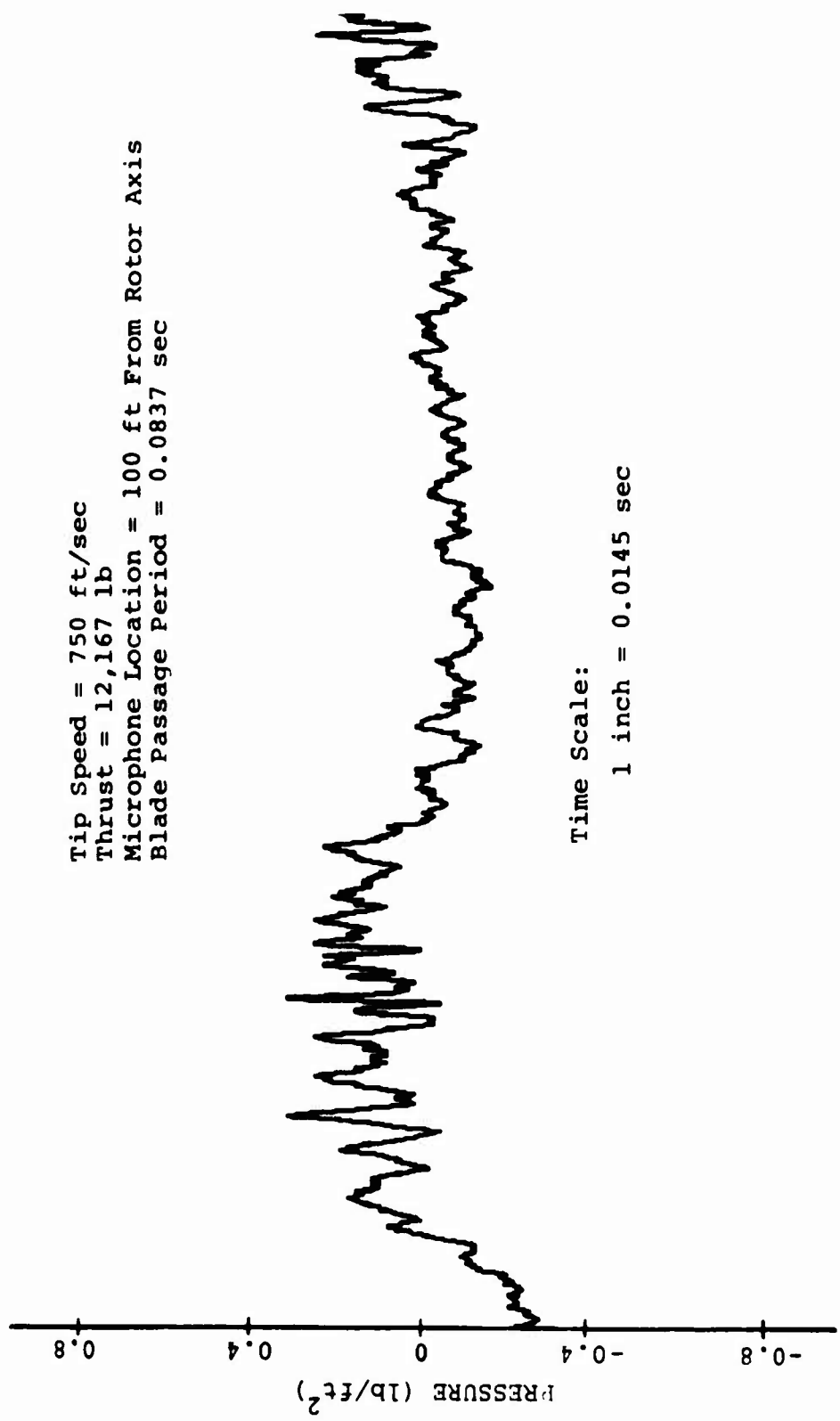


Figure 10. Pressure Time History of Recorded Noise Generated From CH-47B Rotor on a Whirl Tower.

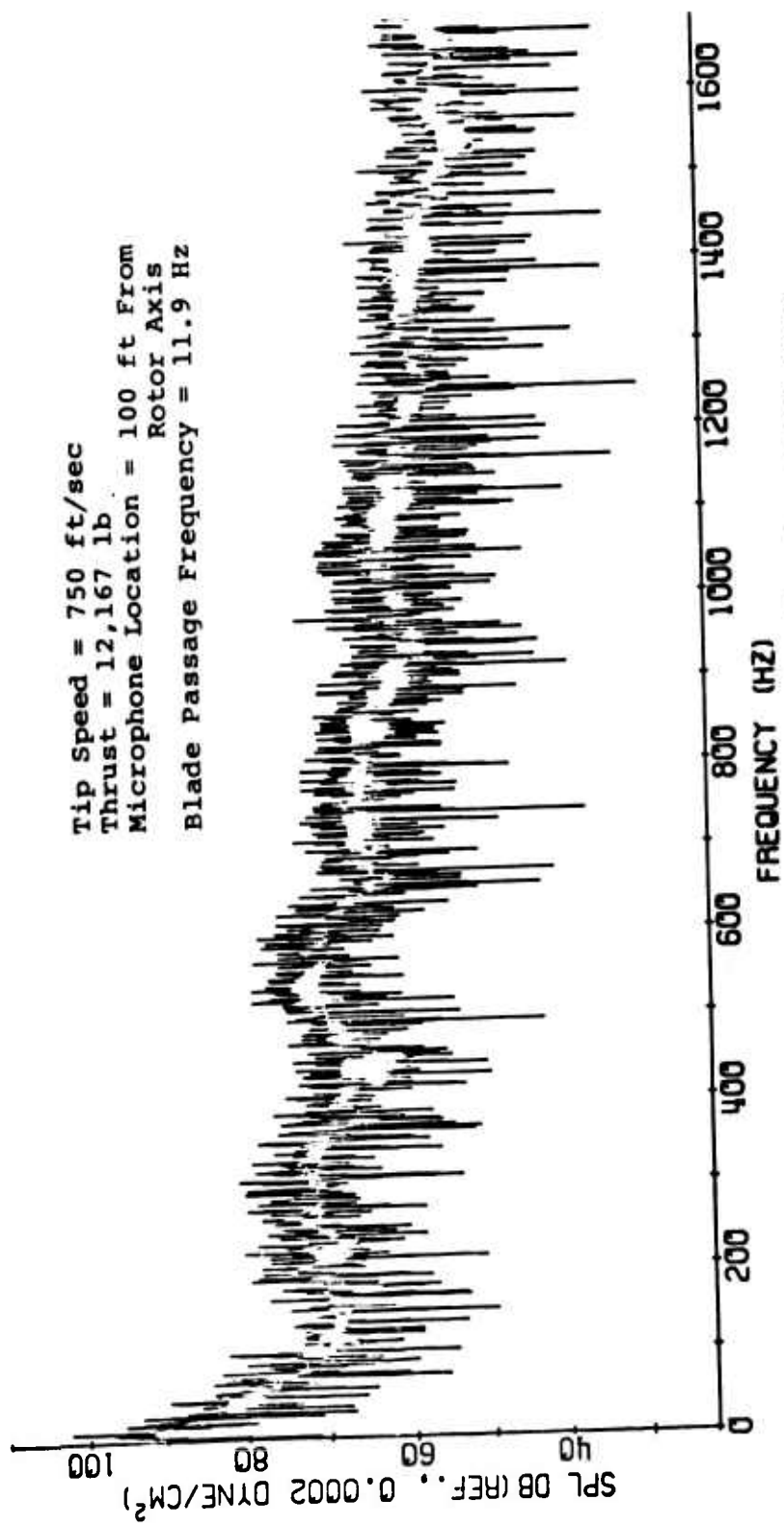


Figure 11. Spectrum of Recorded Noise Generated From CH-47B Rotor on a Whirl Tower (Referenced Figure 10).

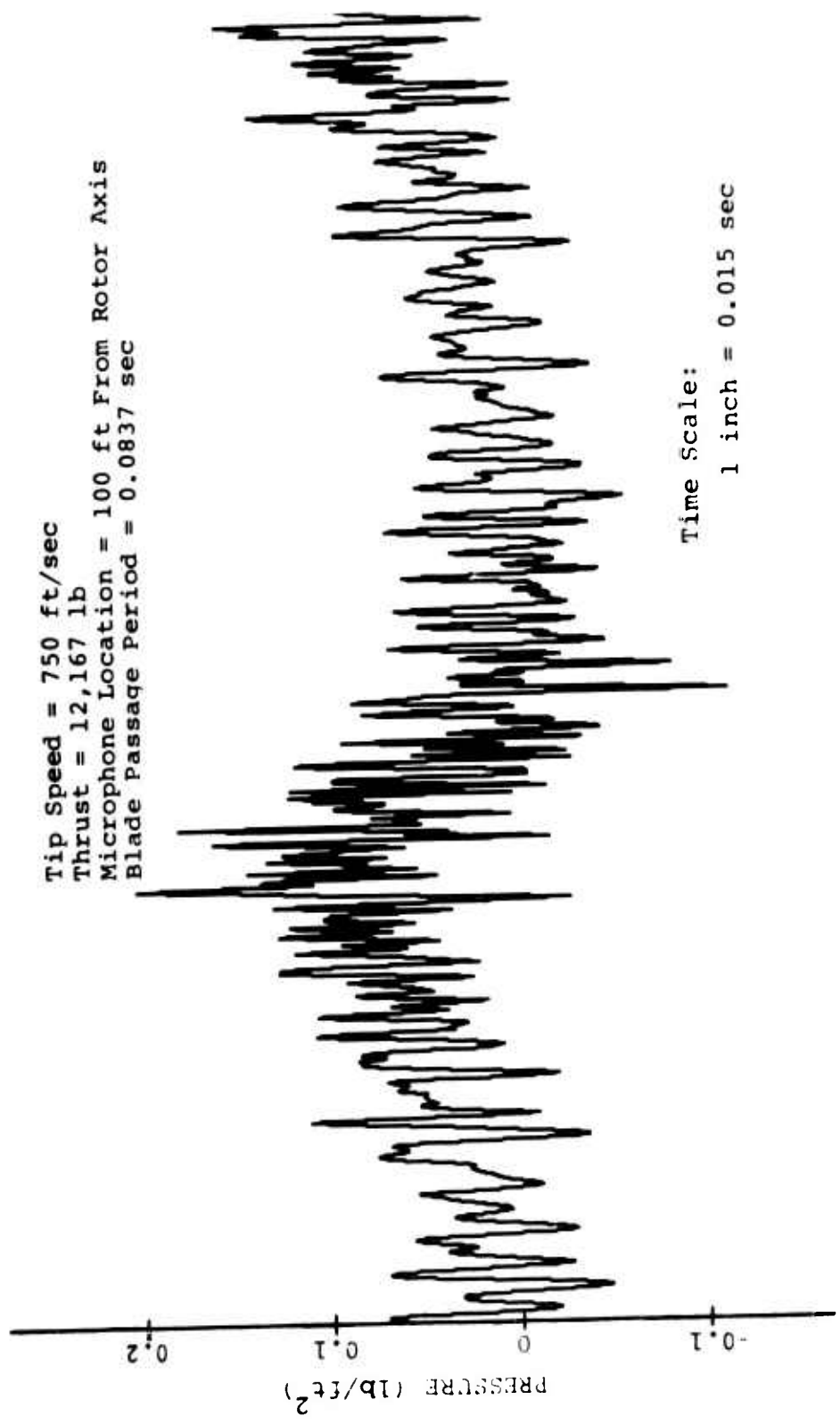


Figure 12. Pressure Time History of Predicted Noise Generated From CH-47B Rotor on a Whirl Tower.

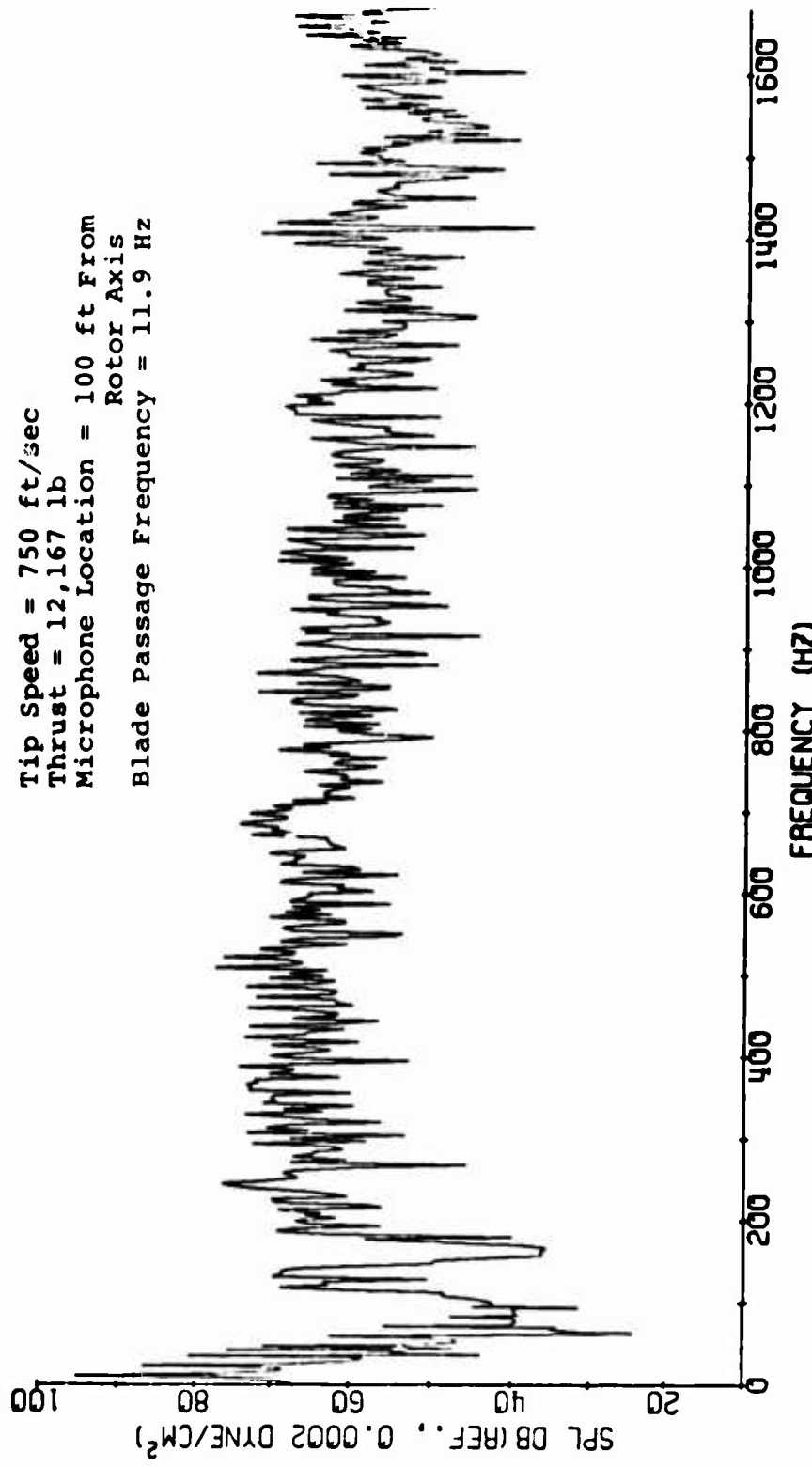


Figure 13. Spectrum of Predicted Noise Generated From
 CH-47B Rotor on a Whirl Tower (Reference
 Figure 12).

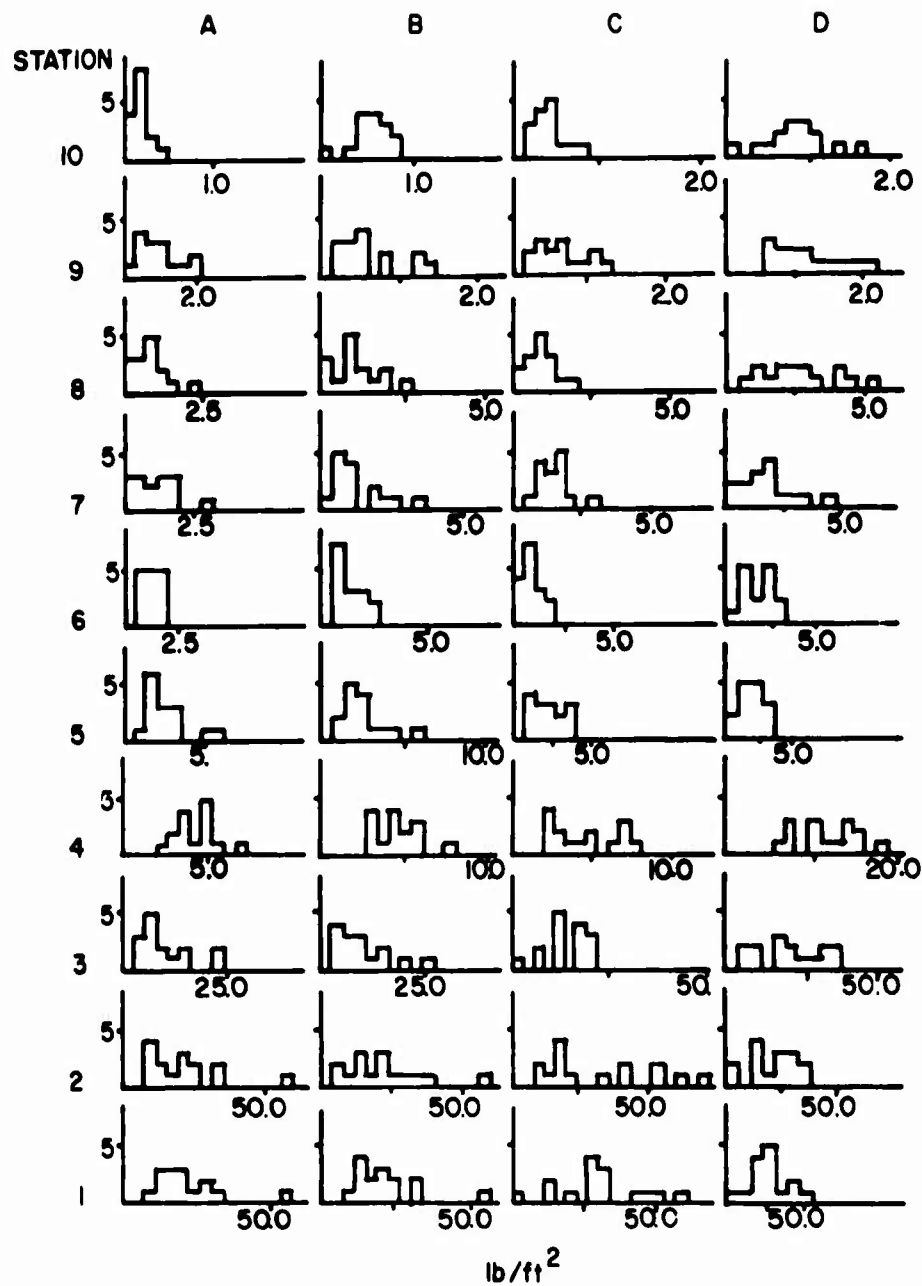


Figure 14. Distribution of the Magnitude of Oscillatory Lift Over Ten Radial Stations for Four Cases.

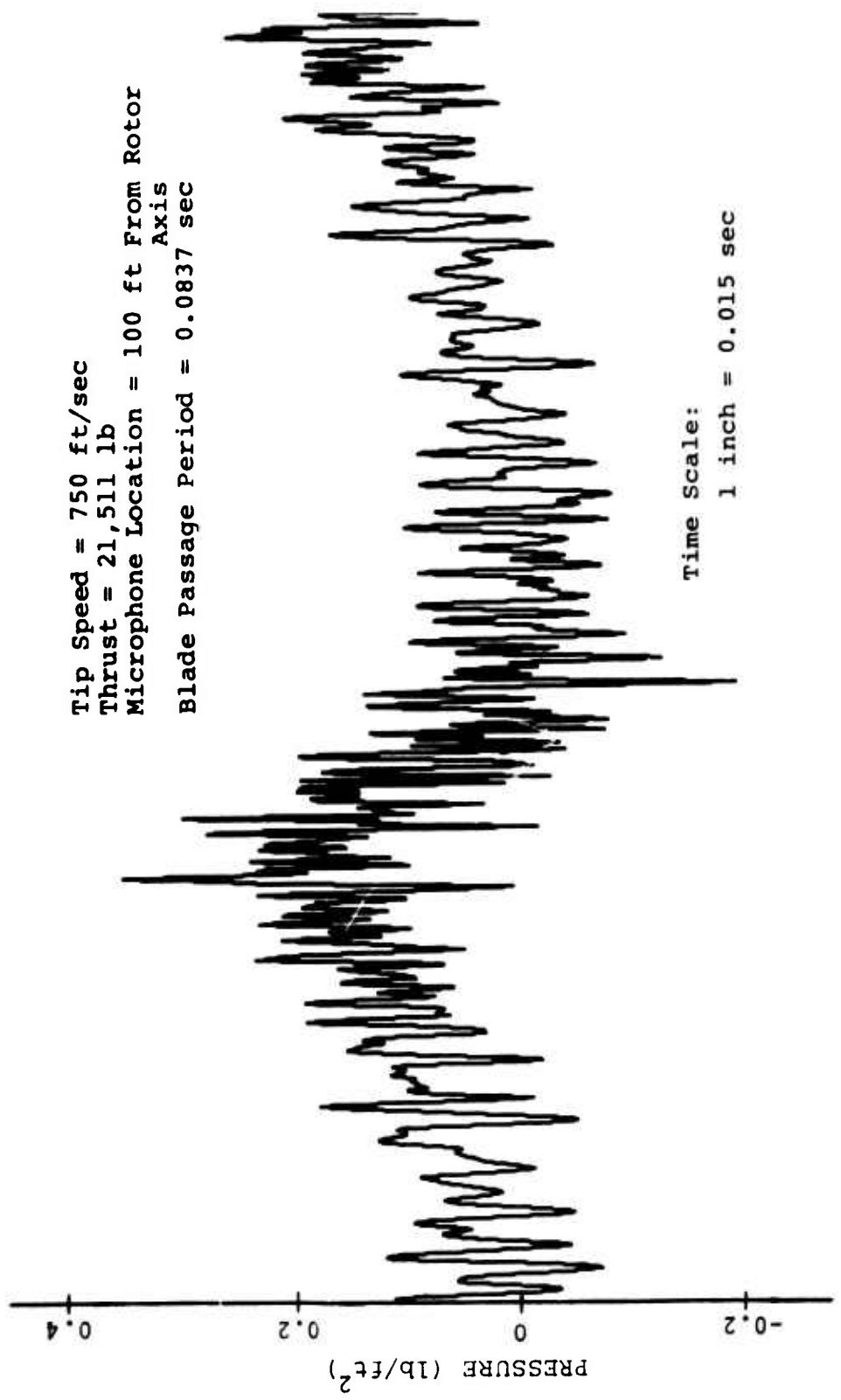


Figure 15. Pressure Time History of Predicted Noise Generated From CH-47B Rotor on a Whirl Tower.

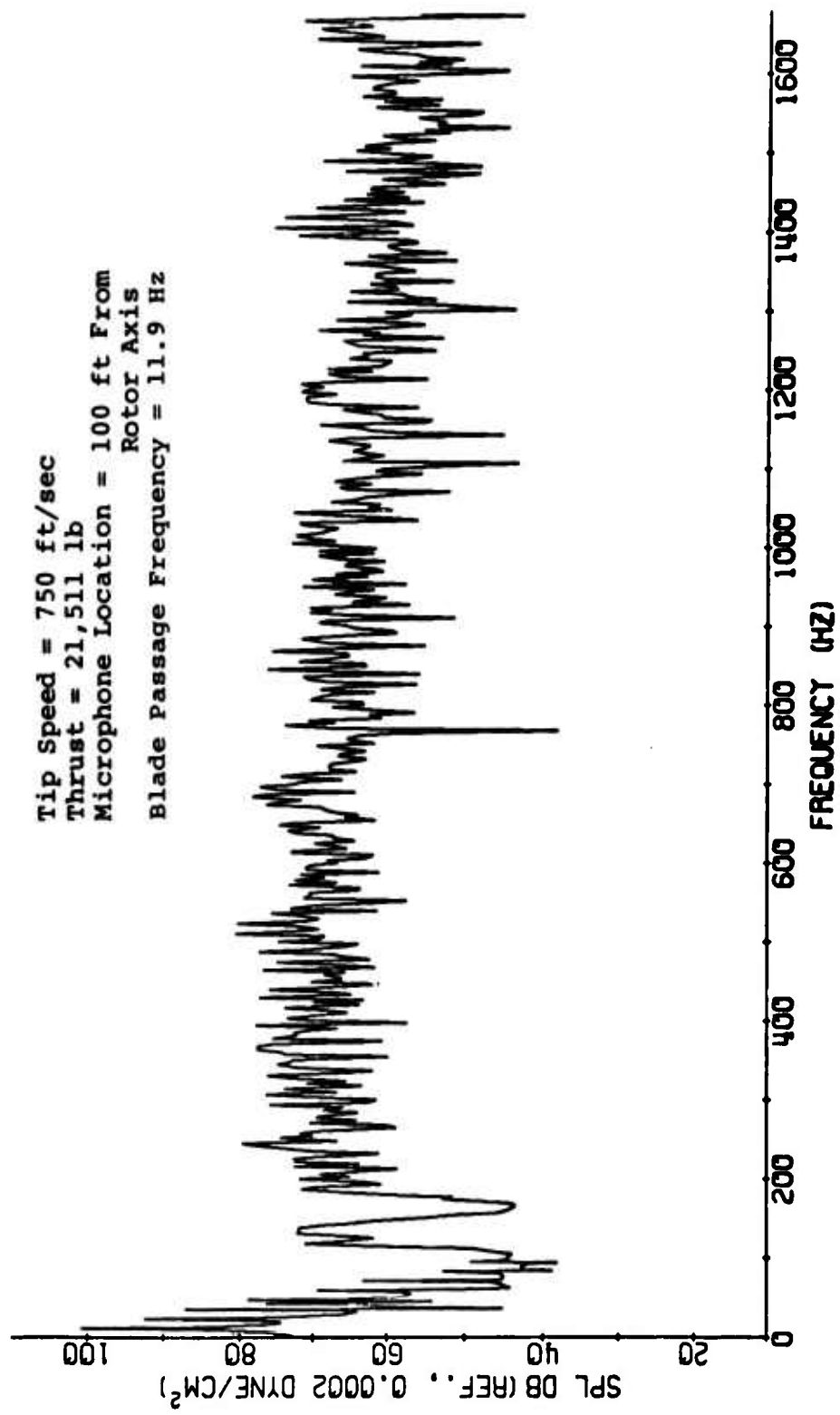


Figure 16. Spectrum of Predicted Noise Generated From CH-47B Rotor on a Whirl Tower (Reference Figure 15).

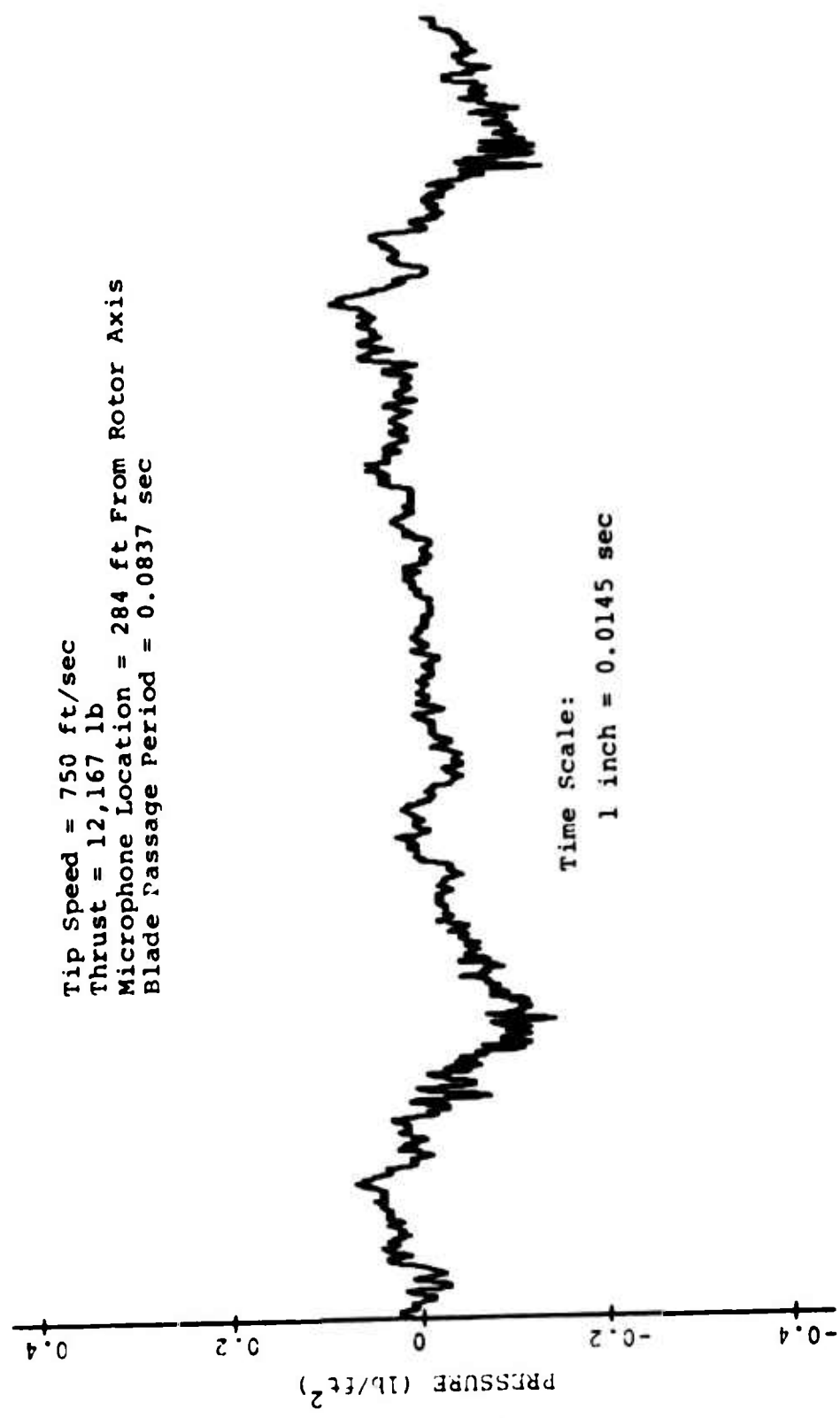


Figure 17. Pressure Time History of Recorded Noise Generated From CH-47B Rotor on a Whirl Tower.

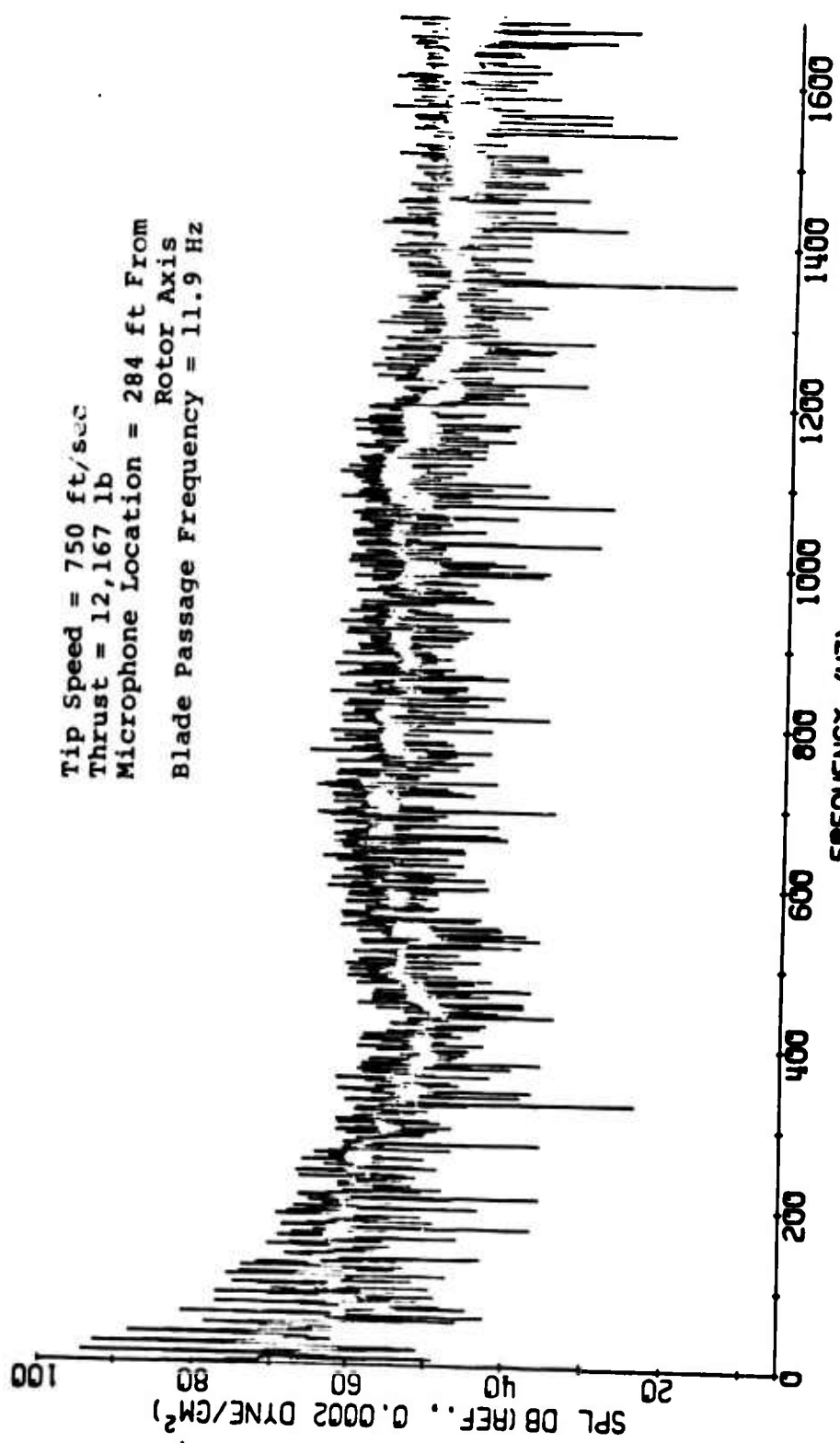


Figure 18. Spectrum of Recorded Noise Generated From CH-47B Rotor on a Whirl Tower (Reference Figure 17).

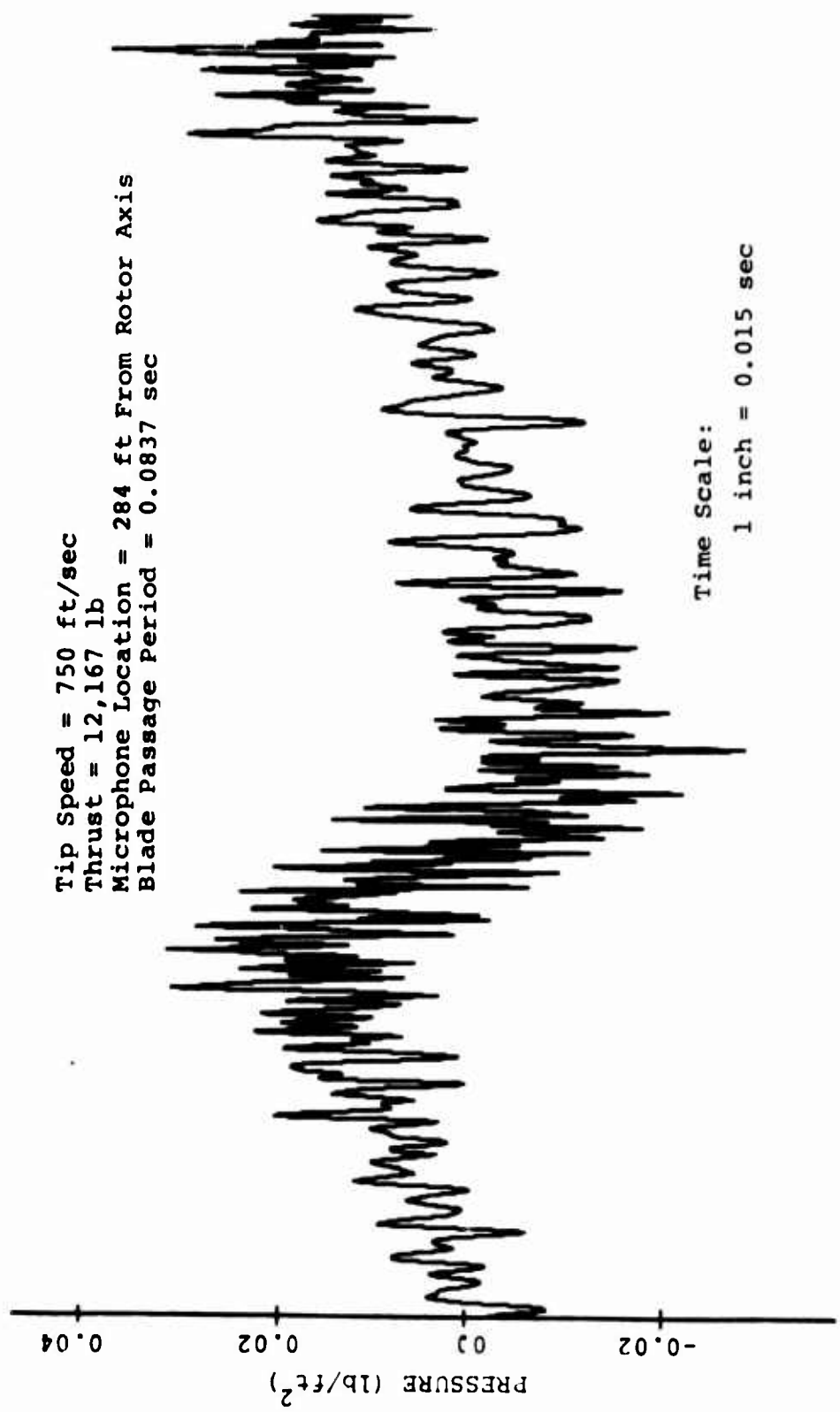


Figure 19. Pressure Time History of Predicted Noise Generated From CH-47B Rotor on a Whirl Tower.

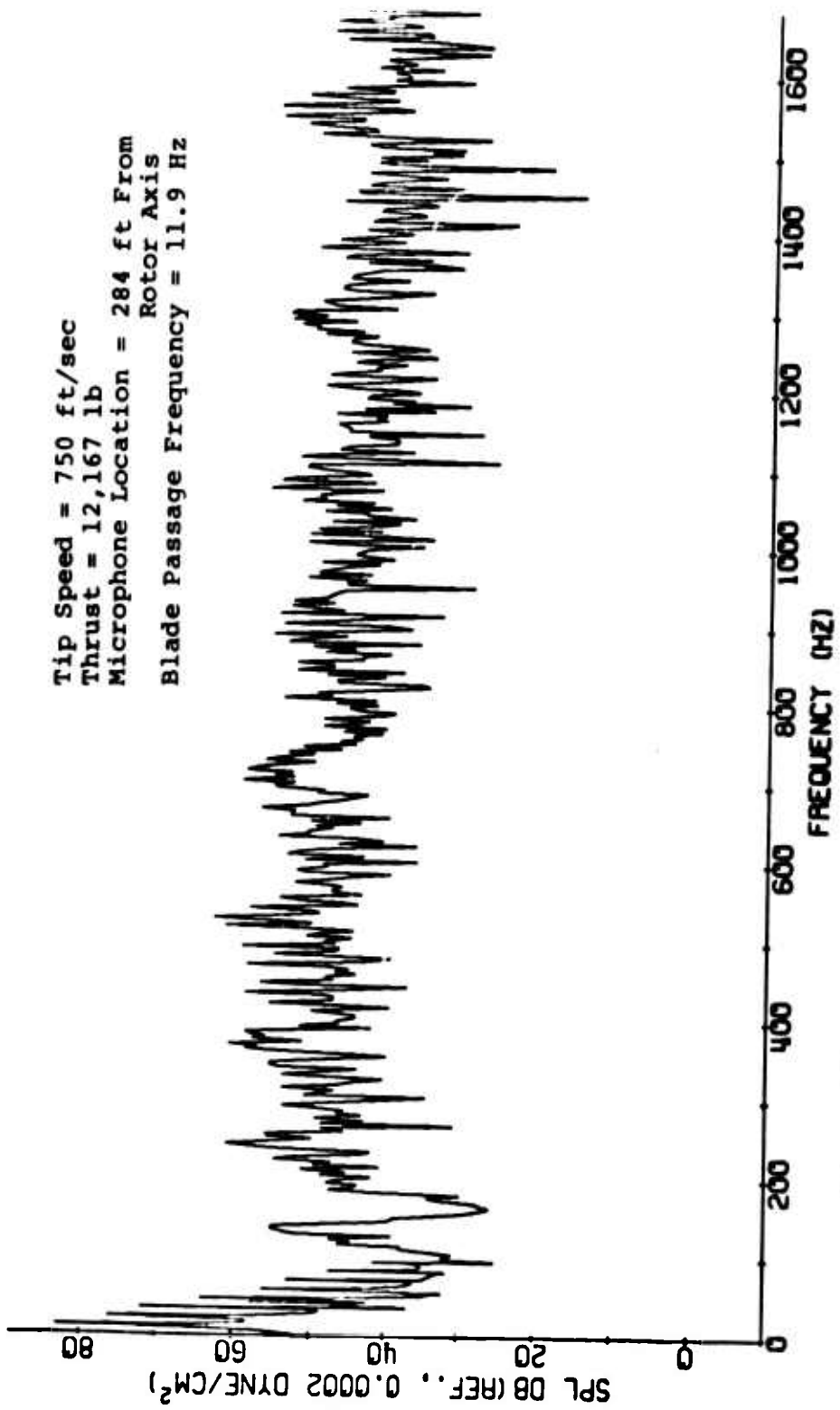


Figure 20. Spectrum of Predicted Noise Generated From
 CH-47B Rotor on a Whirl Tower (Reference
 Figure 19).

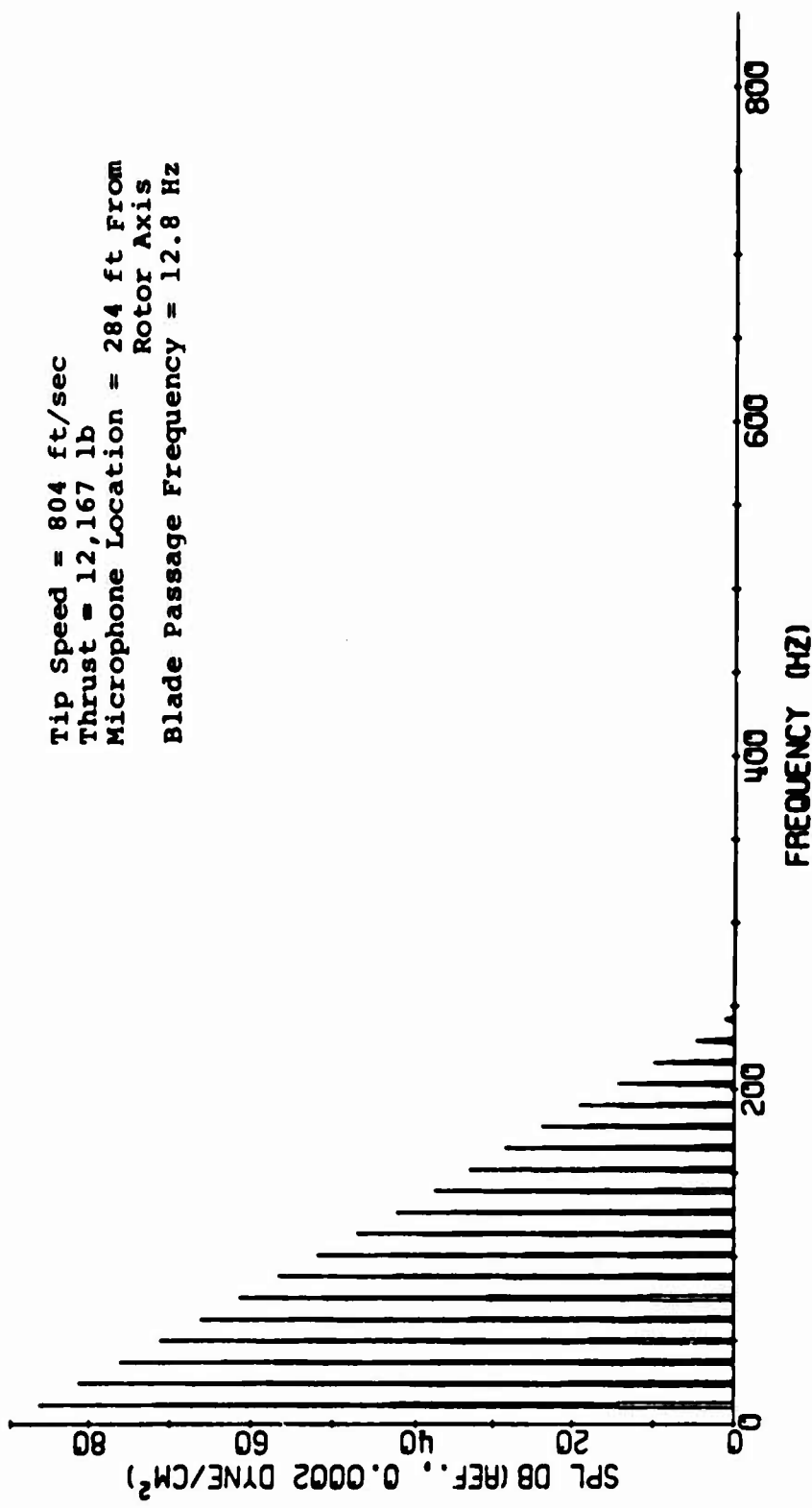


Figure 21. Spectrum of Predicted Rotational Noise Generated From CH-47B Rotor on a Whirl Tower.

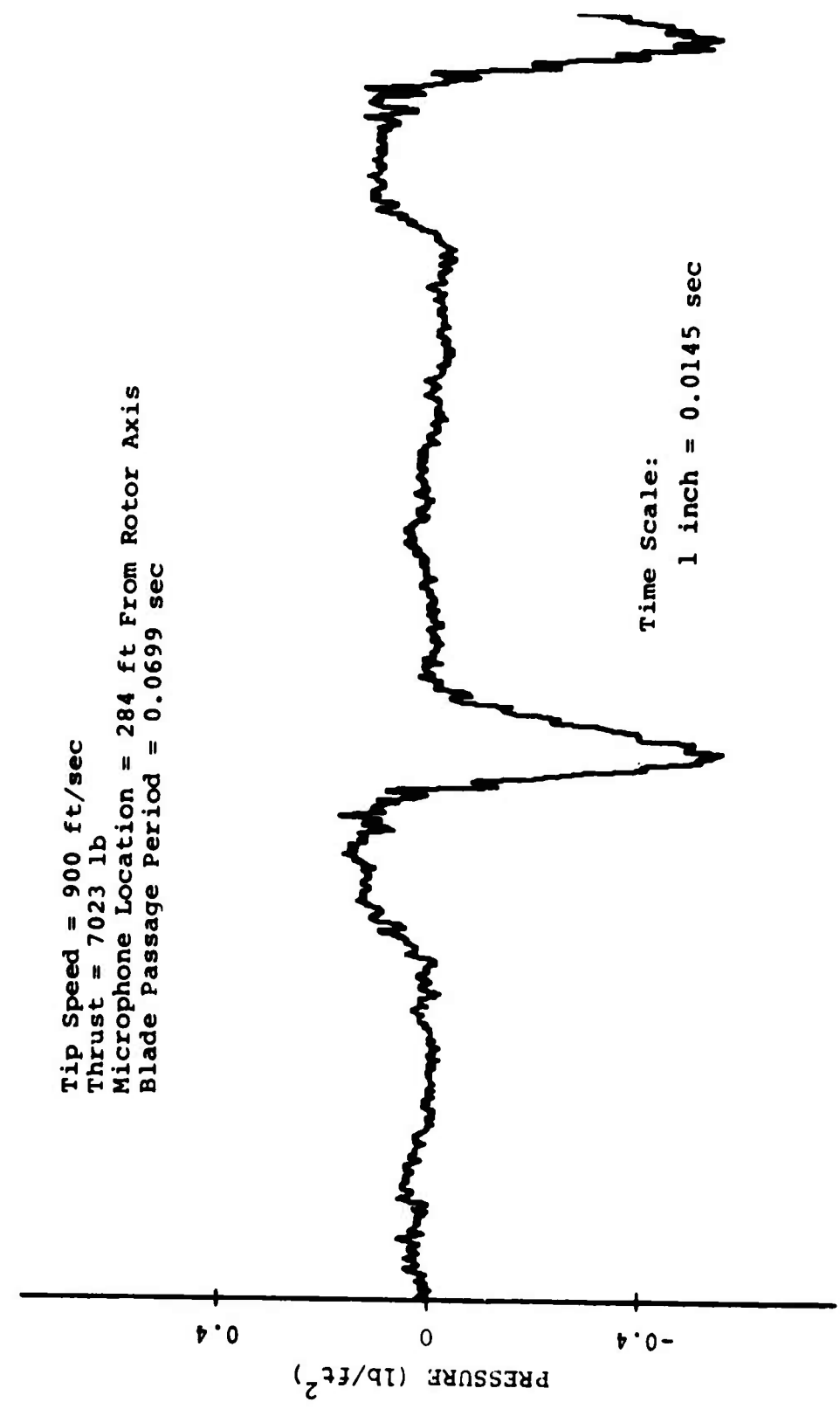


Figure 22. Pressure Time History of Recorded Noise Generated From CH-47B Rotor on a Whirl Tower.

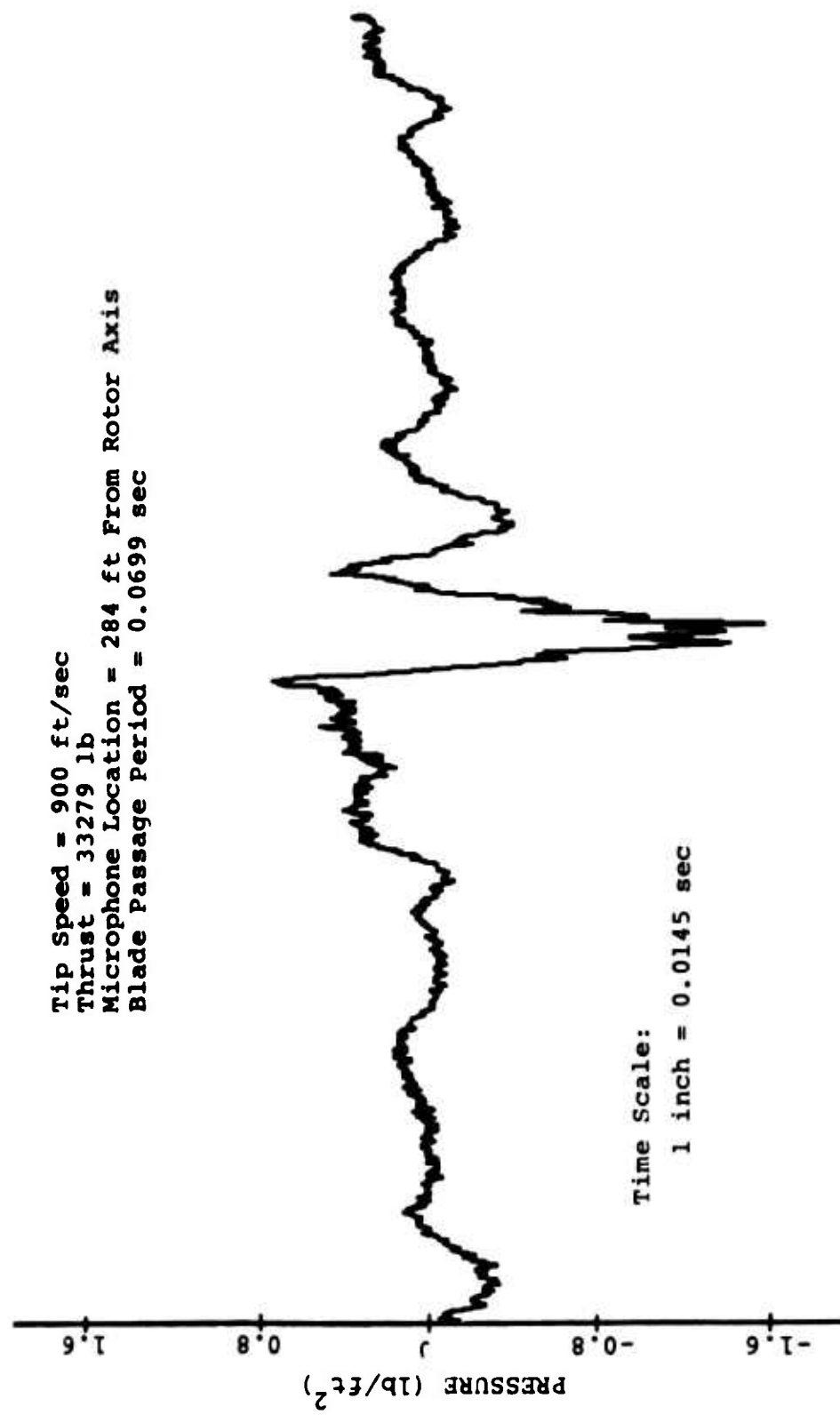


Figure 23. Pressure Time History of Recorded Noise Generated From CH-47B Rotor on a Whirl Tower.

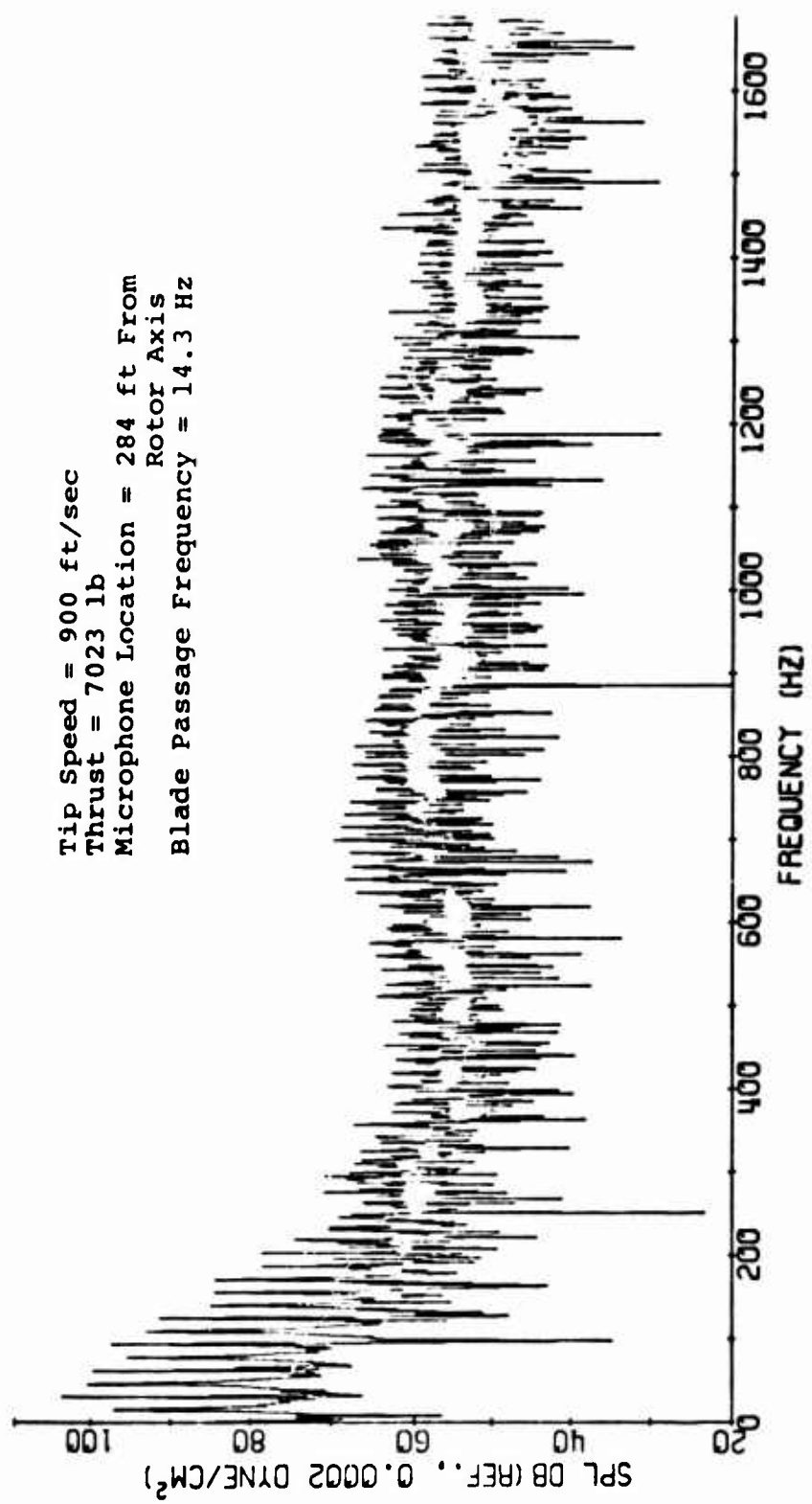


Figure 24. Spectrum of Recorded Noise Generated From CH-47B Rotor on a Whirl Tower (Reference Figure 22).

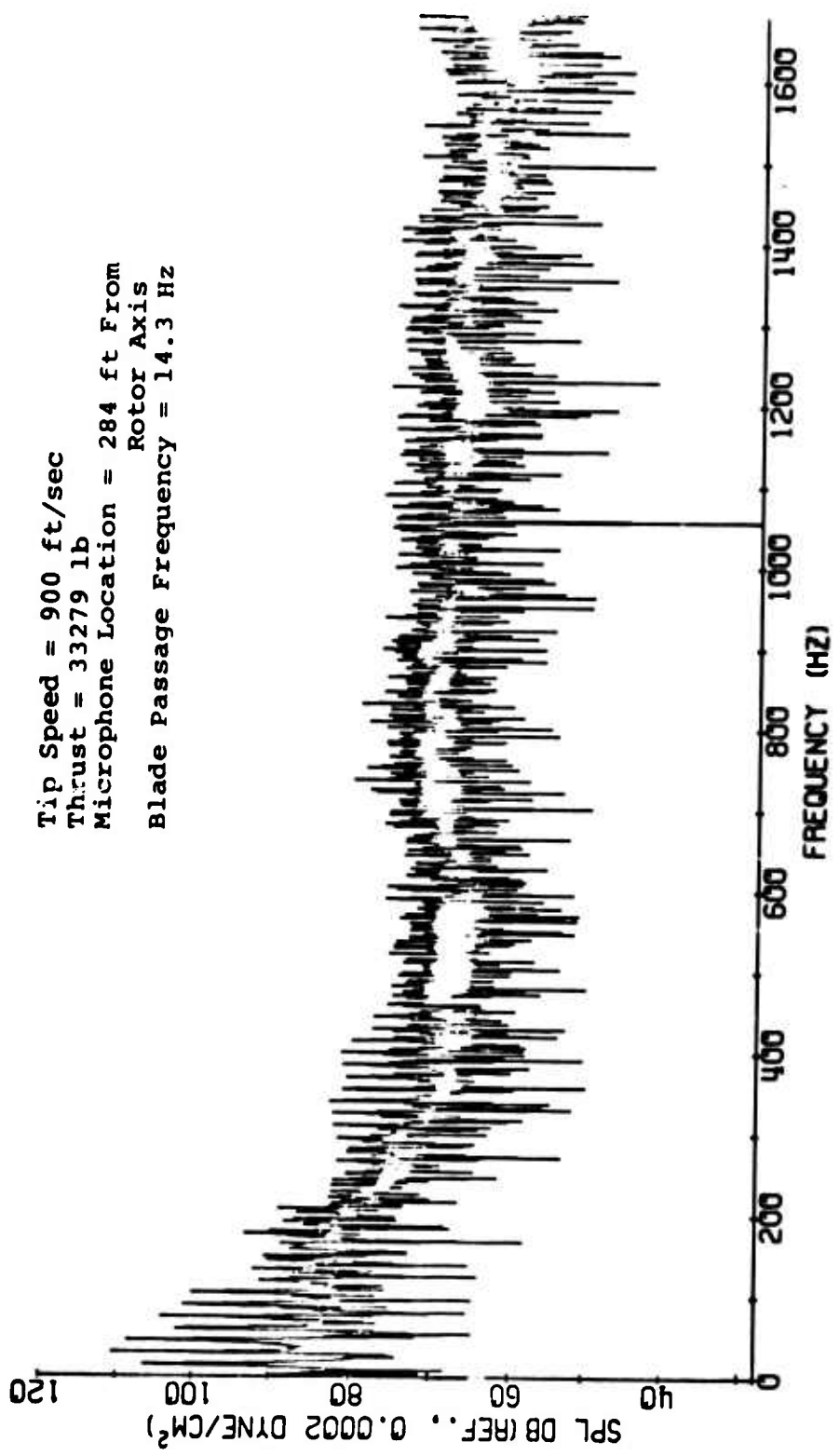


Figure 25. Spectrum of Recorded Noise Generated From
 CH-47B Rotor on a Whirl Tower (Reference
 Figure 23).

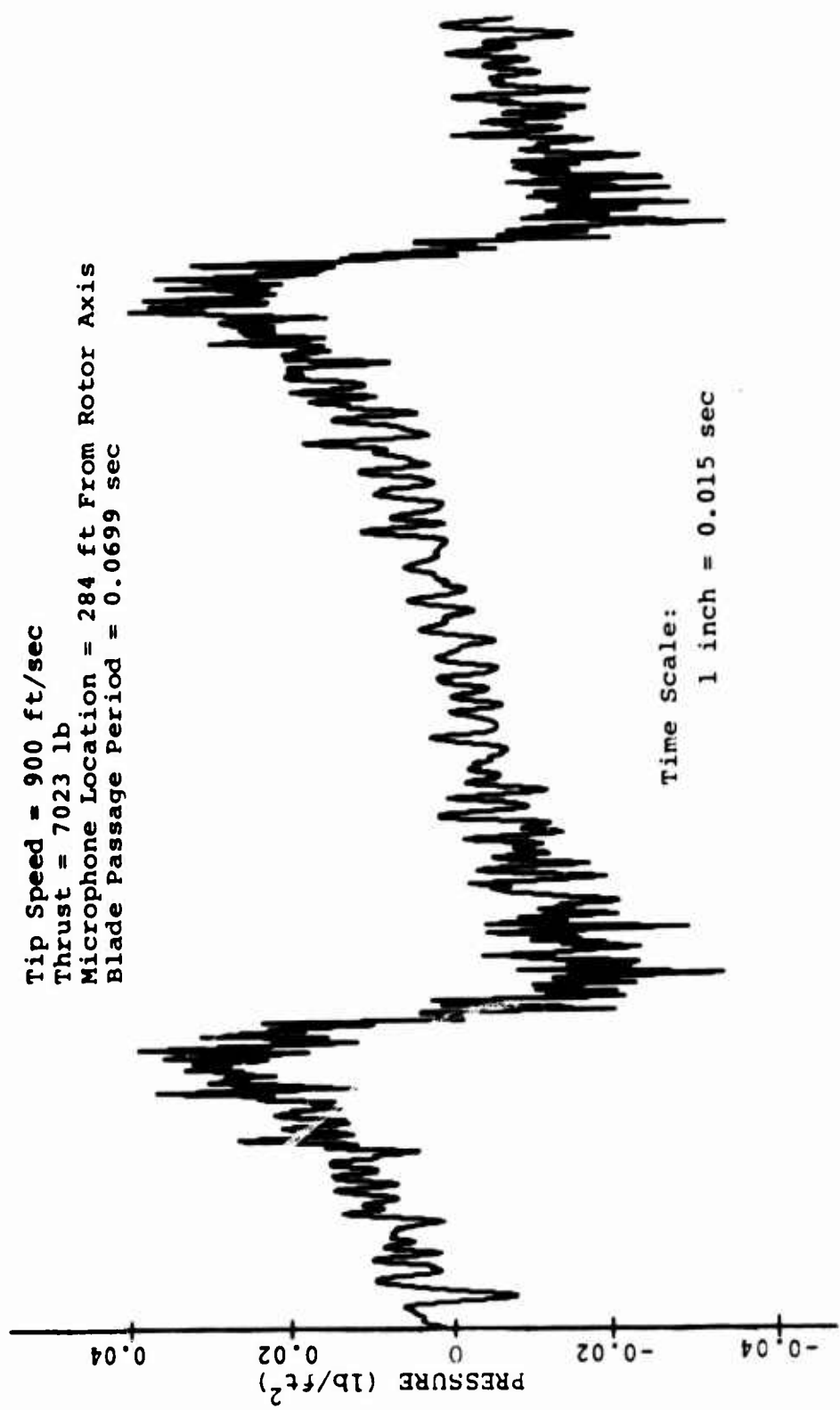


Figure 26. Pressure Time History of Predicted Noise Generated From CH-47B Rotor on a Whirl Tower.

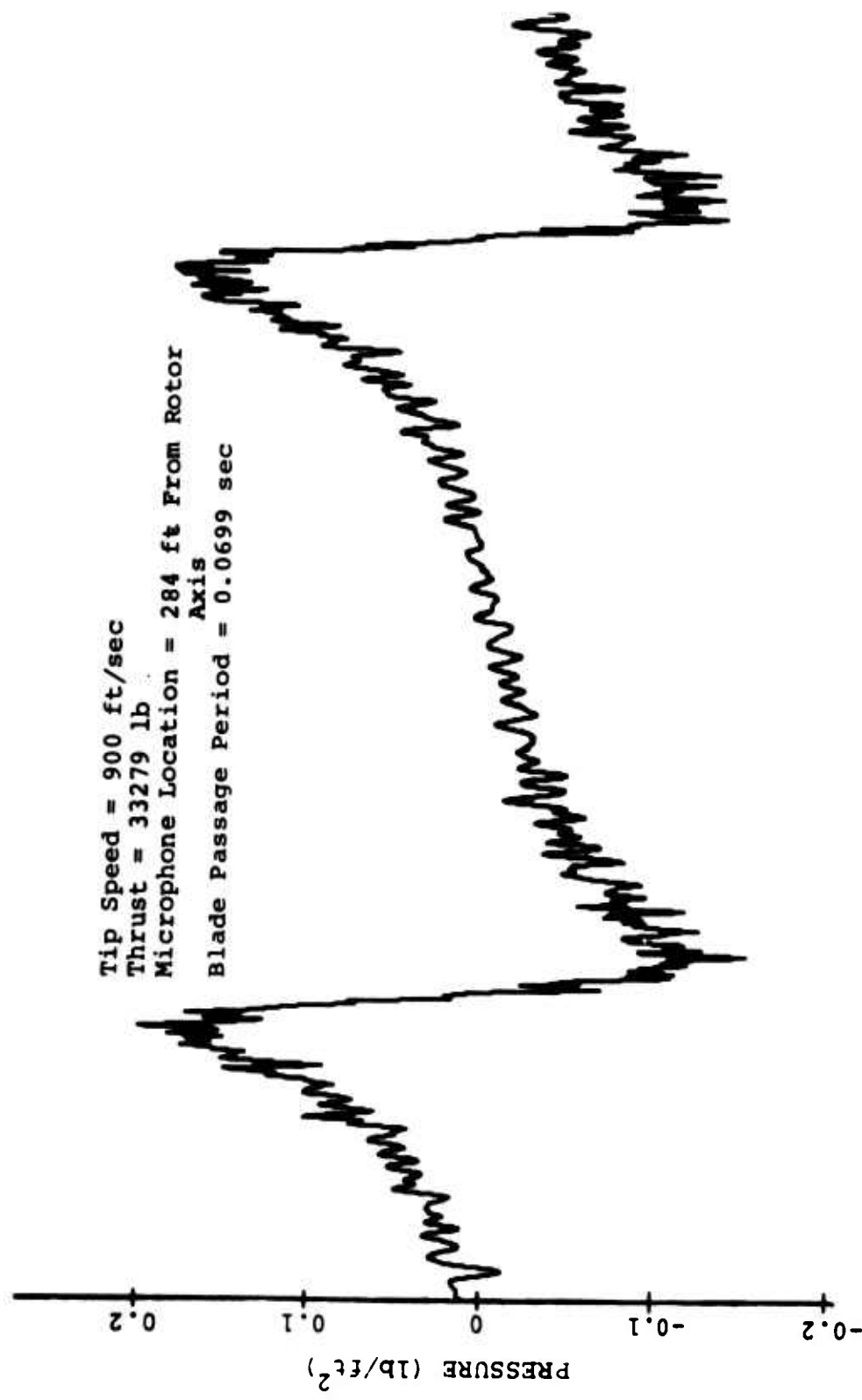


Figure 27. Pressure Time History of Predicted Noise Generated From CH-47B Rotor on a Whirl Tower.

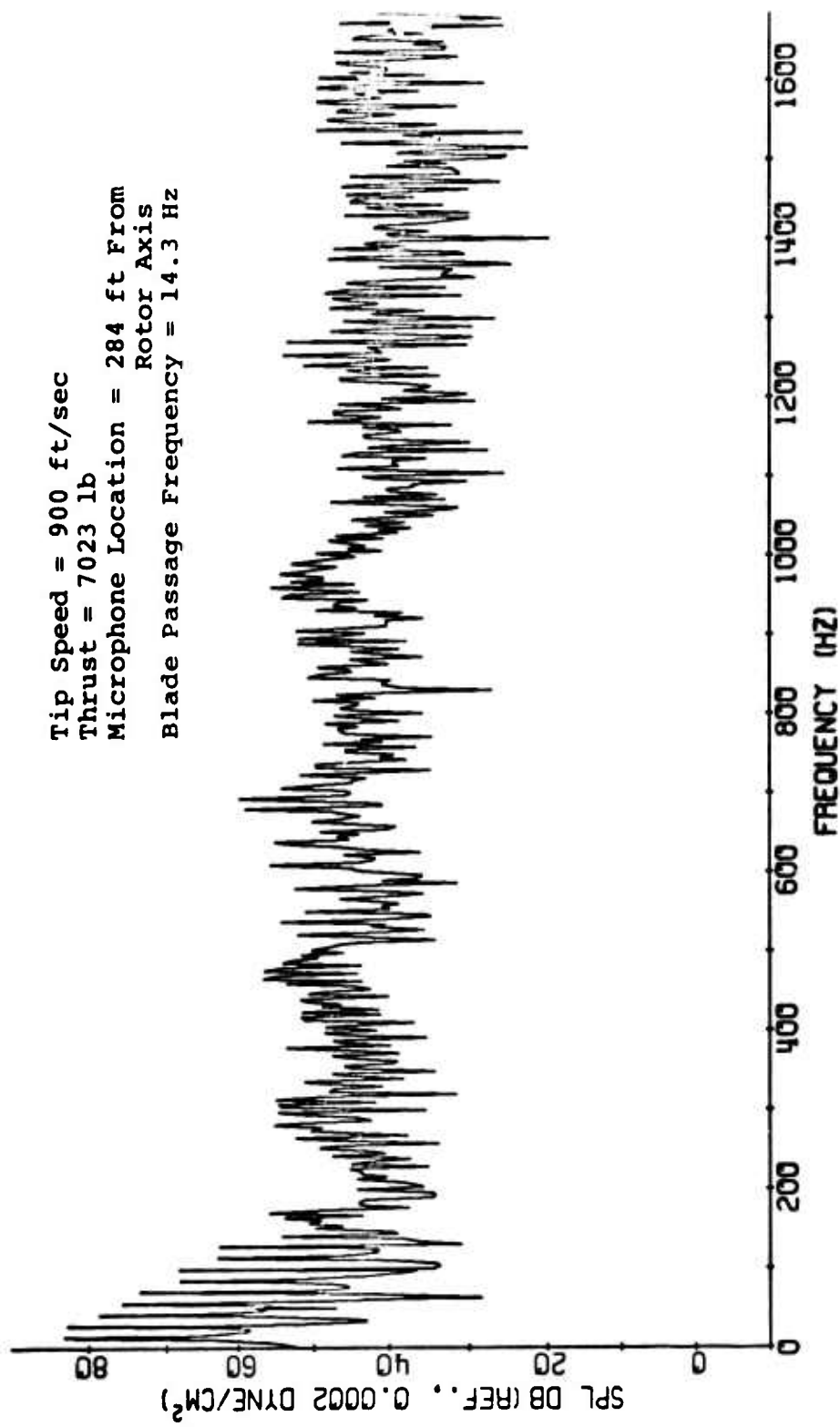


Figure 28. Spectrum of Predicted Noise Generated From
 CH-47B Rotor on a Whirl Tower (Reference
 Figure 26).

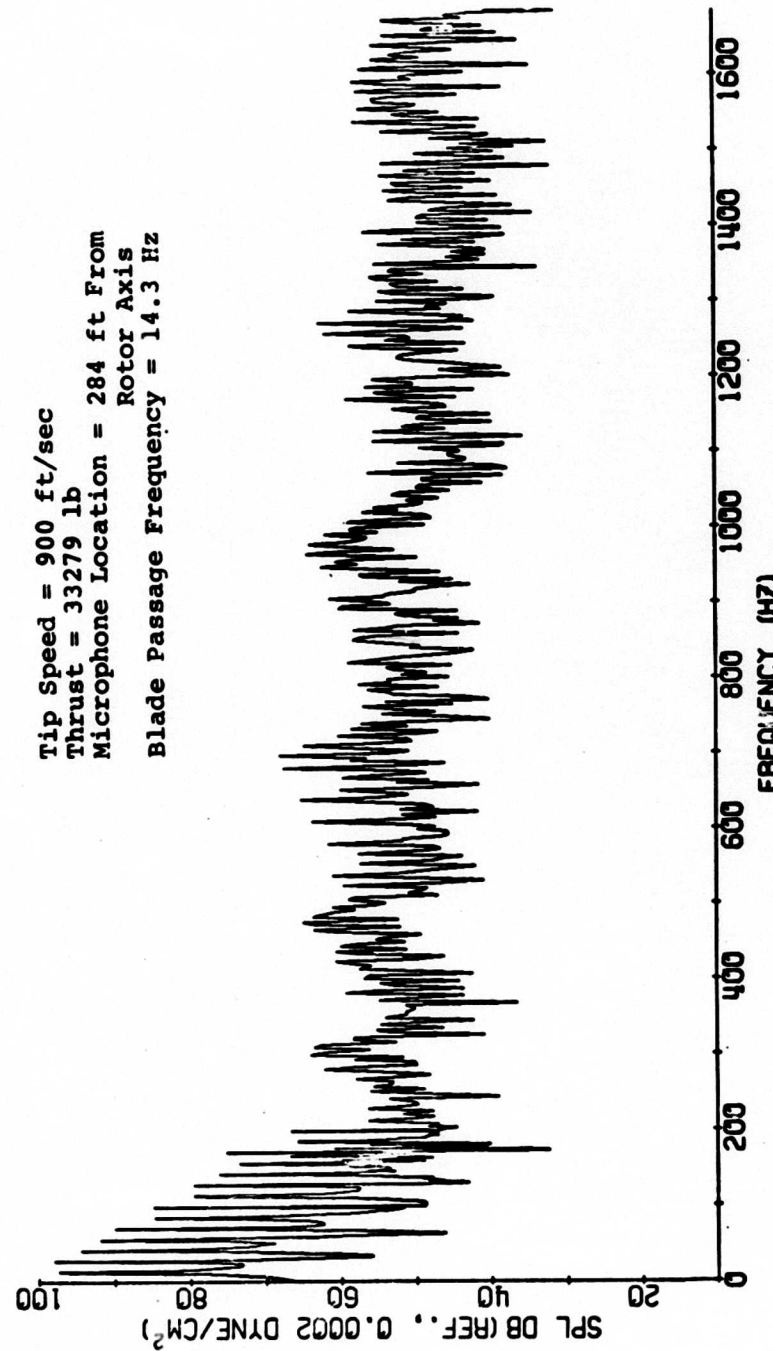


Figure 29. Spectrum of Predicted Noise Generated From
 CH-47B Rotor on a Whirl Tower (Reference
 Figure 27).

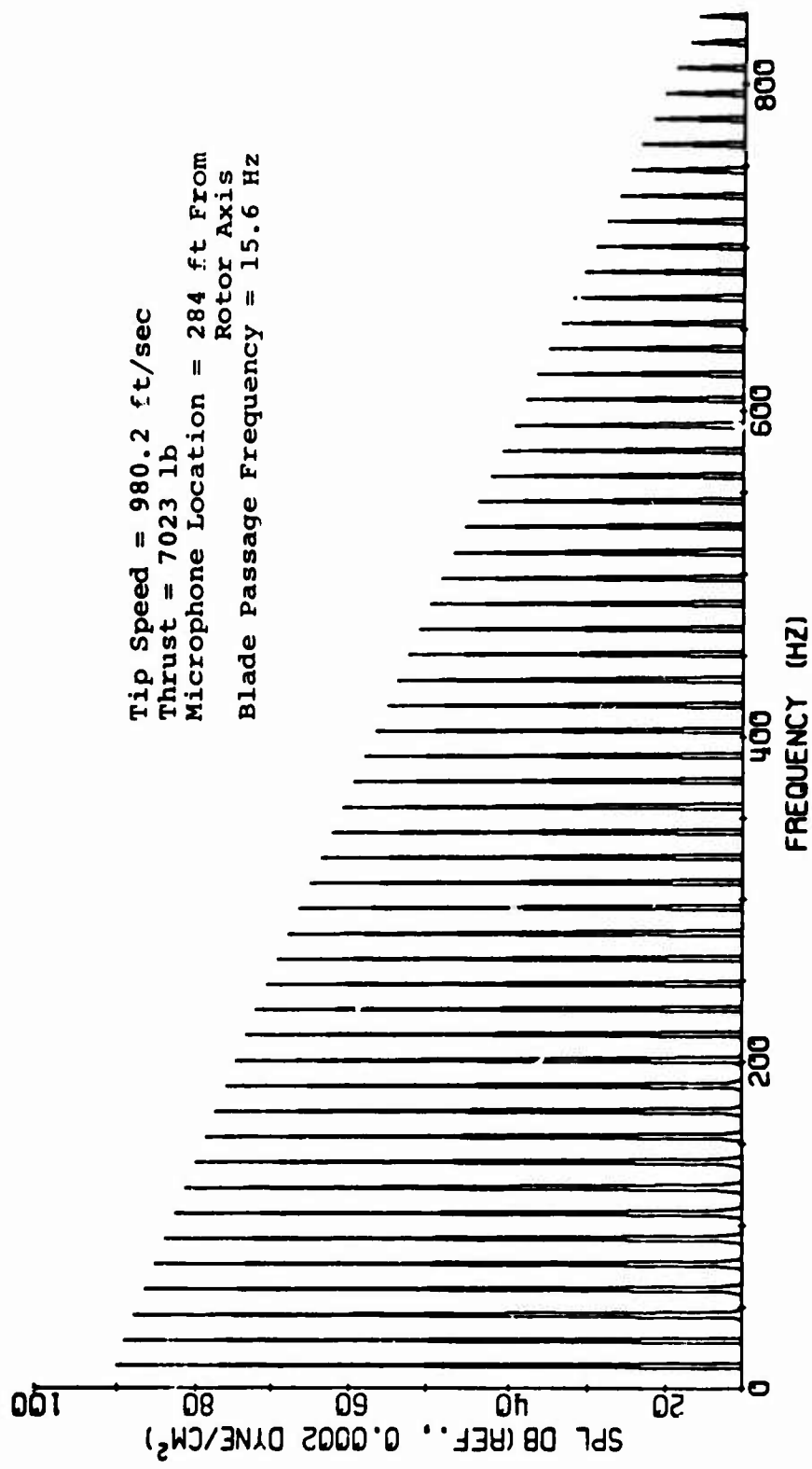


Figure 30. Spectrum of Predicted Rotational Noise Generated
 From CH-47B Rotor on a Whirl Tower.

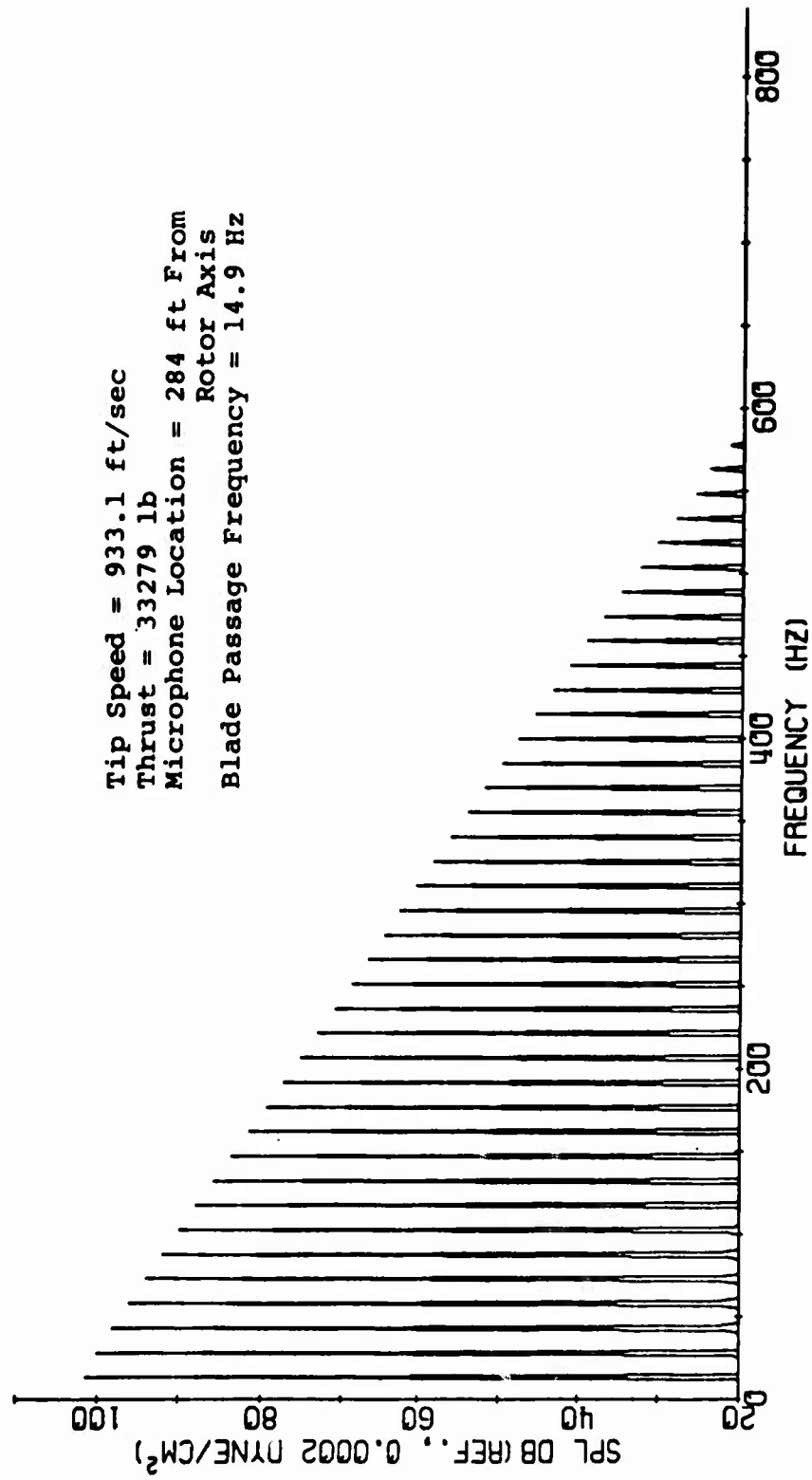
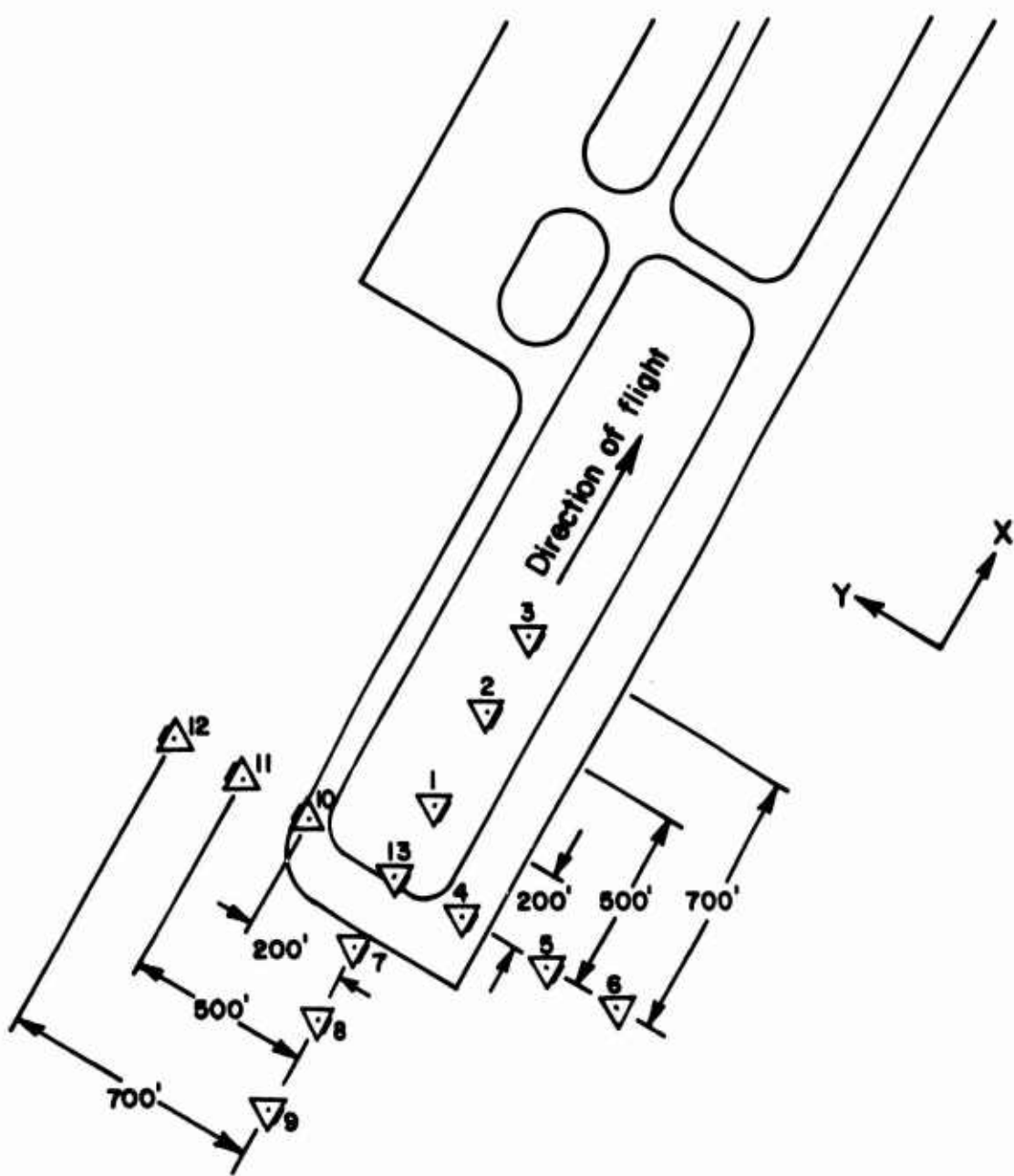


Figure 31. Spectrum of Predicted Rotational Noise Generated
 From CH-47B Rotor on a Whirl Tower.



▲ Microphone location and direction during flyby

Figure 32. Relative Positions of Microphones at Wallops Island Air Station.

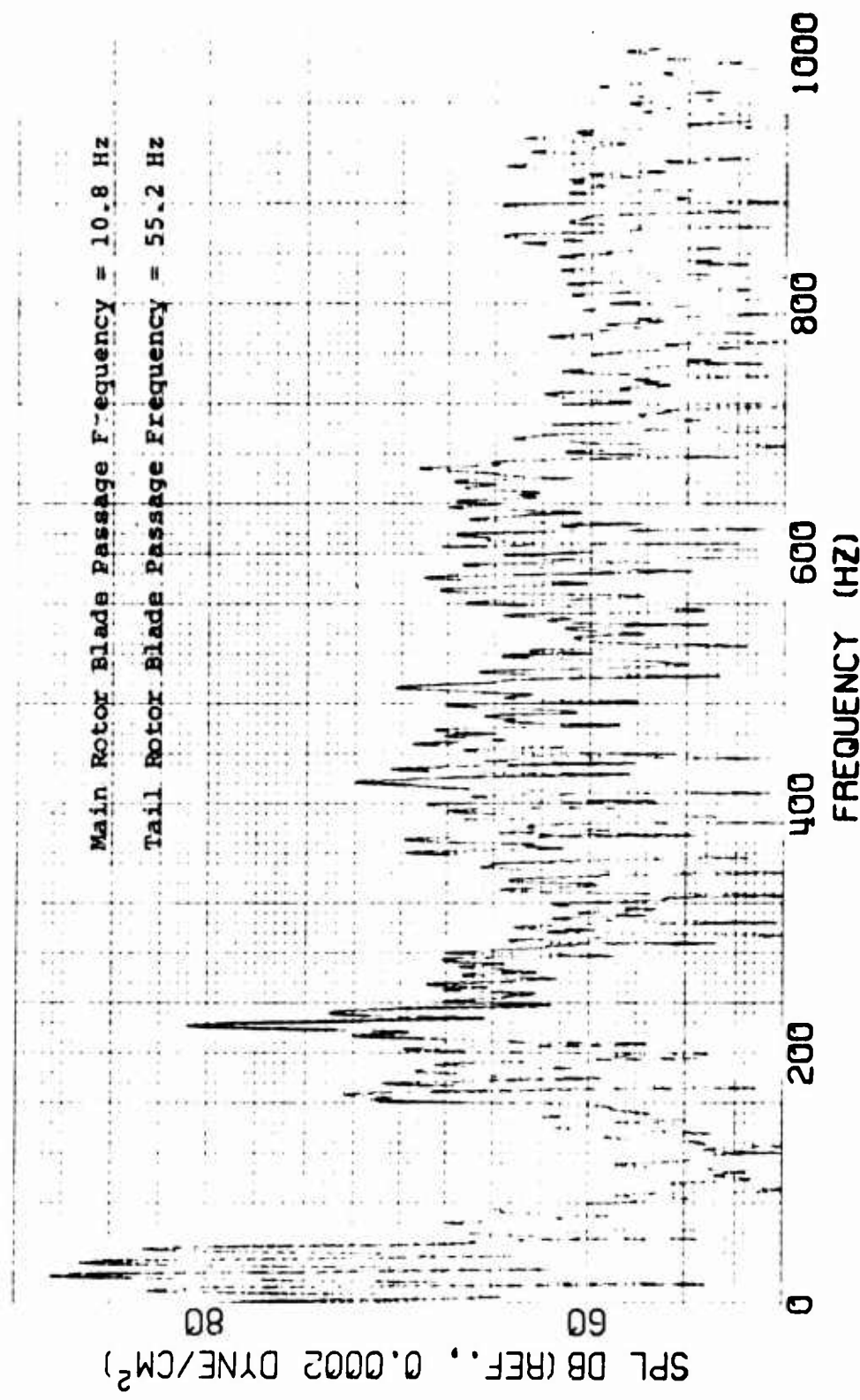


Figure 33. Noise Spectrum by Ubiquitous Analyzer for UH-1B Helicopter in 100-Ft Hover, Recorded 200 Ft to the Right (Microphone 4).

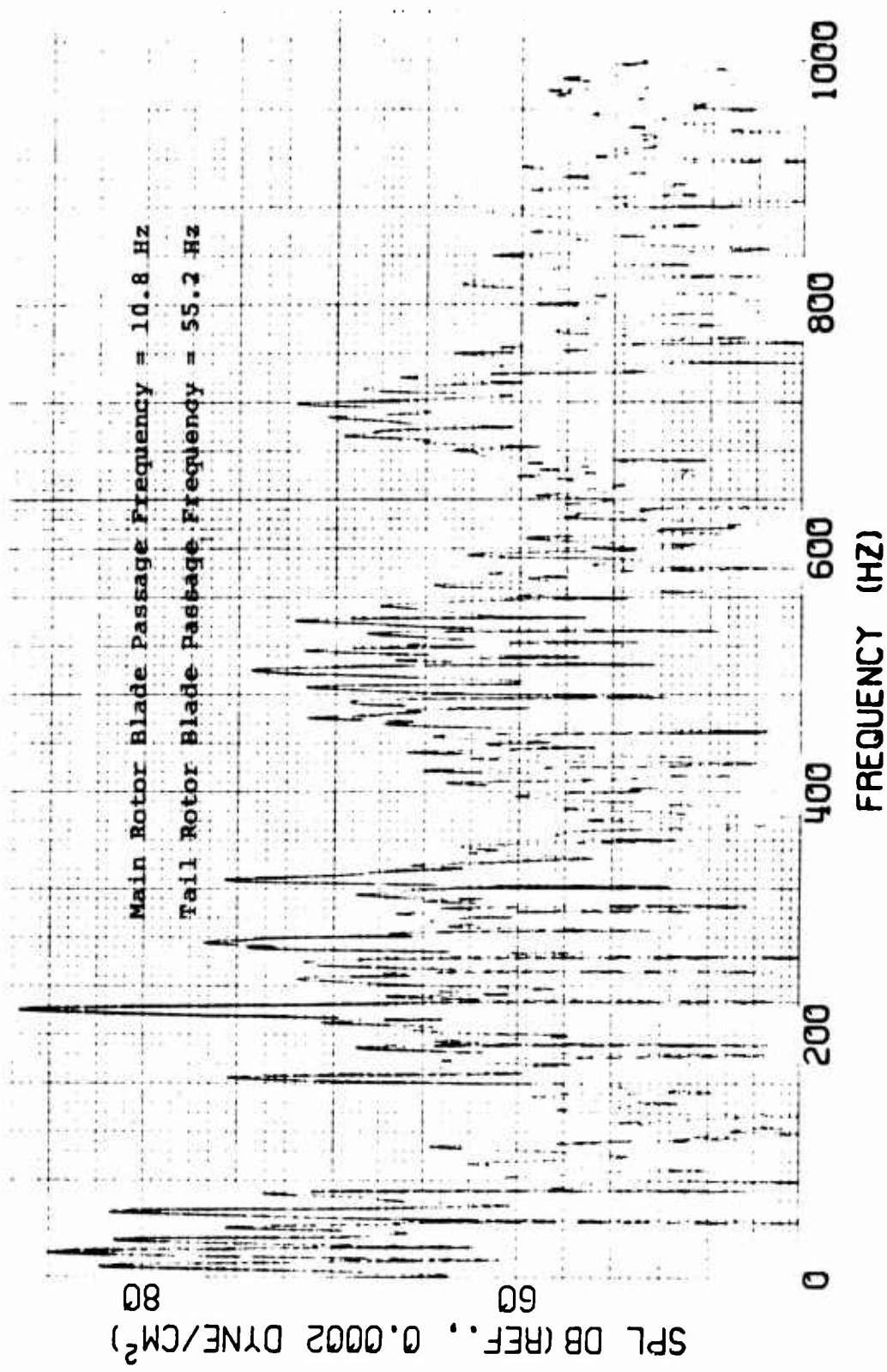


Figure 34. Noise Spectrum by Ubiquitous Analyzer for UH-1B Helicopter in 100-Ft Hover, Recorded 200 Ft to the Left (Microphone 10).

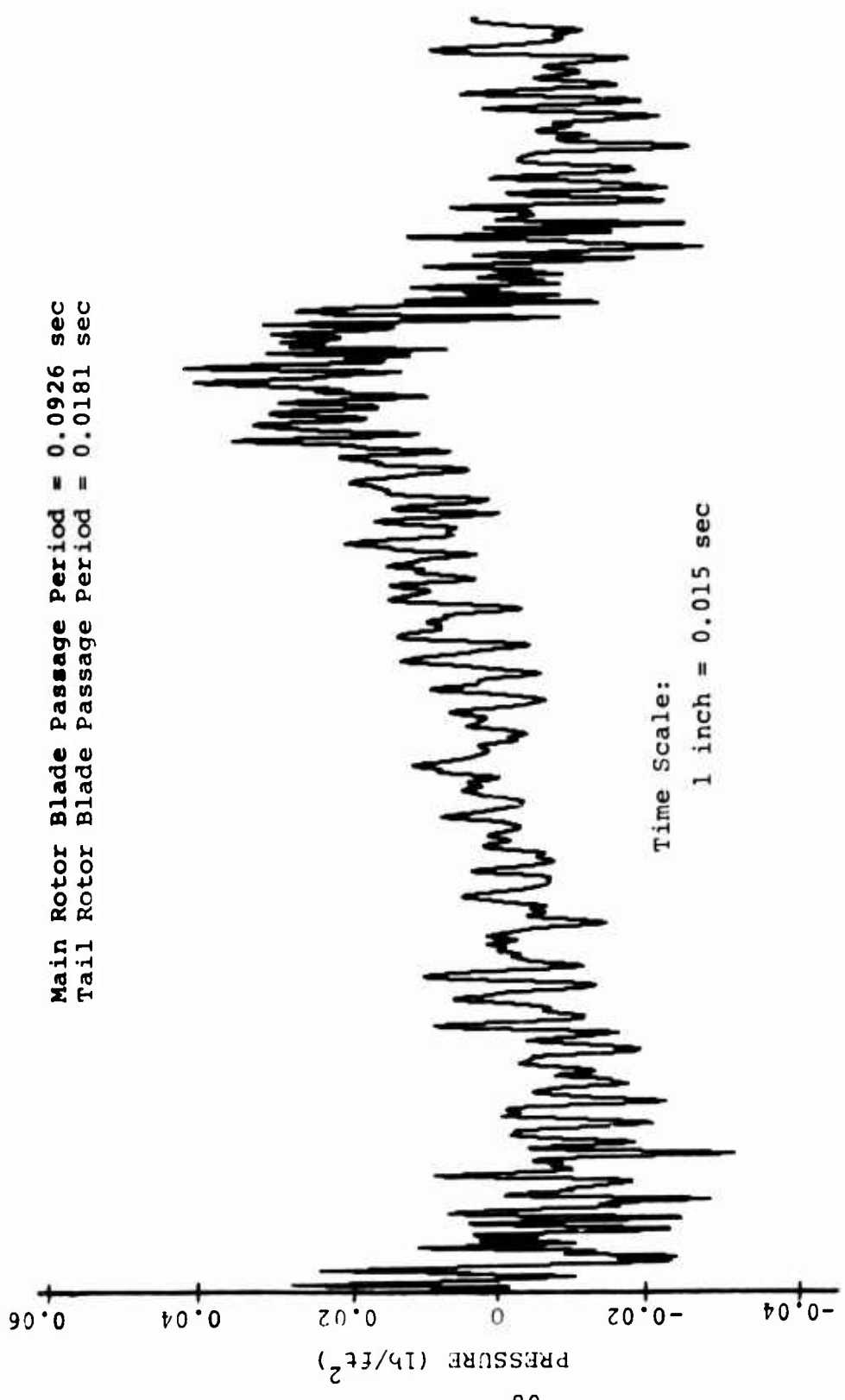


Figure 35. Pressure Time History of Predicted Noise Generated
 From a UH-1B in 100 Ft Hover, Recorded 200 Ft to
 the Left (Microphone 10).

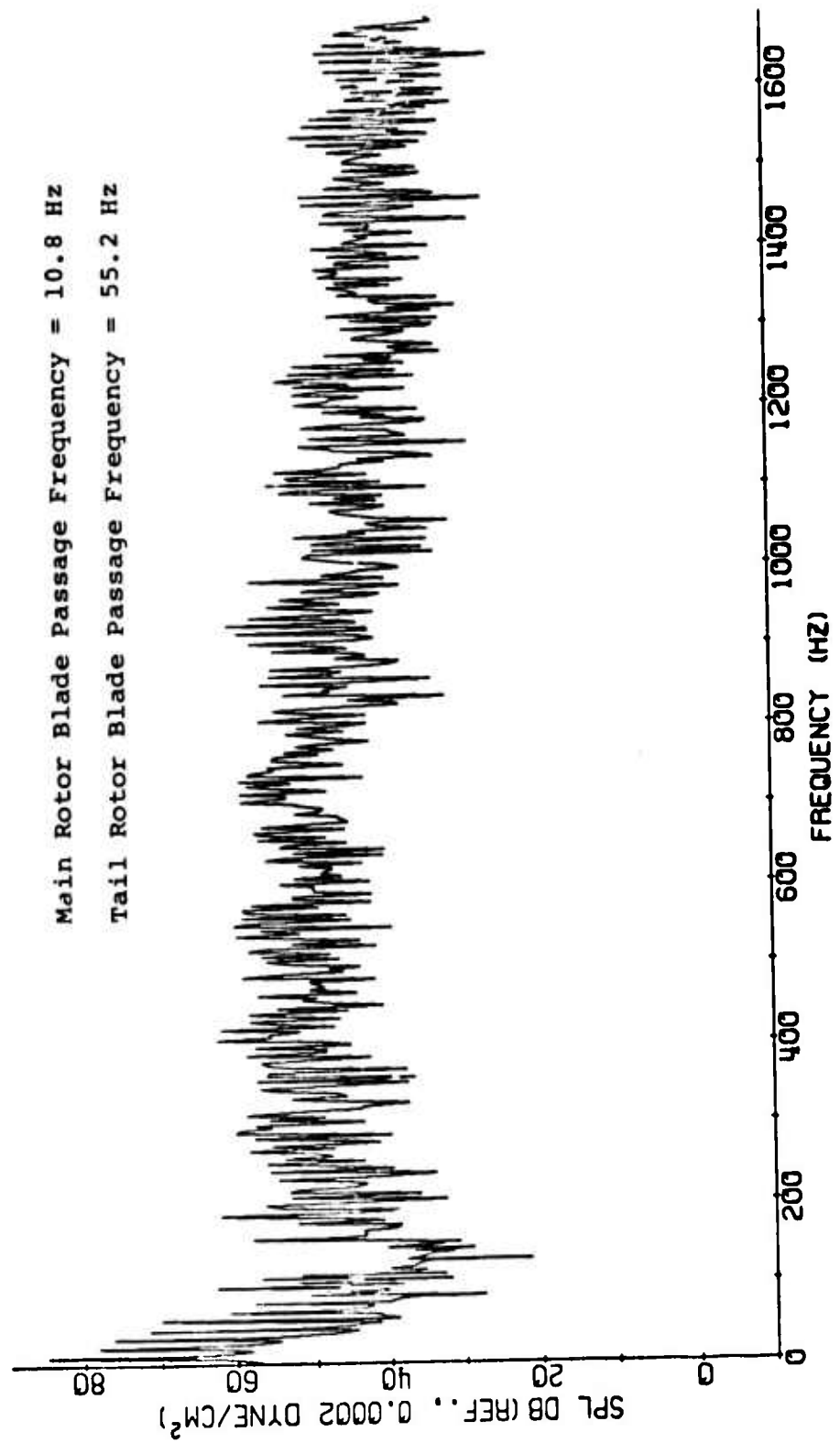


Figure 36. Spectrum of Predicted Noise Generated From a UH-1B in 100-Ft Hover, Recorded 200 Ft to the Left (Microphone 10) (Reference Figure 35).

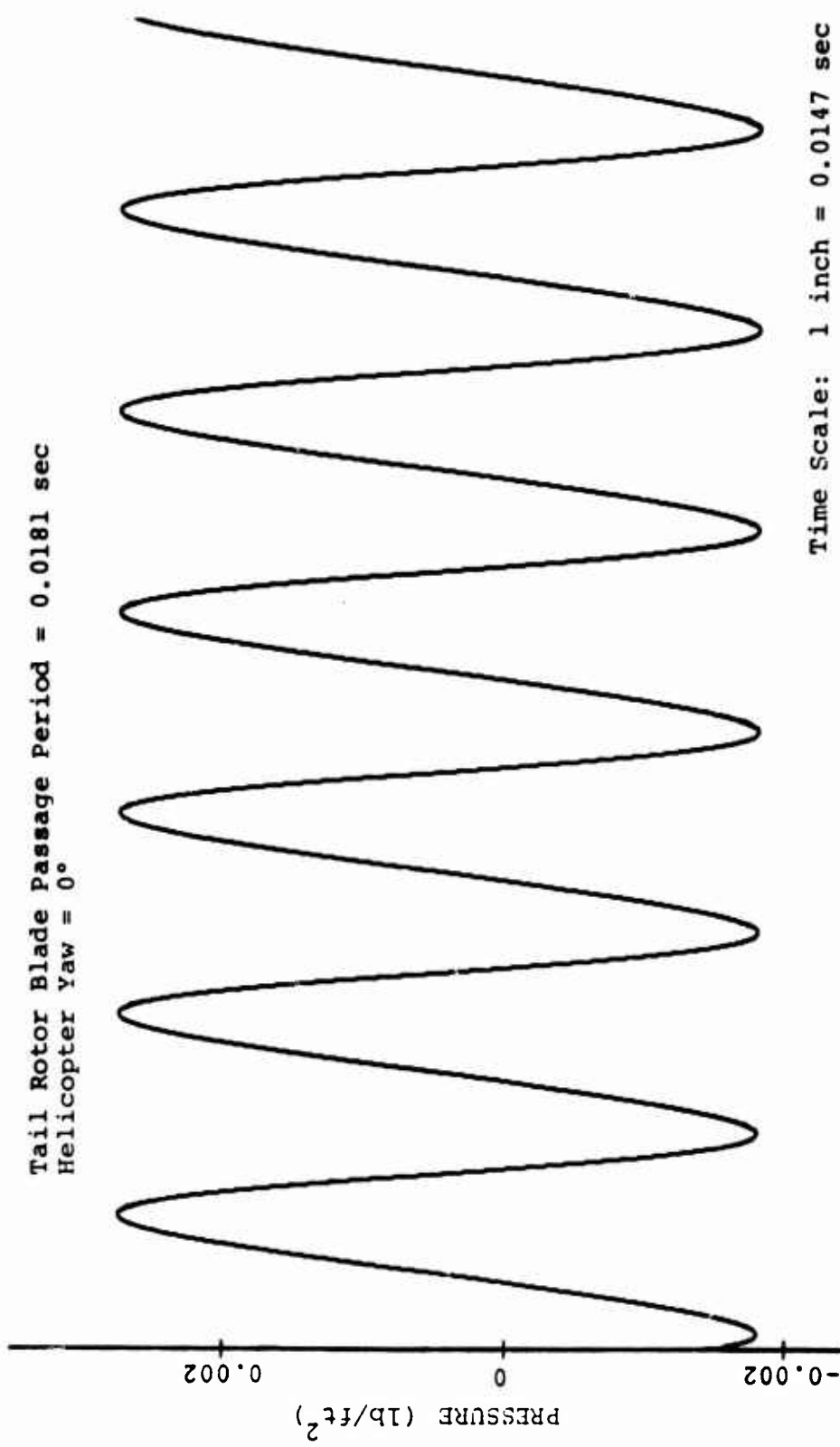


Figure 37. Pressure Time History of Predicted Tail Rotor Rotational Noise Generated From a UH-1B in 100-Ft Hover.

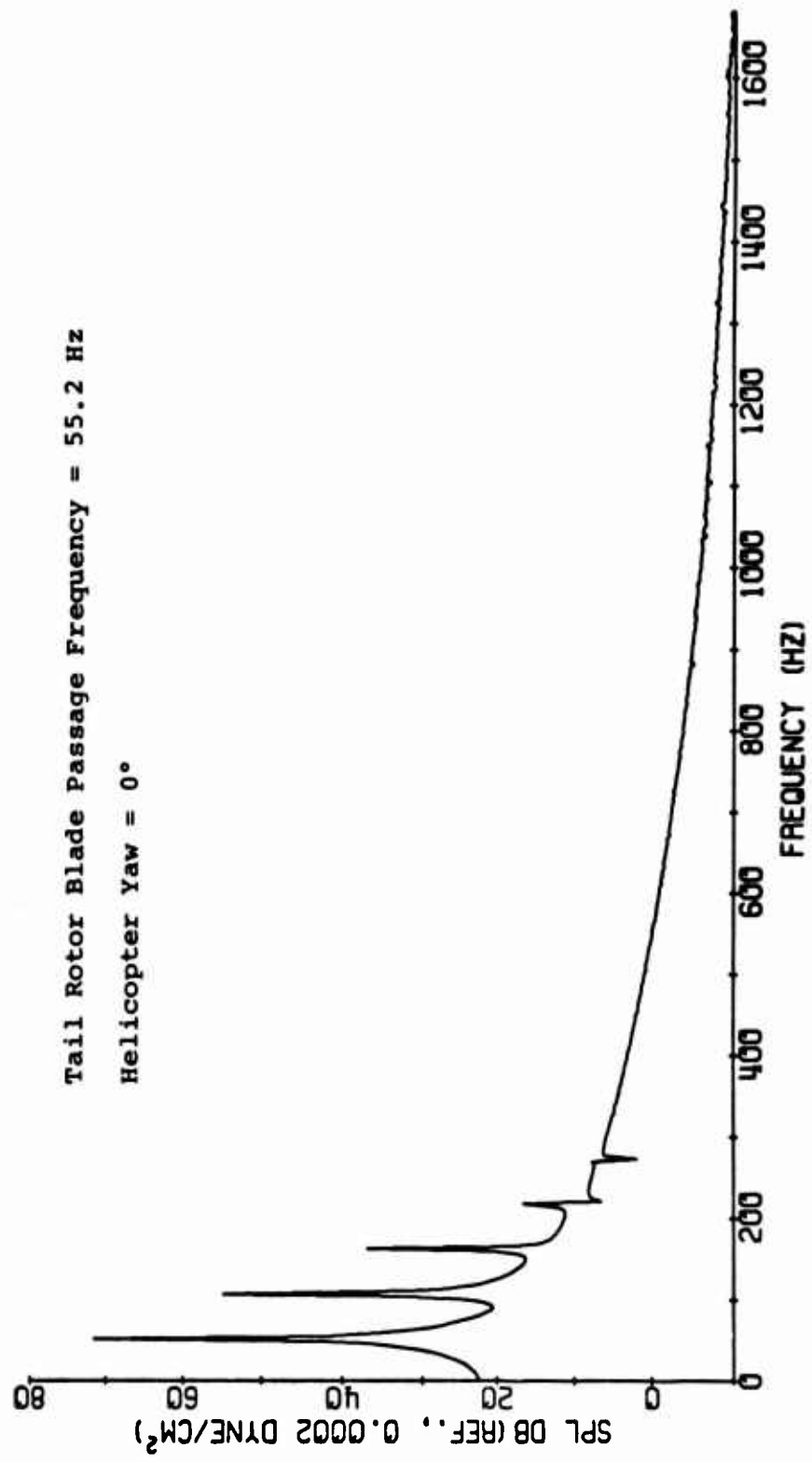


Figure 38. Spectrum of Predicted Tail Rotor Rotational Noise Generated From a UH-1B in 100-ft Hover (Reference Figure 37).

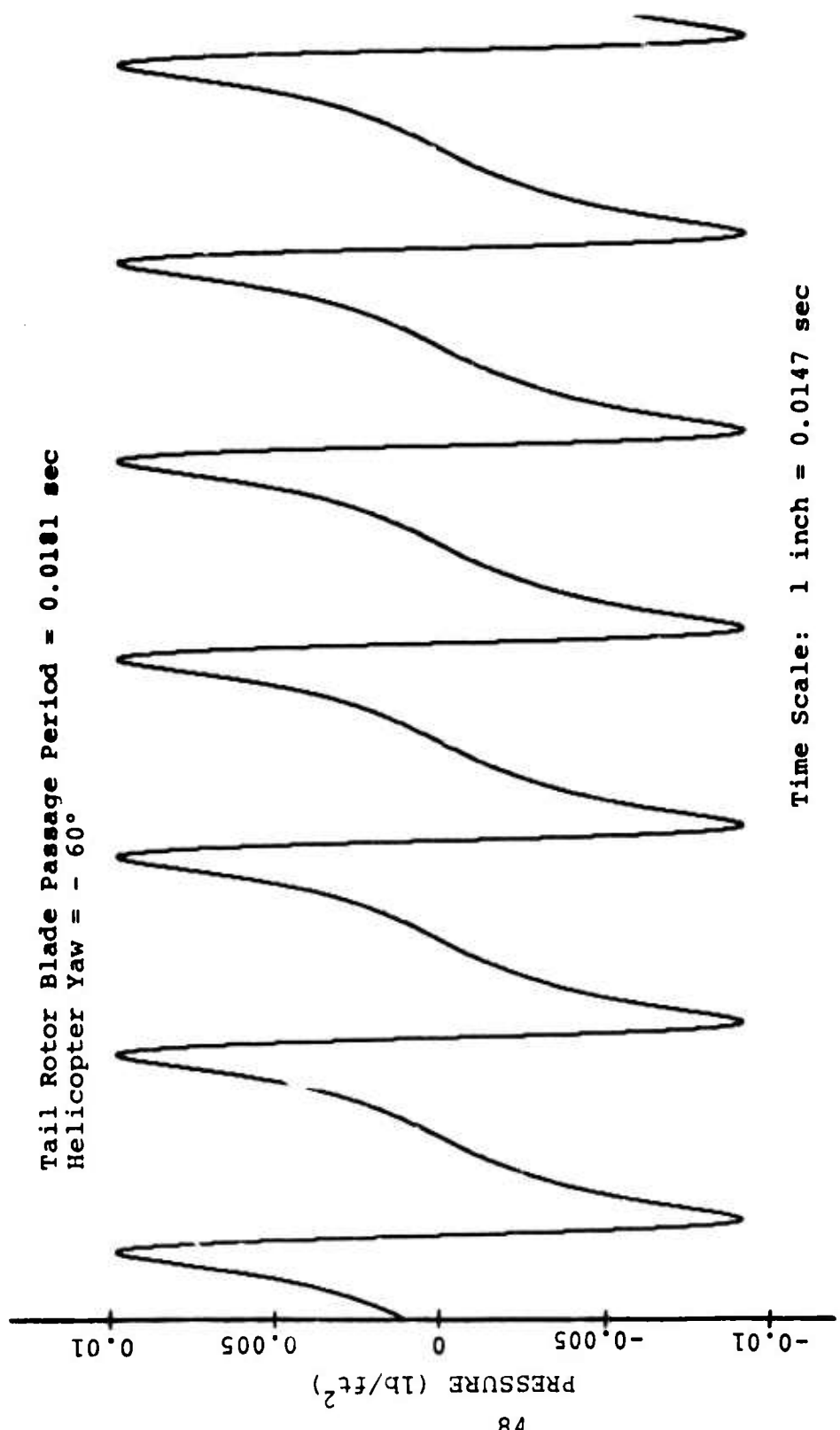


Figure 39. Pressure Time History of Predicted Tail Rotor Rotational Noise Generated From a UH-1B in 100-Ft Hover.

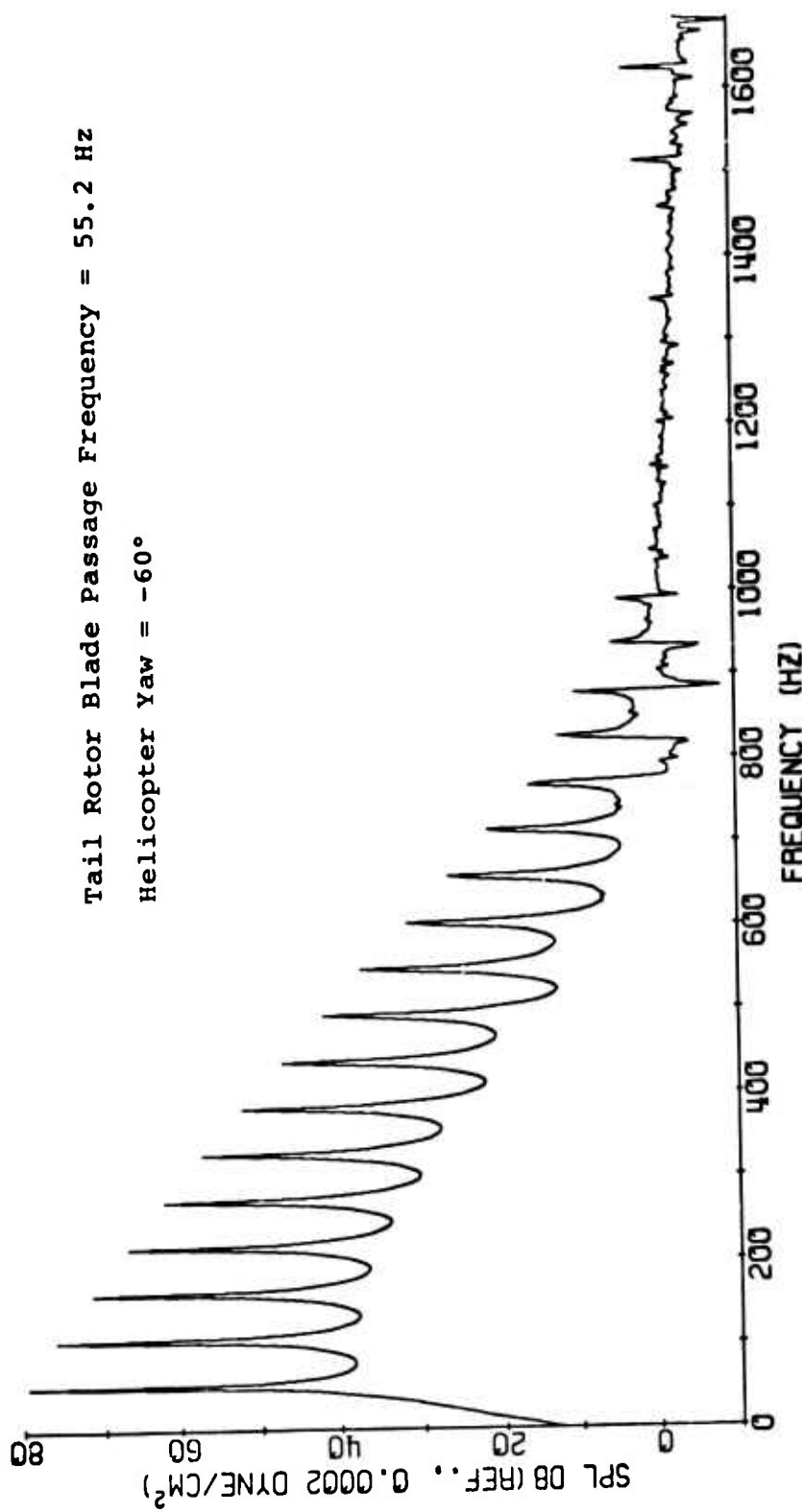


Figure 40. Spectrum of Predicted Tail Rotor Rotational Noise Generated From a UH-1B in 100-Ft Hover (Reference Figure 39).

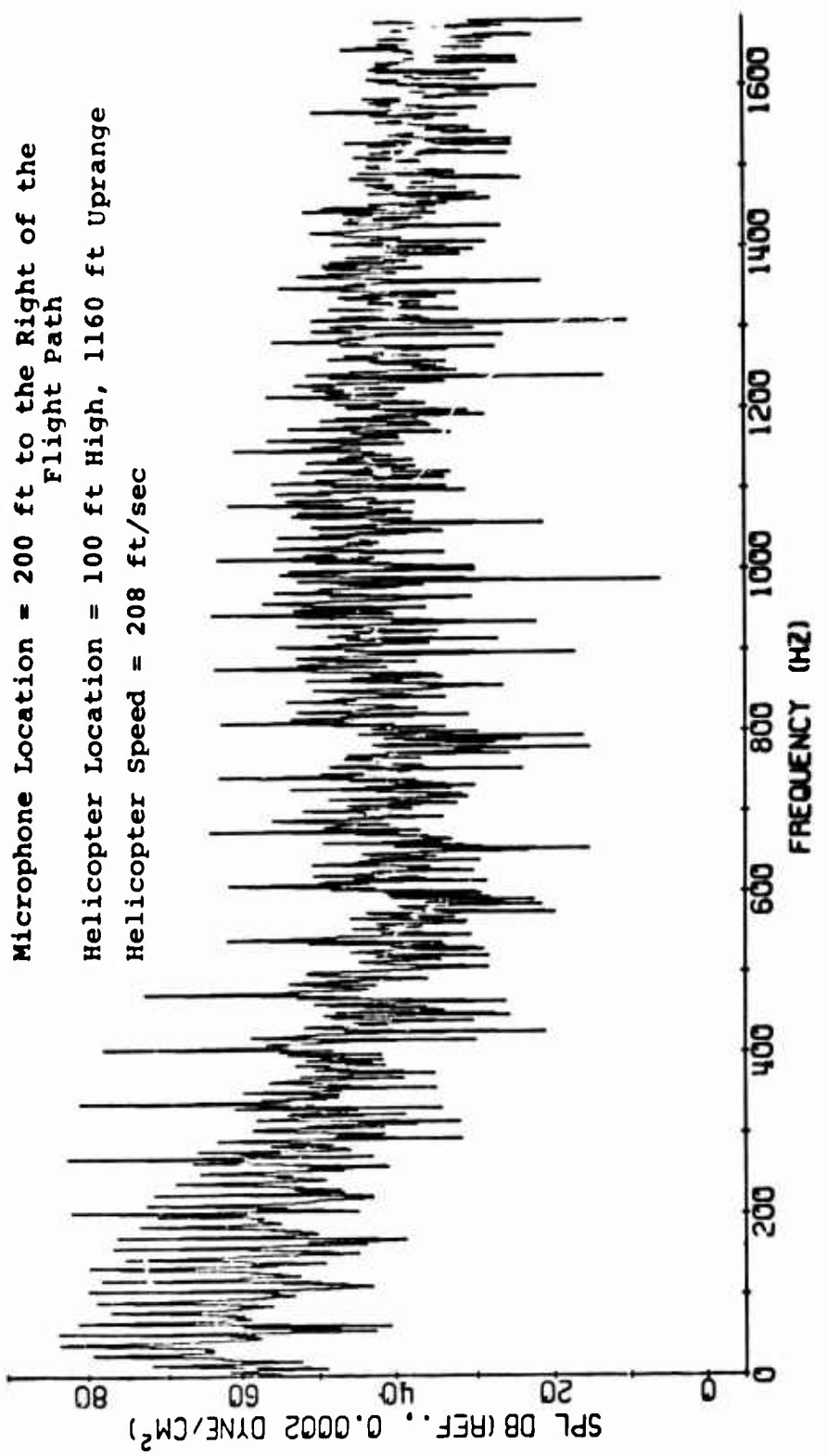


Figure 41. Spectrum of Recorded Noise Generated From a UH-1B in Level Flight.

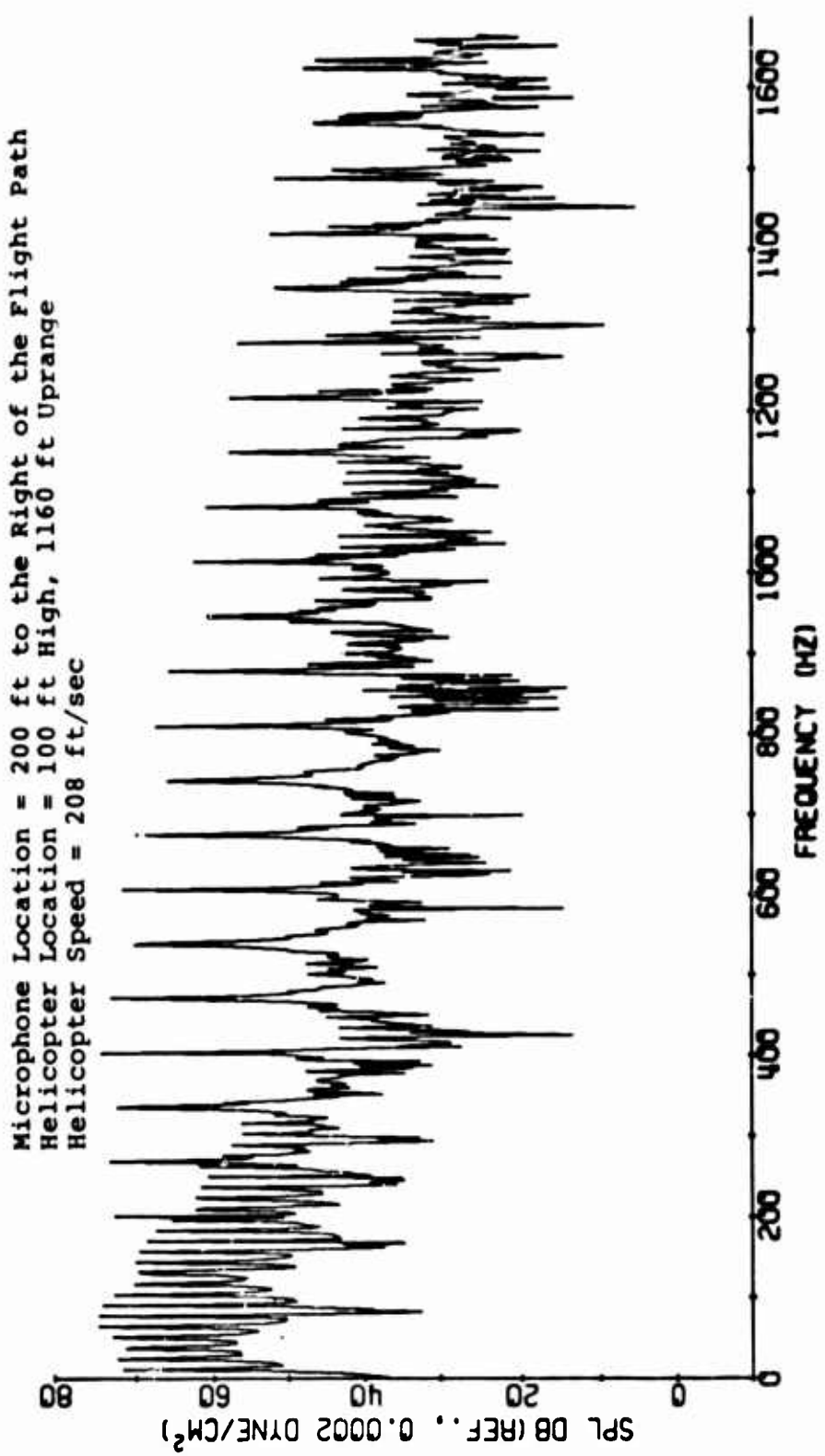


Figure 42. Spectrum of Predicted Noise Generated from a UH-1B in Level Flight.

Microphone Location = 200 ft to the Right of the Flight Path
Helicopter Position = 100 ft High, 1000 ft Uprange
Helicopter Speed = 208 ft/sec

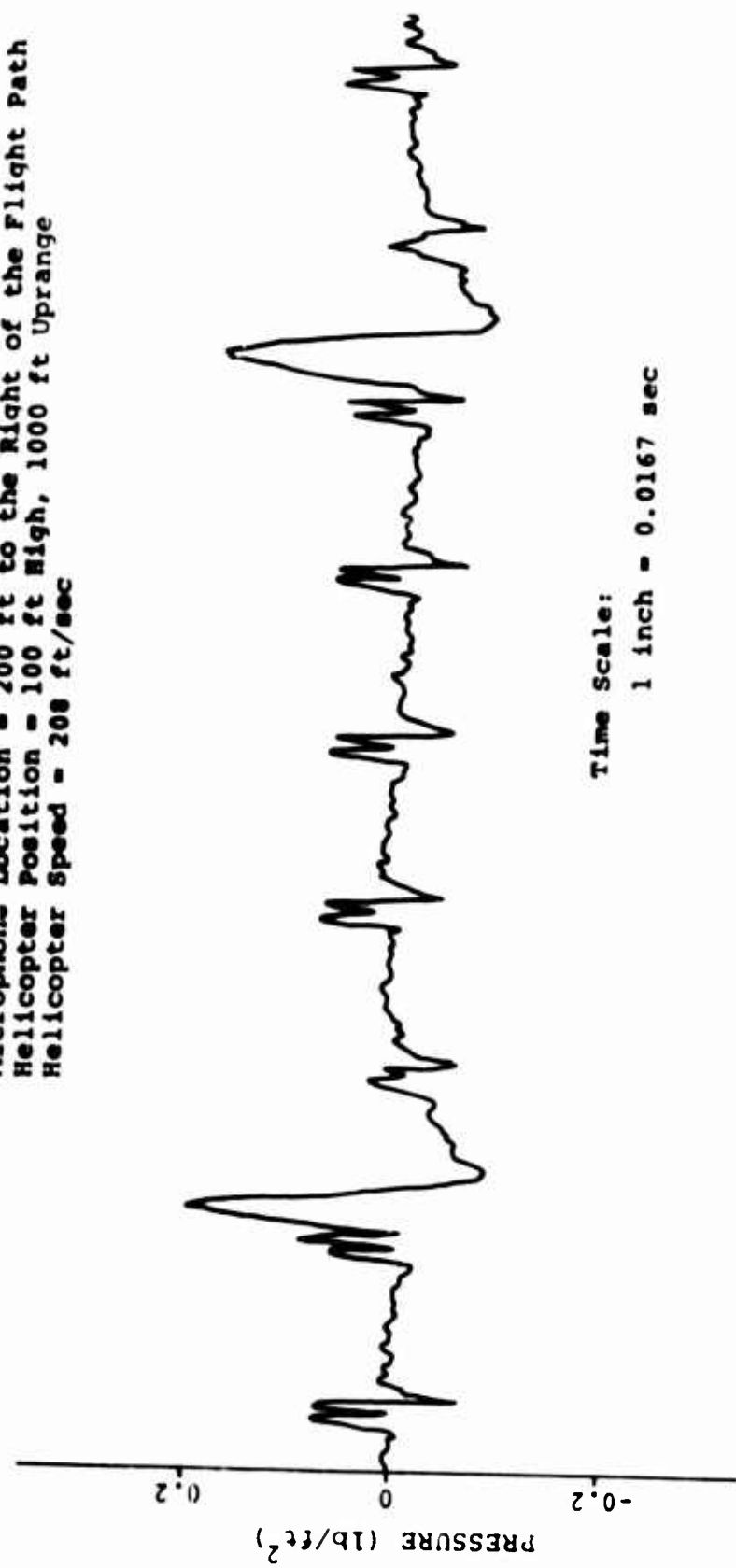


Figure 43. Pressure Time History of Recorded Noise Generated From a UH-1B in Level Flight.

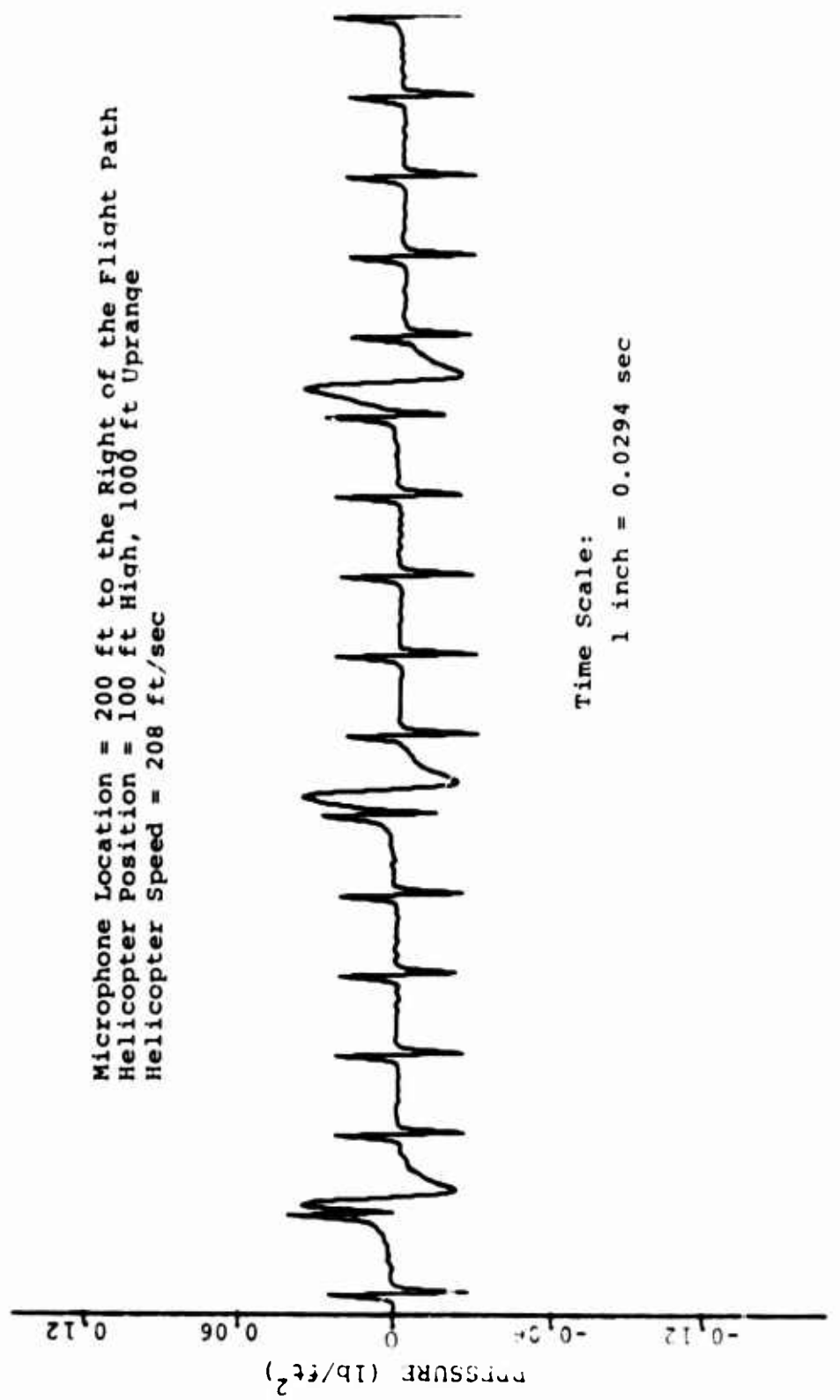


Figure 44. Pressure Time History of Predicted Noise Generated From a UH-1B in Level Flight.

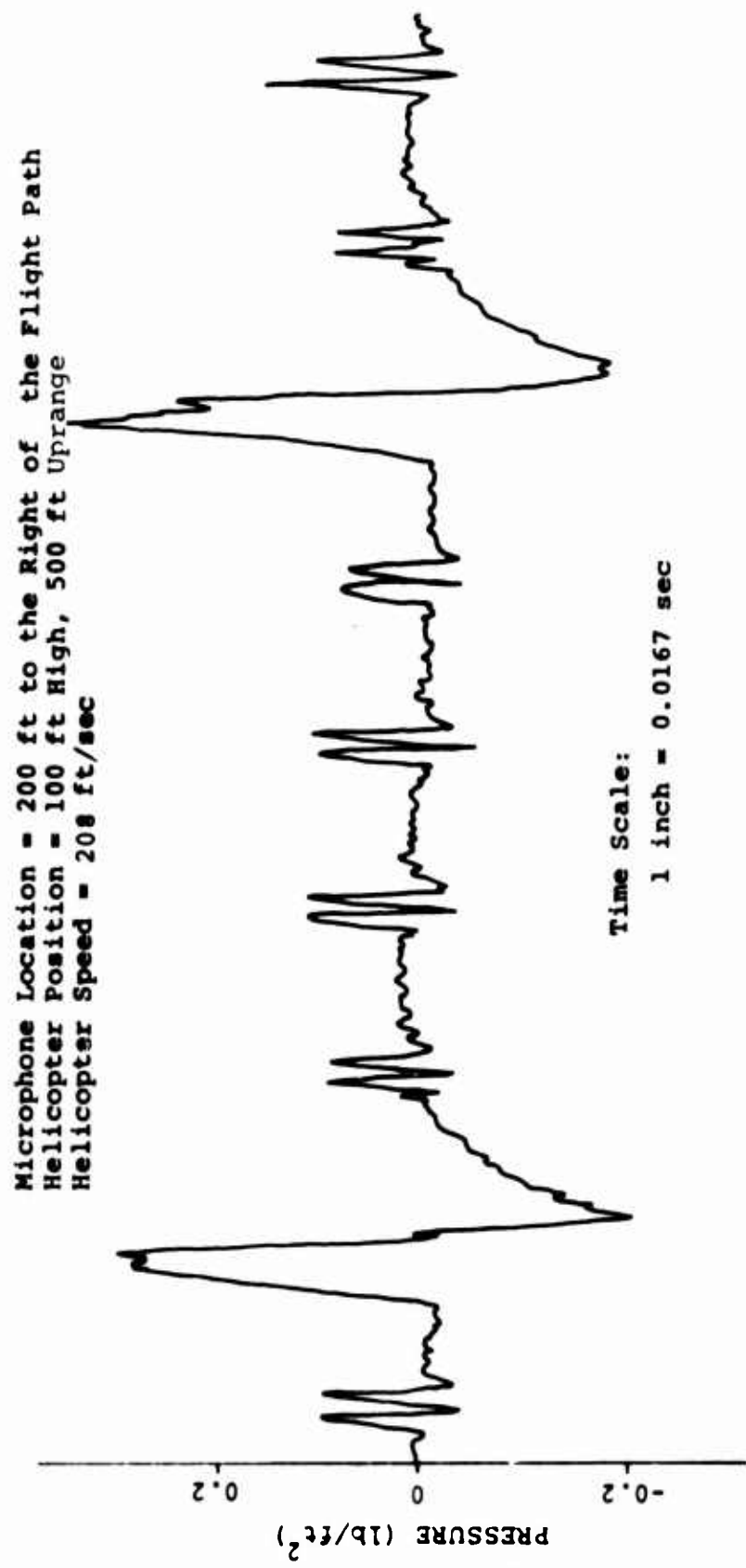


Figure 45. Pressure Time History of Recorded Noise Generated From a UH-1B in Level Flight.

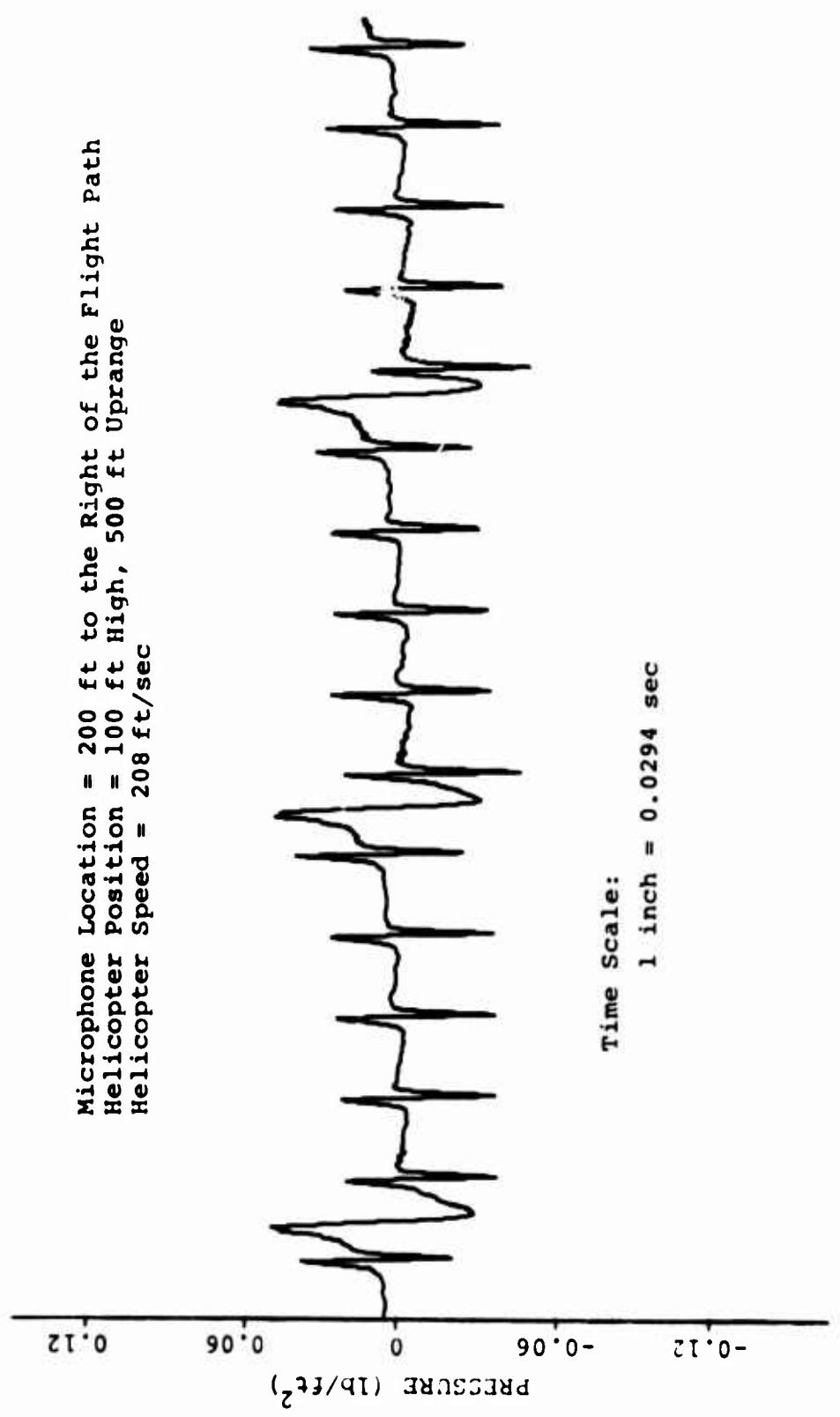


Figure 46. Pressure Time History of Predicted Noise Generated From a UH-1B in Level Flight.

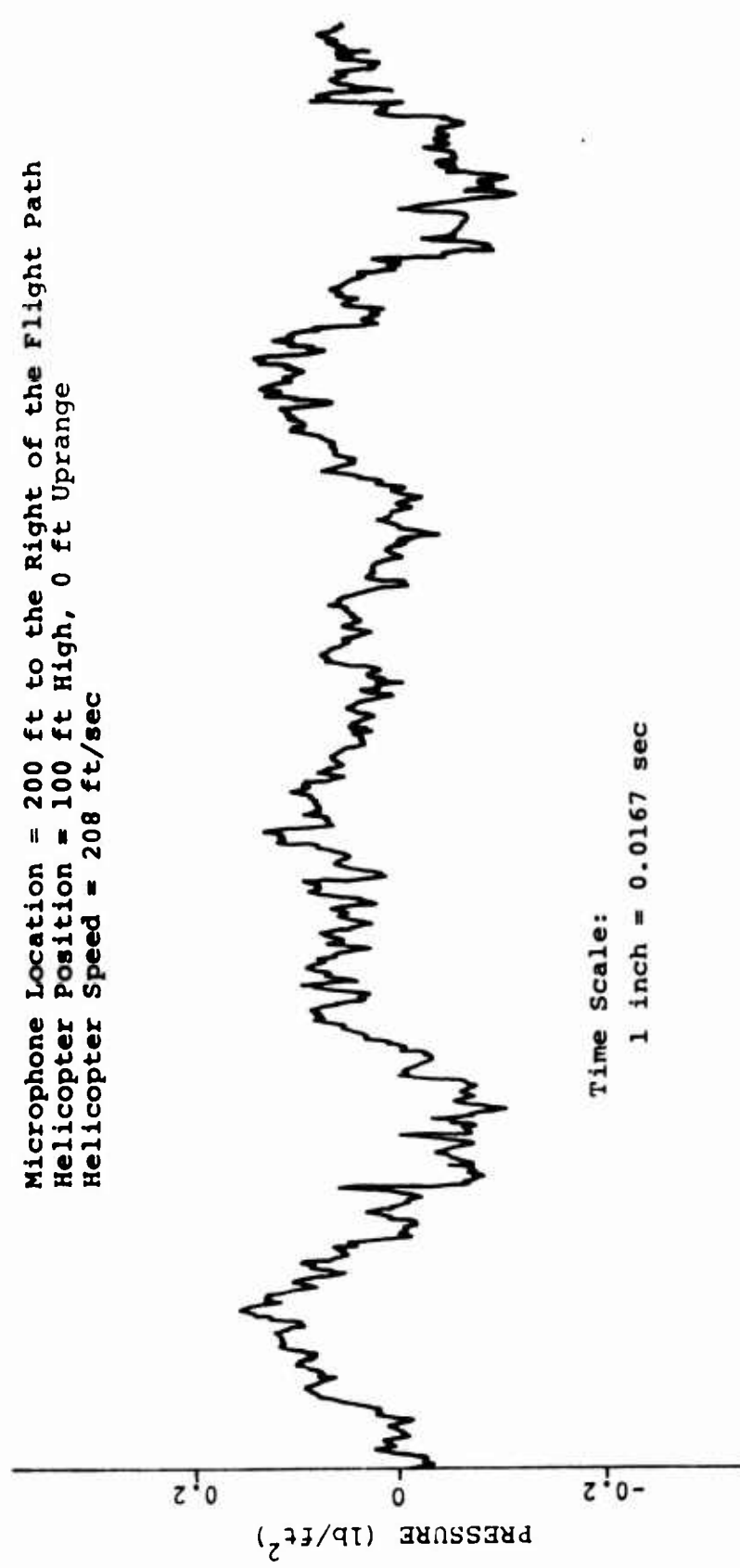


Figure 47. Pressure Time History of Recorded Noise Generated From a UH-1B in Level Flight.

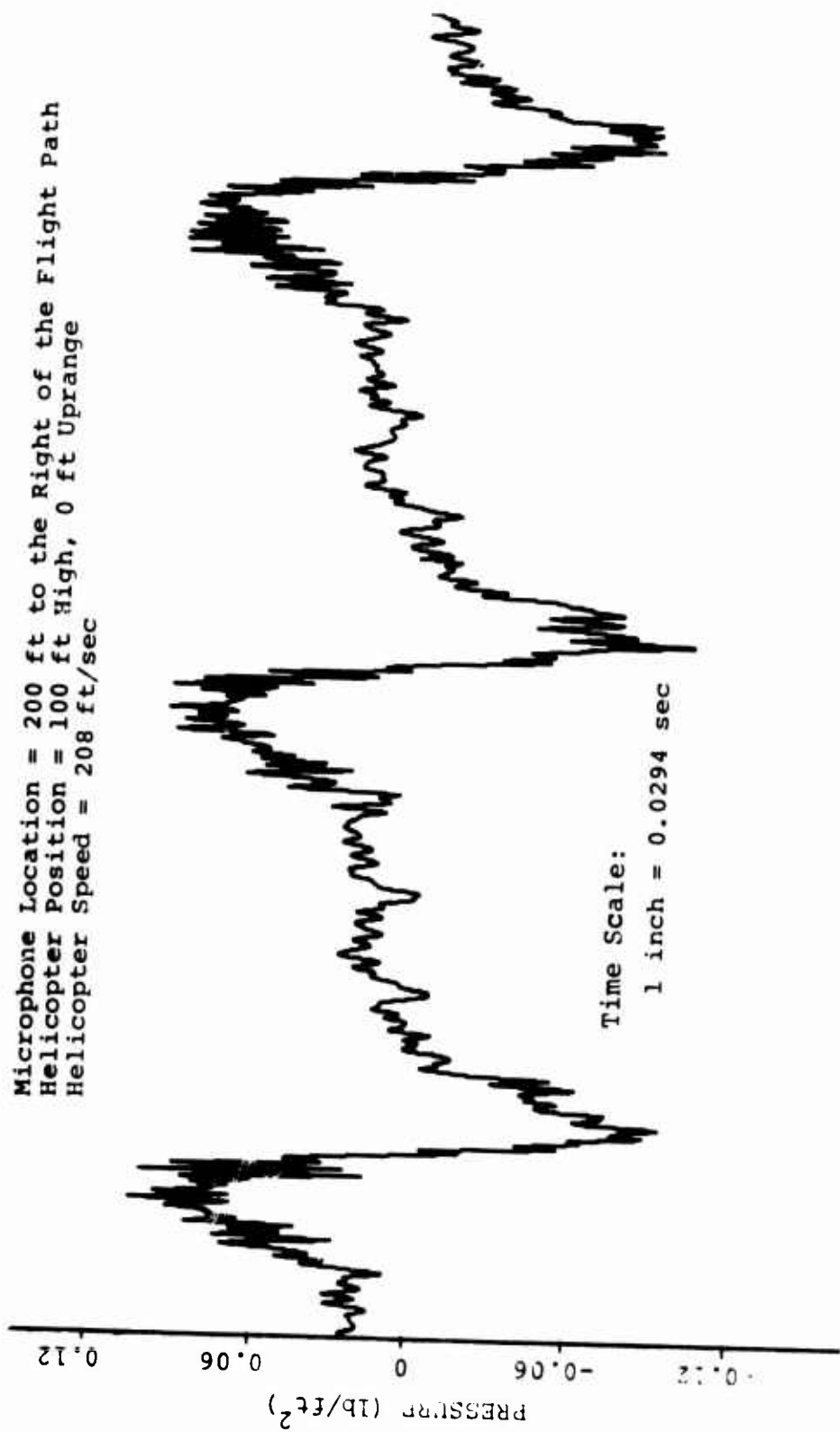


Figure 48. Pressure Time History of Predicted Noise Generated
 From a UH-1B in Level Flight.

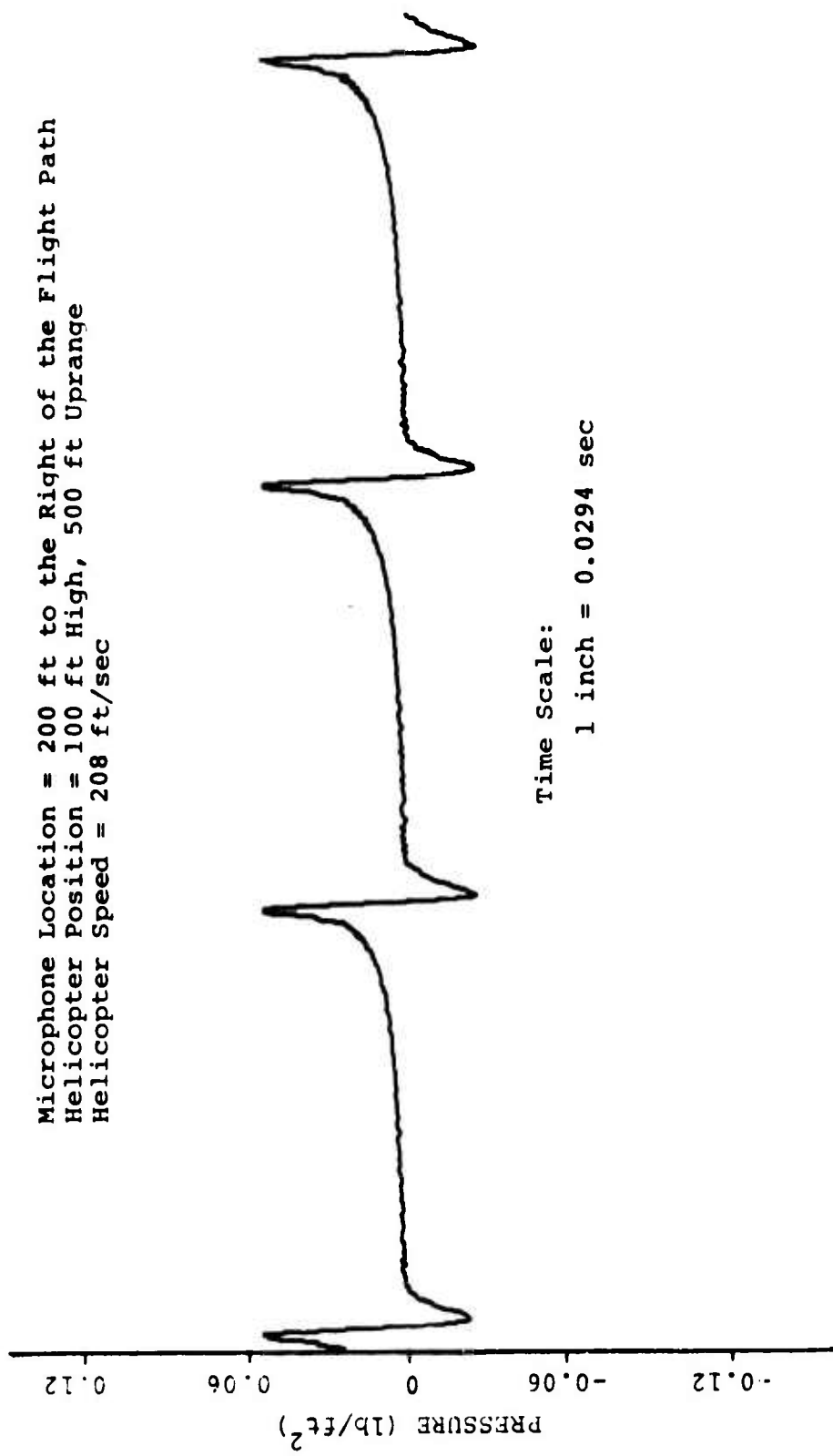


Figure 49. Pressure Time History of Predicted Noise Generated From a UH-1B Main Rotor in Level Flight.

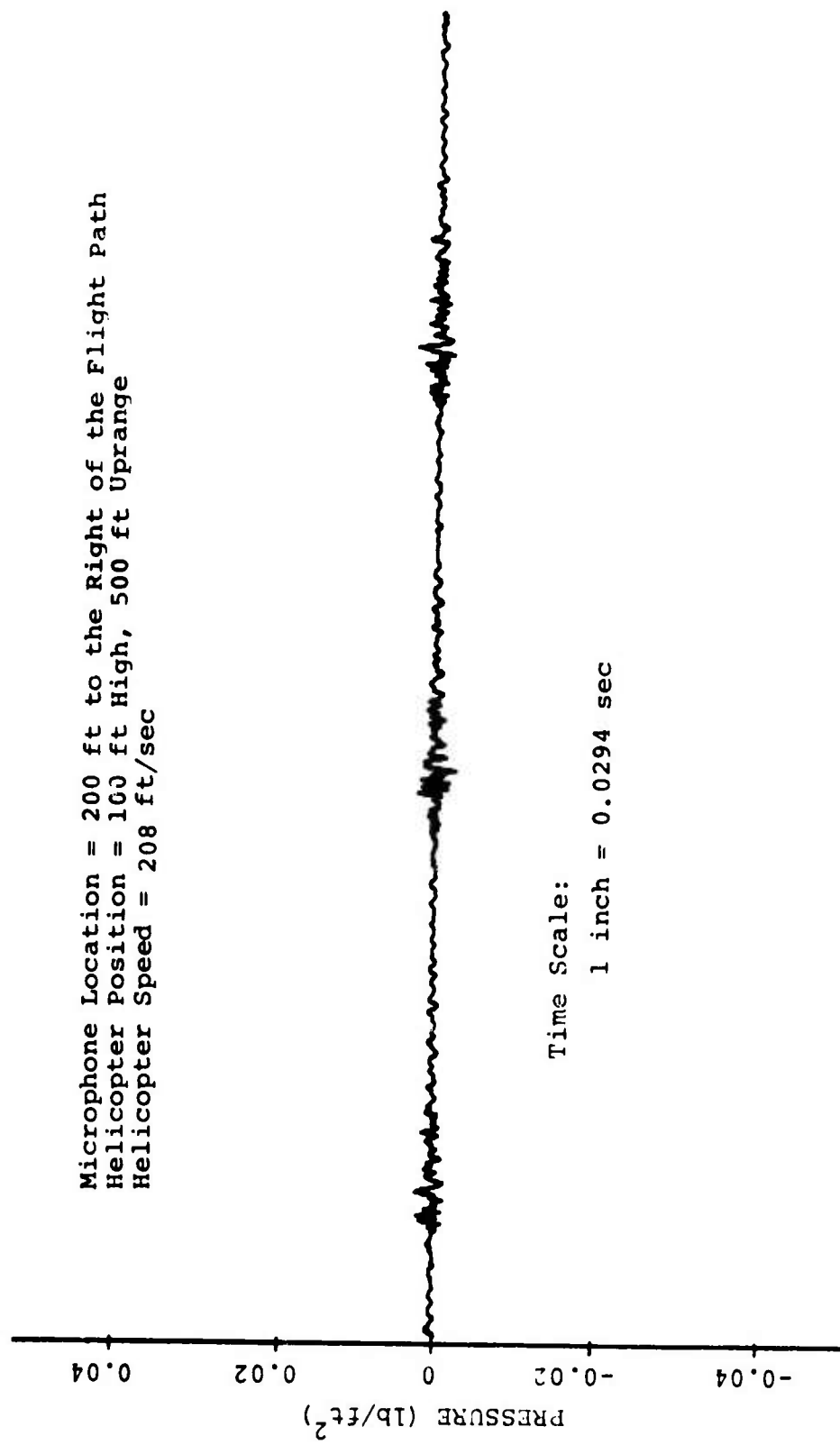


Figure 50. Pressure Time History of Predicted Vortex Noise Generated From a UH-1B Main Rotor in Level Flight.

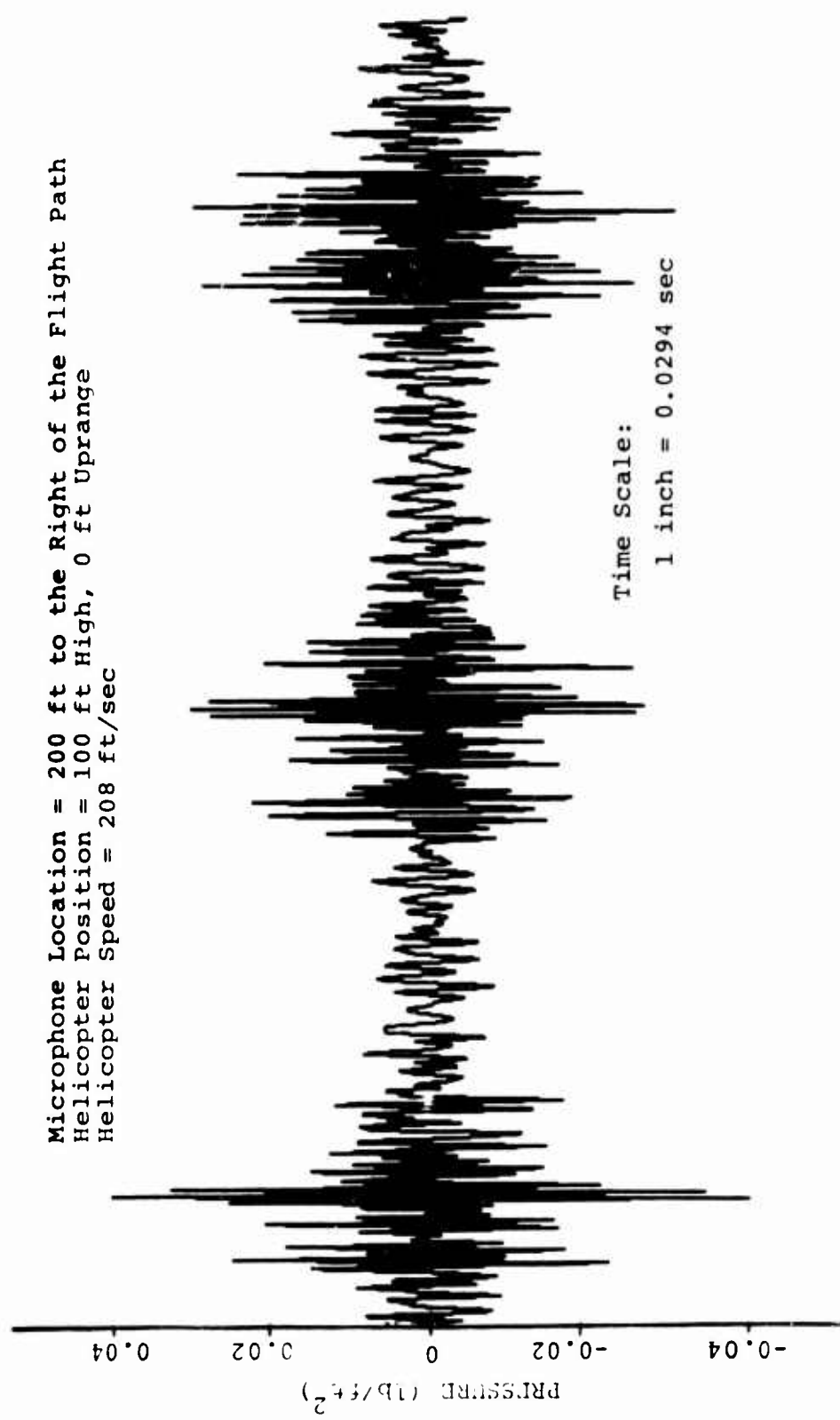


Figure 51. Pressure Time History of Predicted Vortex Noise Generated From a UH-1B Main Rotor in Level Flight.

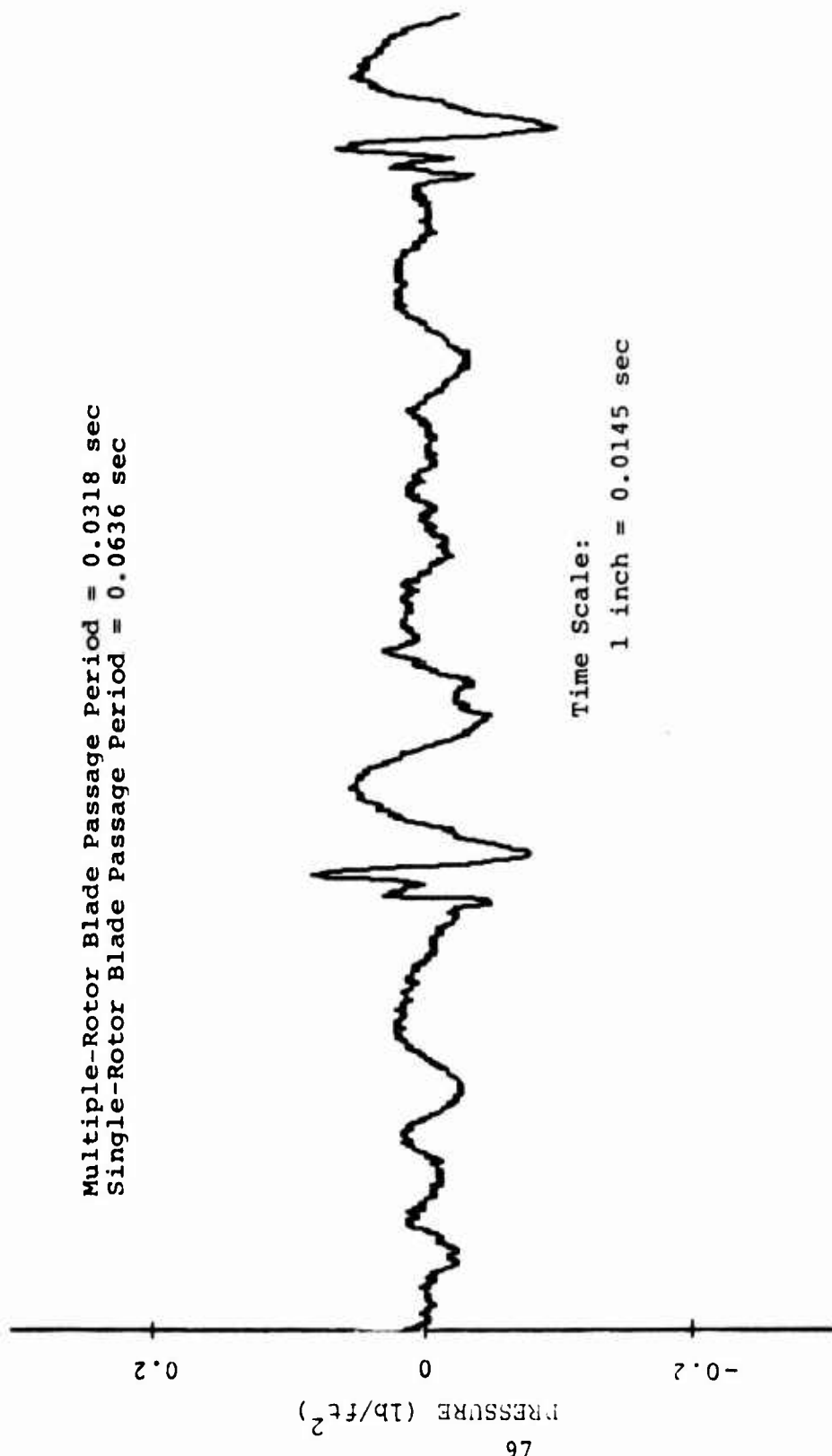


Figure 52. Pressure Time History of Recorded Noise Generated From a Boeing-Vertol Model 347 Helicopter Hovering in Ground Effect, Microphone 200 Ft to the Right.

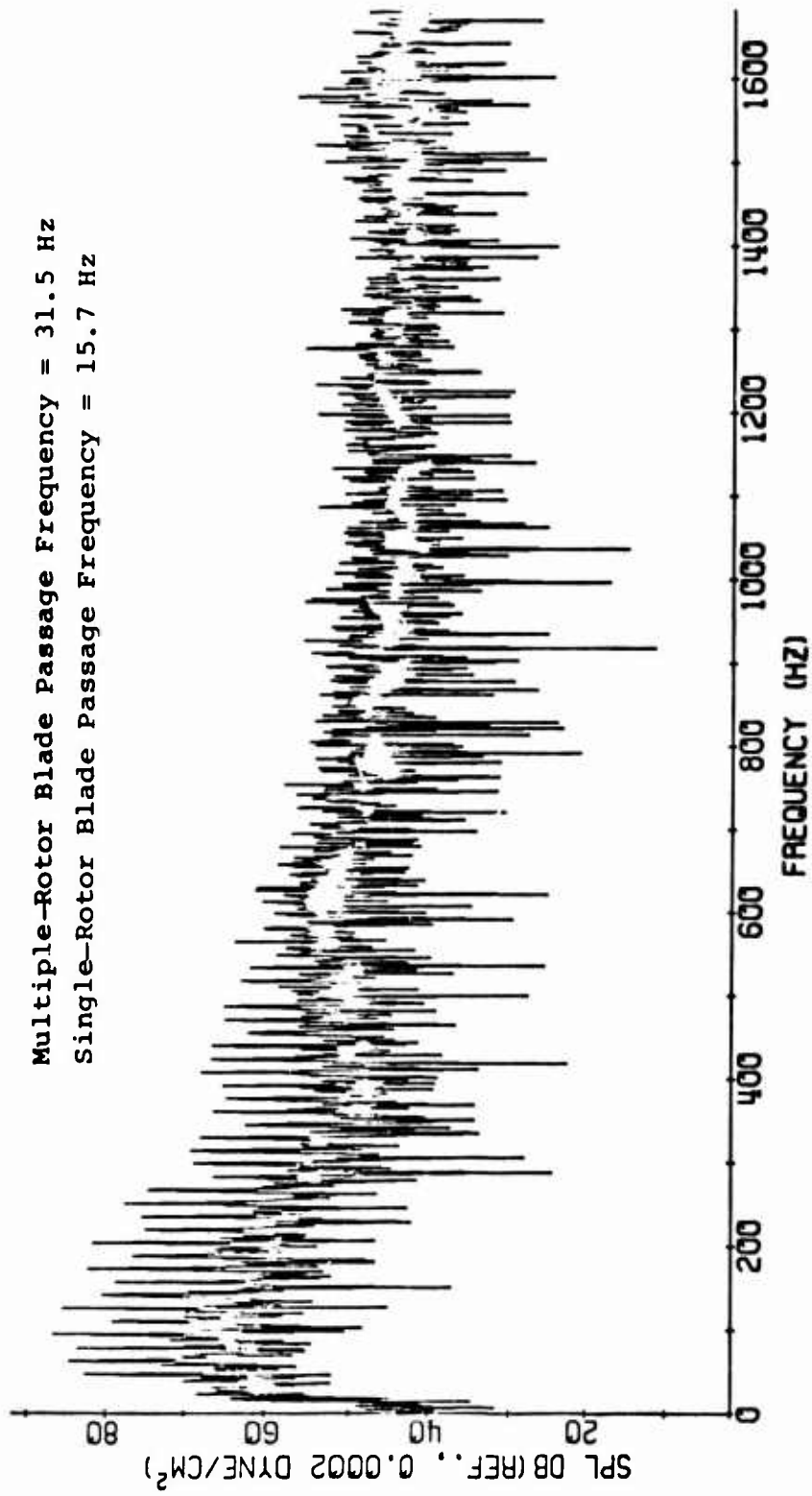


Figure 53. Spectrum of Recorded Noise Generated From a Boeing-Vertol Model 347 Helicopter Hovering in Ground Effect, Microphone 200 Ft to the Right (Reference Figure 52).

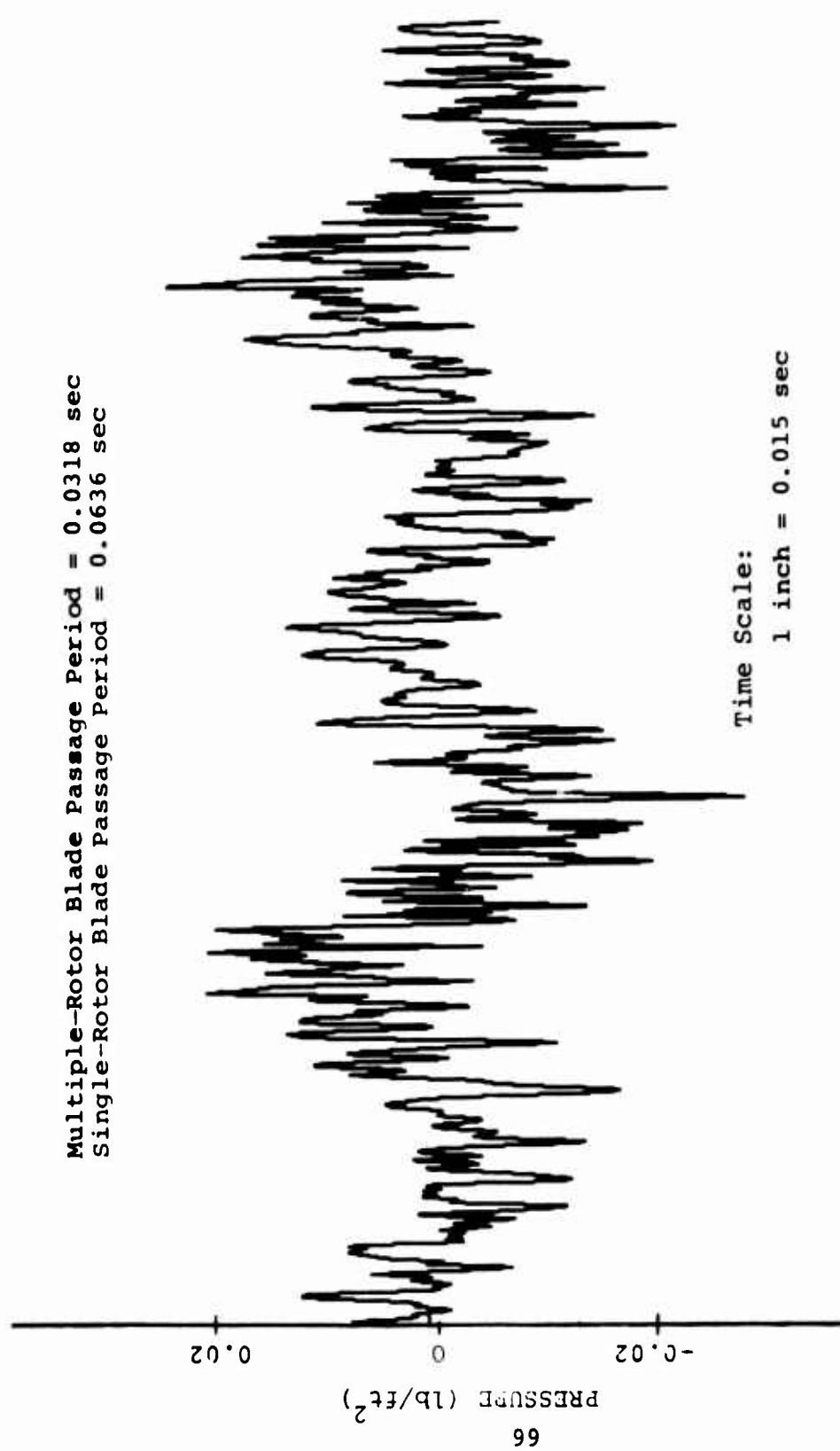


Figure 54. Pressure Time History of Predicted Noise Generated From a Boeing-Vertol Model 347 Helicopter Hovering in Ground Effect, Microphone 200 Ft to the Right.

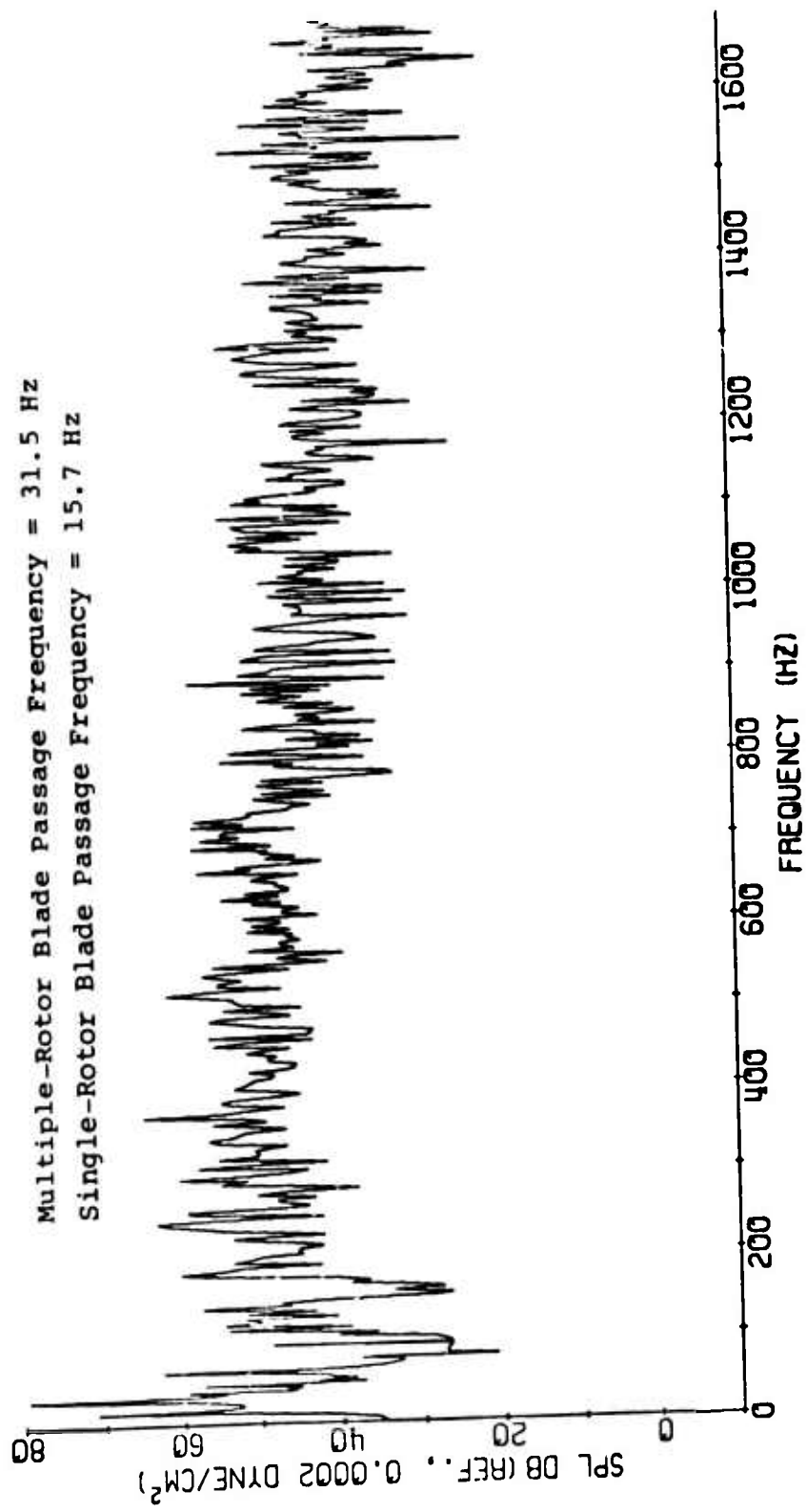


Figure 55. Spectrum of Predicted Noise Generated From a Boeing-Vertol Model 347 Helicopter Hovering in Ground Effect. Microphone 200 Ft to the Right (Reference Figure 54).

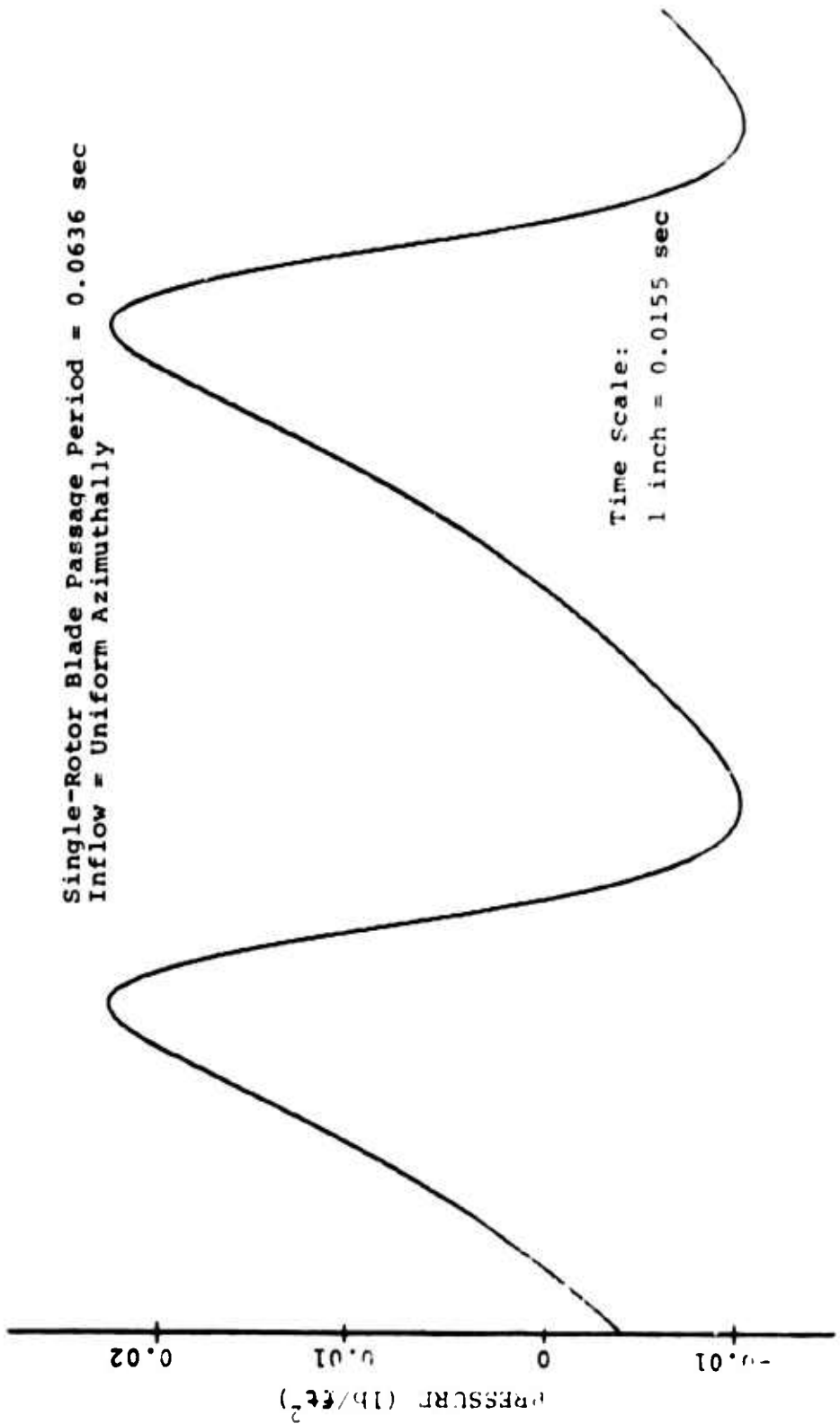


Figure 56. Pressure Time History of Predicted Single-Rotor Rotational Noise Generated From a Boeing-Vertol Model 347 Hovering in Ground Effect.

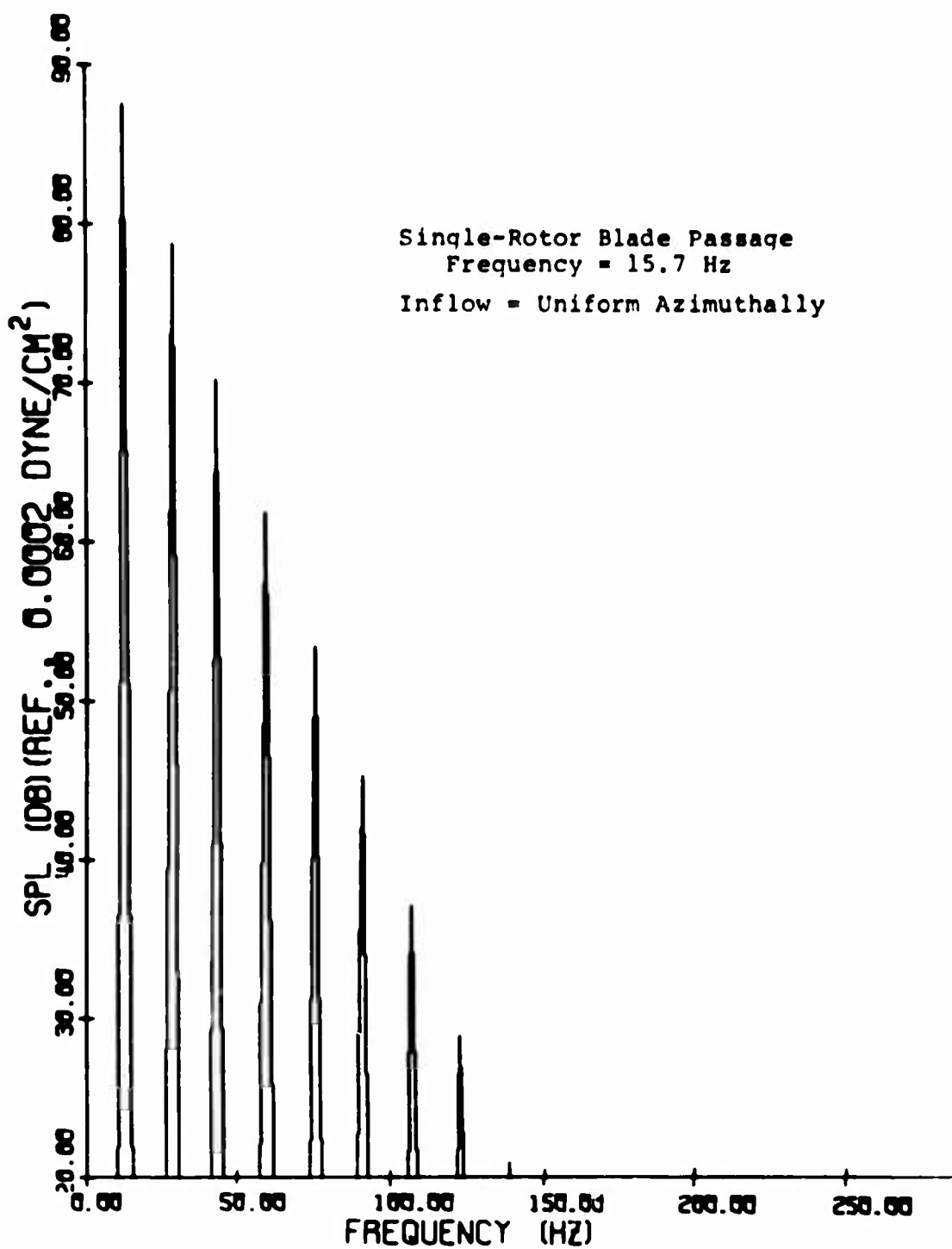


Figure 57. Spectrum of Predicted Single-Rotor Rotational Noise Generated from a Boeing-Vertol Model 347 Hovering in Ground Effect (Reference Figure 56).

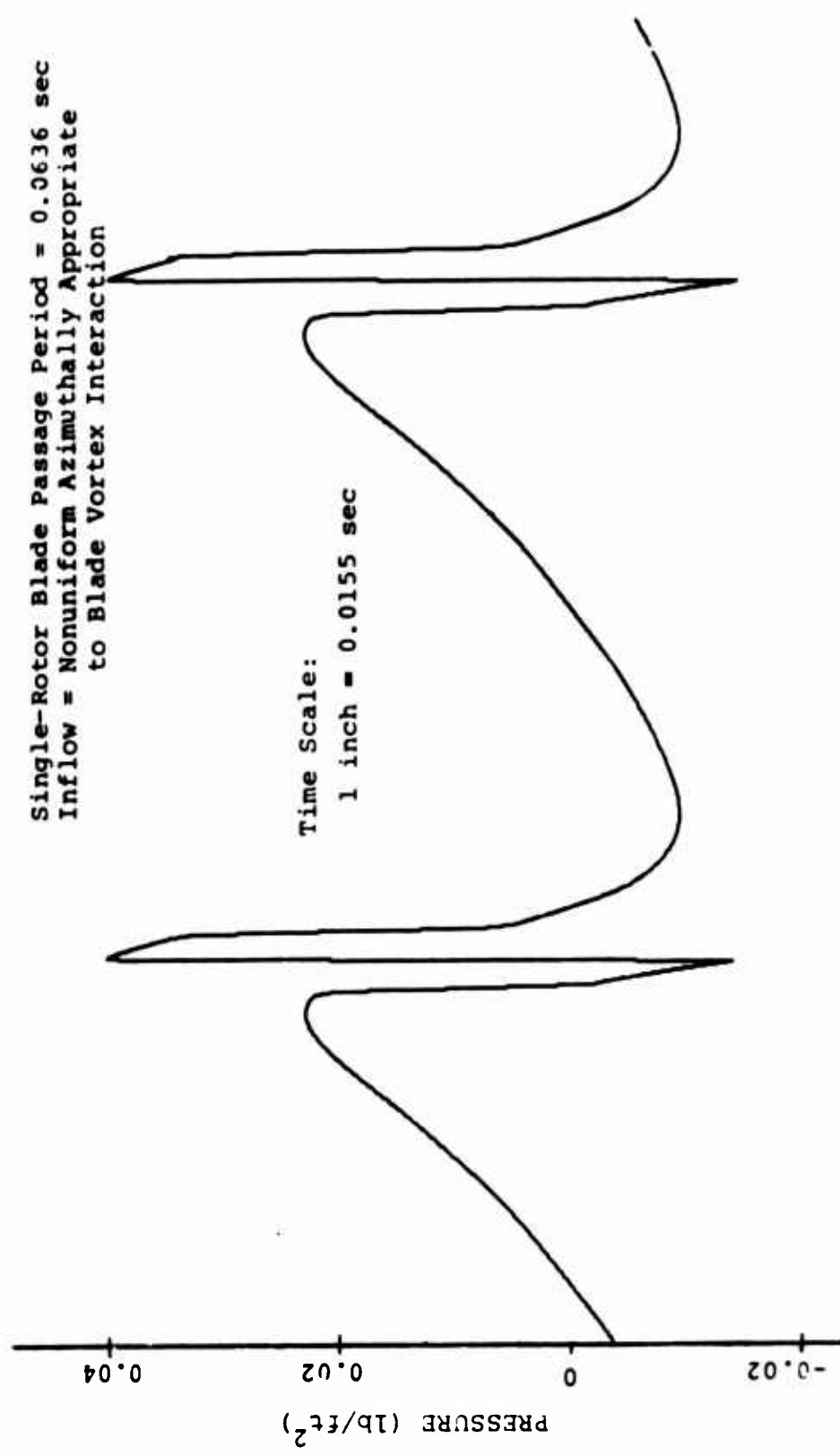


Figure 58. Pressure Time History of Predicted Single-Rotor Rotational Noise Generated From a Boeing-Vertol Model 347 Hovering in Ground Effect.

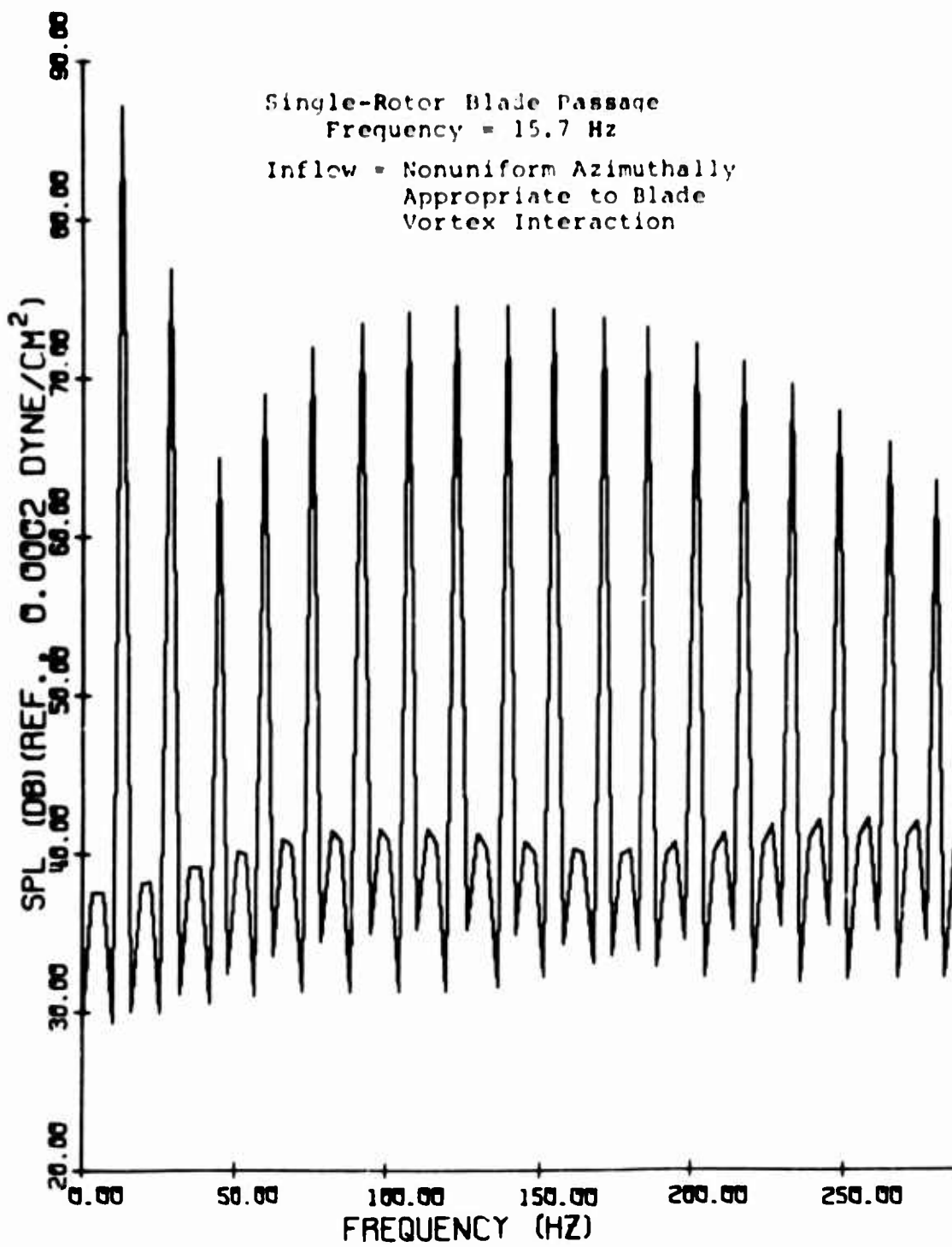


Figure 59. Spectrum of Predicted Single-Rotor Rotational Noise Generated From a Boeing/Vertol Model 347 Hovering in Ground Effect (Reference Figure 58).

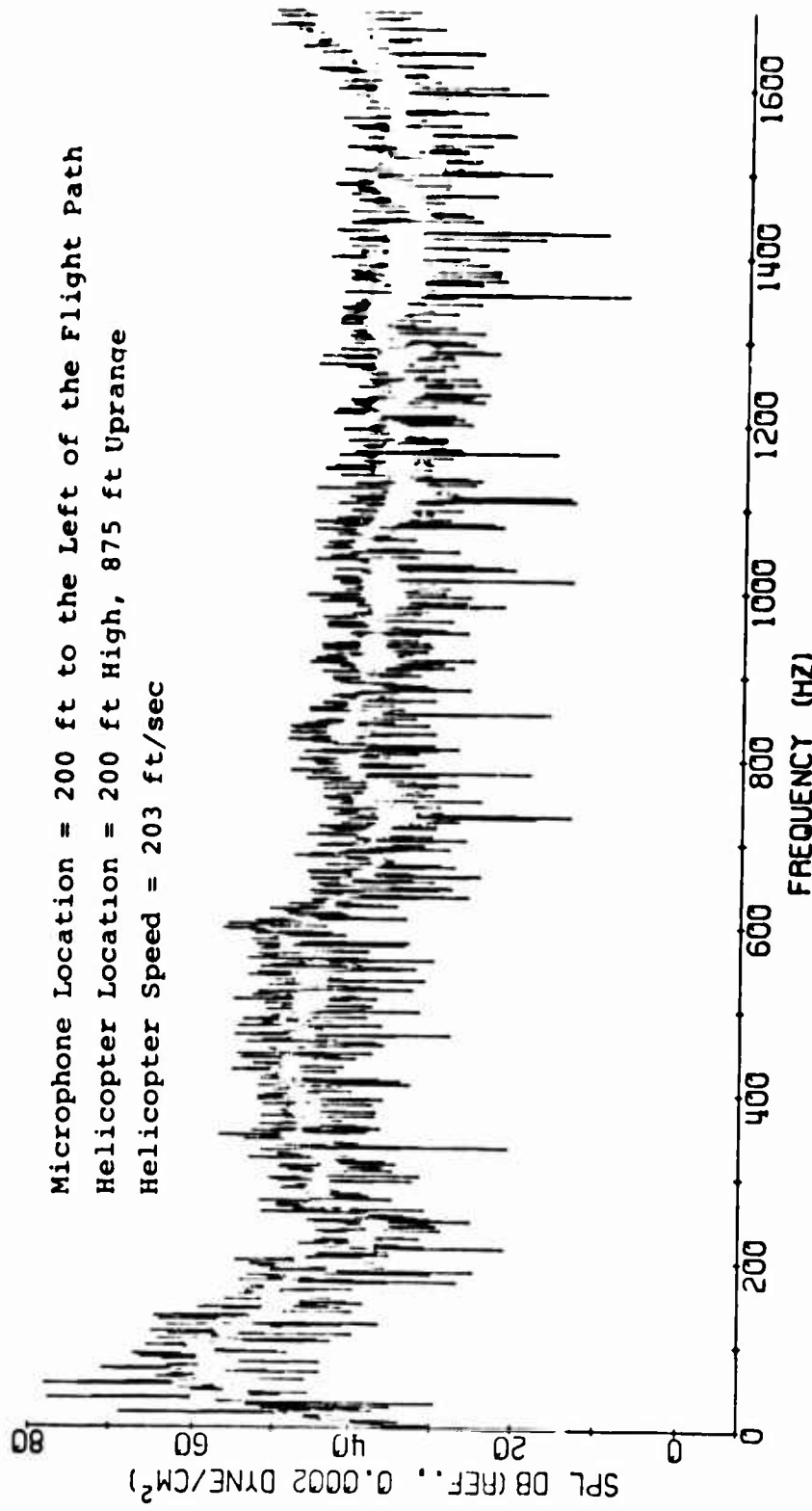


Figure 60. Spectrum of Recorded Noise Generated From a Boeing/Vertol Model 347 Helicopter in Level Flight.

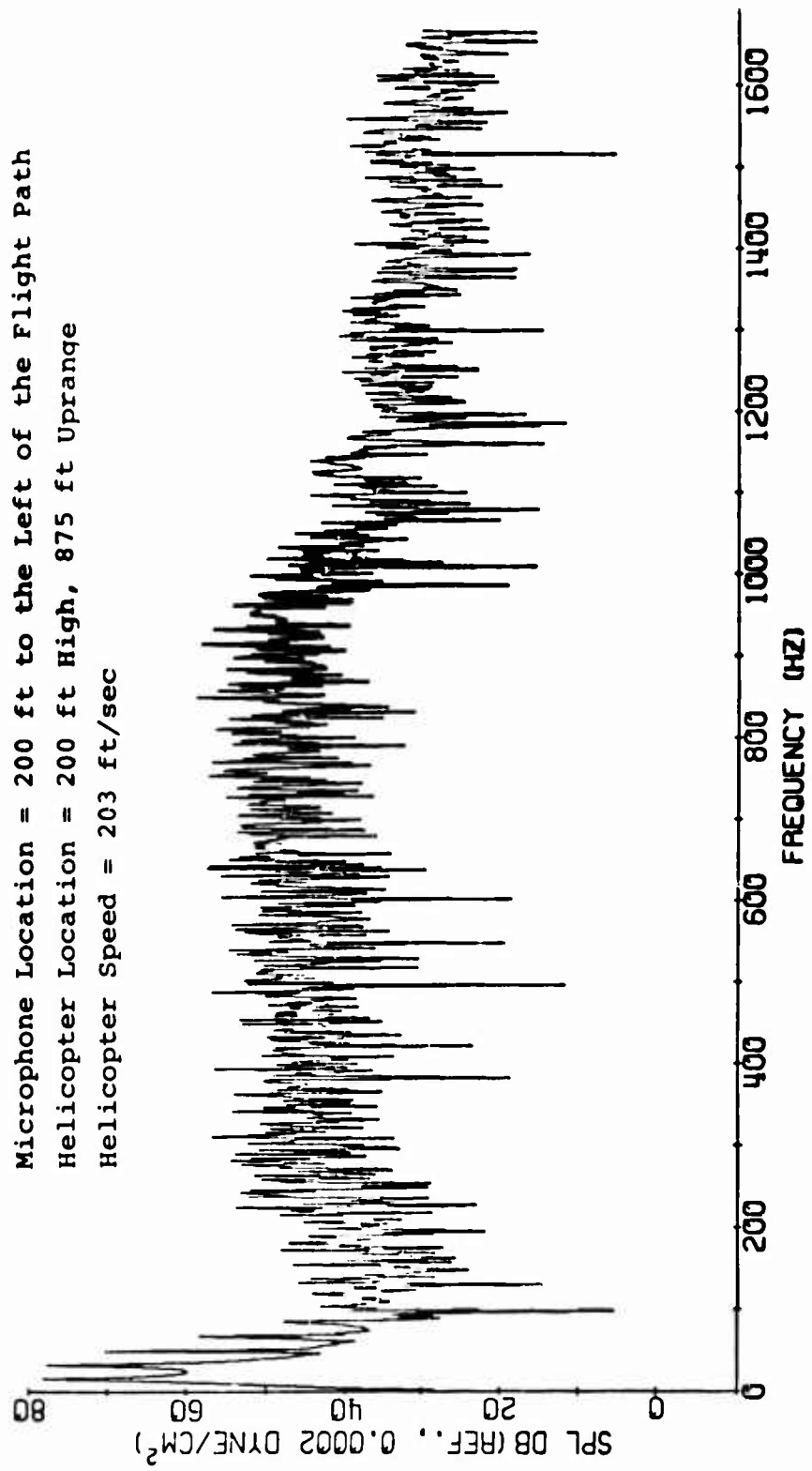


Figure 61. Spectrum of Predicted Noise Generated From a Boeing-Vertol Model 347 Helicopter in Level Flight.

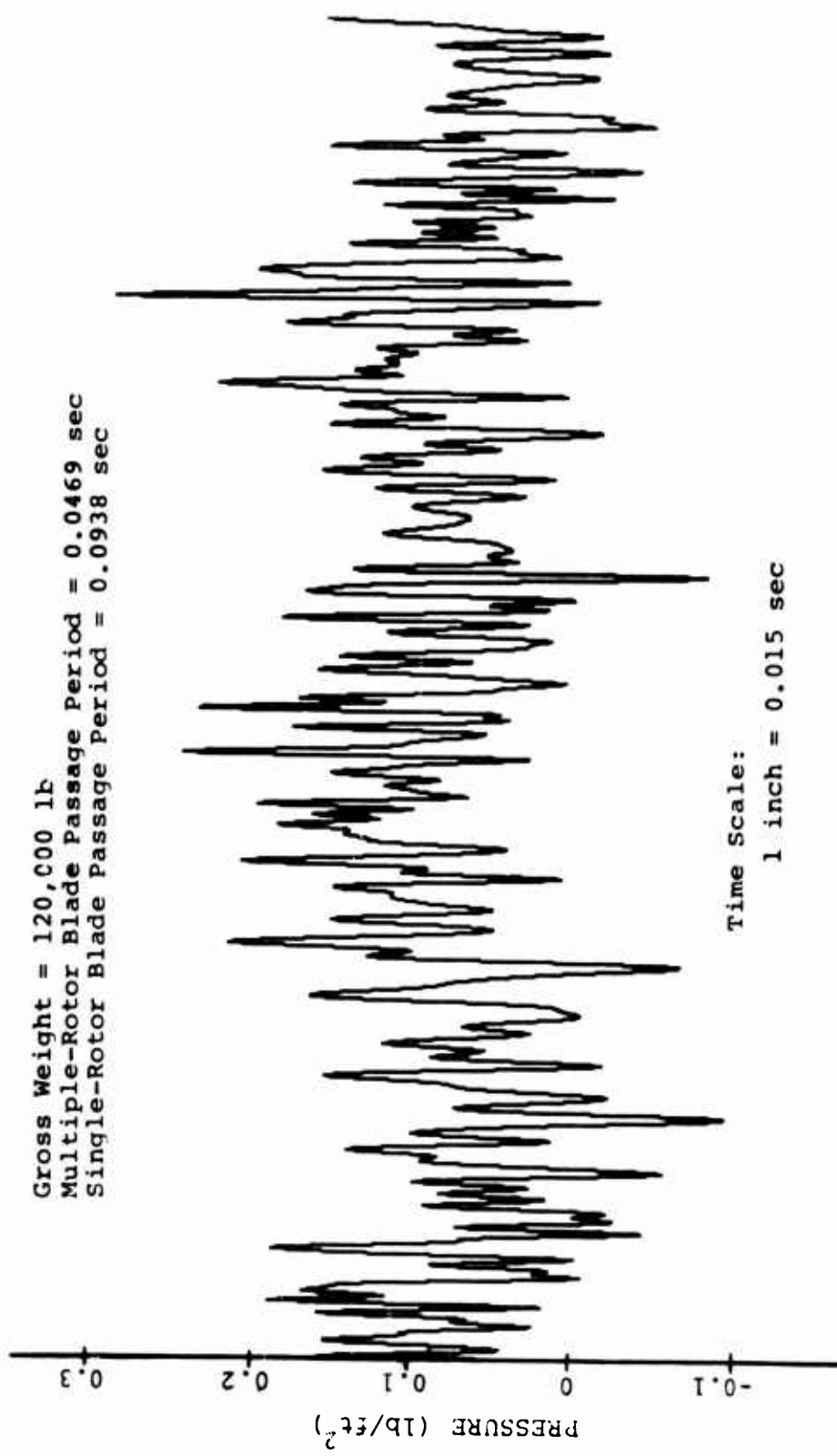


Figure 62. Pressure Time History of Predicted Noise Generated From the Proposed HLH Configuration in 100-Ft Hover, Microphone 200 Ft to the Right.

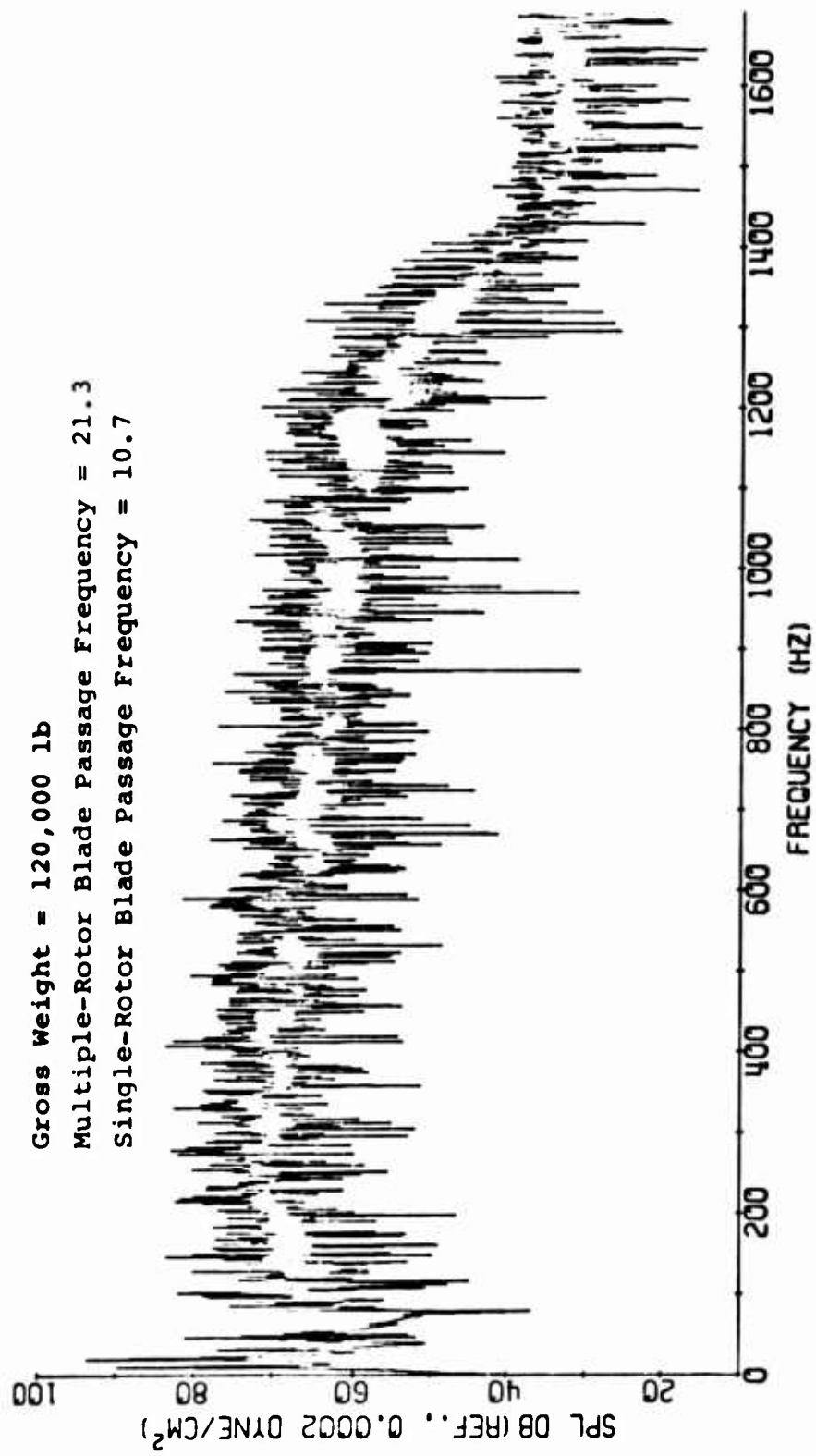


Figure 63. Spectrum of Predicted Noise Generated From the Proposed HLI Configuration in 100-Ft Hover, Microphone 200 Ft to the Right (Reference Figure 62).

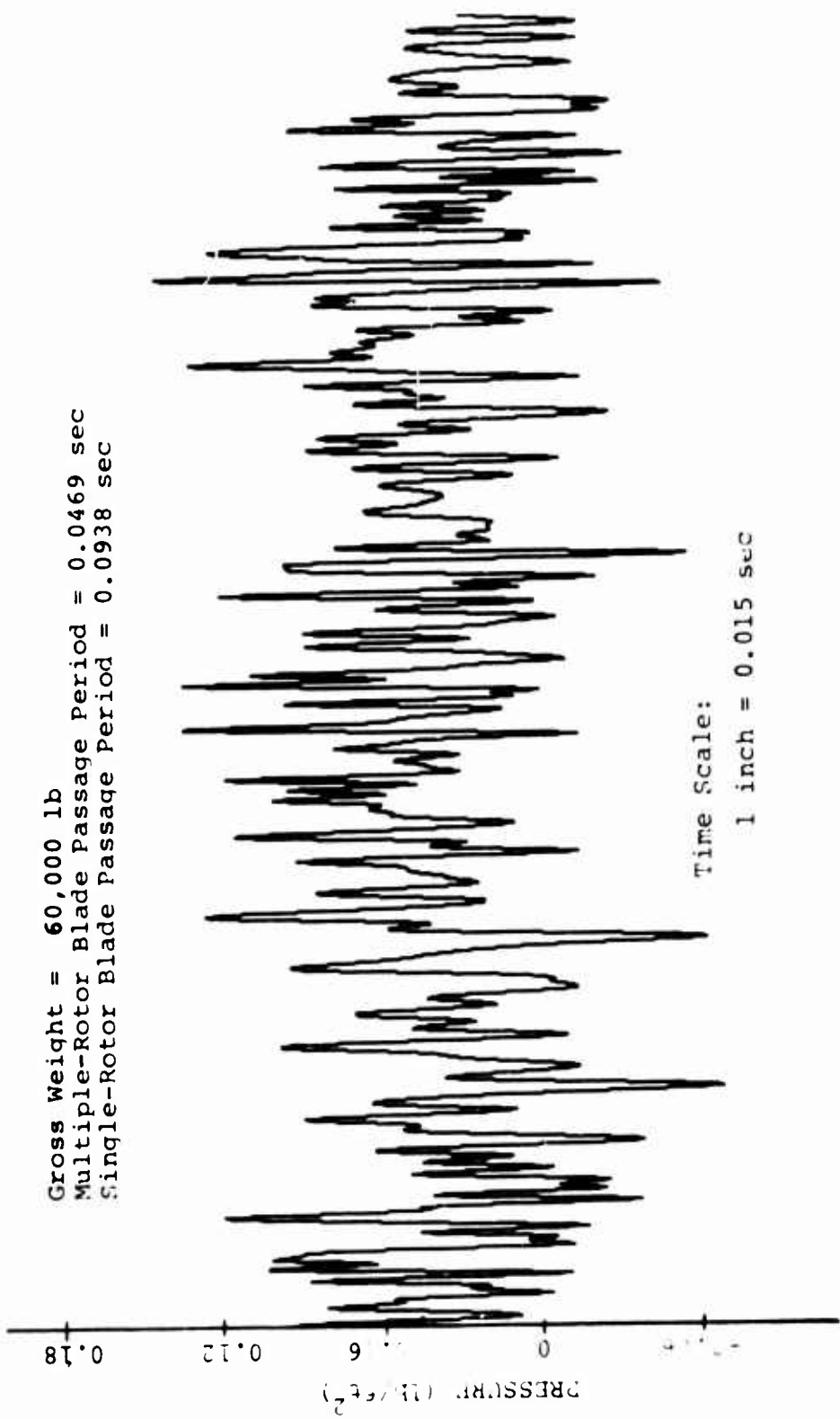


Figure 64. Pressure Time History of Predicted Noise Generated From the Proposed HLH Configuration in 100-Ft Hover, Microphone 200 Ft to the Right.

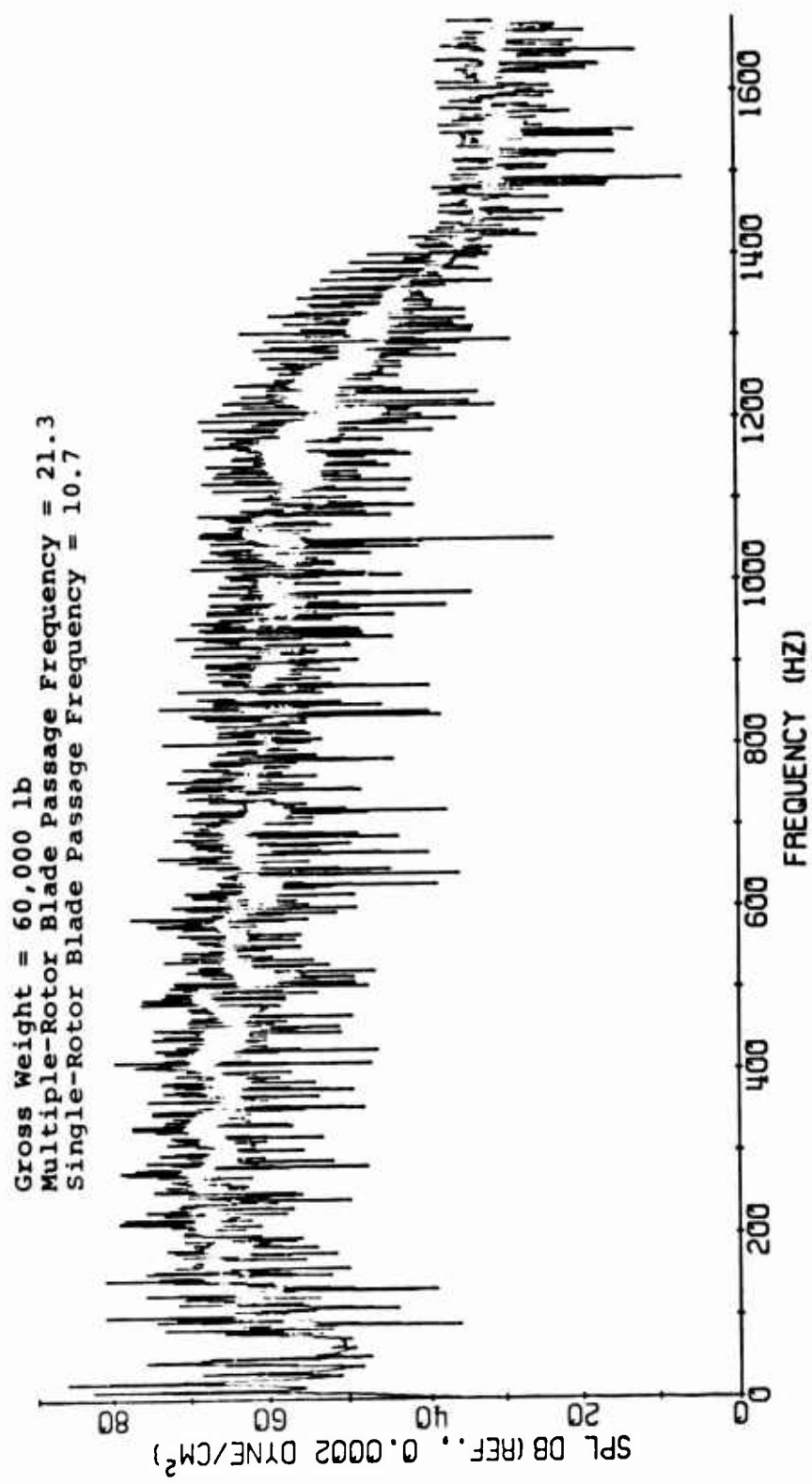


Figure 65. Spectrum of Predicted Noise Generated From the Proposed HLH configuration in 100-Ft Hover, Microphone 200 Ft to the Right (Reference Figure 64).

LITERATURE CITED

1. Lawson, M.V., THE SOUND FIELD FOR SINGULARITIES IN MOTION, Proceedings of the Royal Society, A. Vol. 286, pp. 559-572, 1965.
2. Lawson, M.V., Ollerhead, J.B., STUDIES OF HELICOPTER ROTOR NOISE, USAAVLabs Technical Report 68-70, U. S. Army Aviation Materiel Laboratories, Fort Eustis, Virginia, January 1969, AD 684394.
3. Johnson, H. Kevin, Katz, Walter M., INVESTIGATION OF THE VORTEX NOISE PRODUCED BY A HELICOPTER ROTOR, USAAMRDL Technical Report 72-2, Eustis Directorate, U. S. Army Air Mobility Research and Development Laboratory, Fort Eustis, Virginia, February 1972, AD 741778.
4. Bowes, Michael A., TEST AND EVALUATION OF A QUIET HELICOPTER CONFIGURATION HH-43B, USAAMRDL Technical Report 71-31, Eustis Directorate, U. S. Army Air Mobility Research and Development Laboratory, Fort Eustis, Virginia, January 1972.
5. Barlow, W.H., McCluskey, W.C., Verris, H.W., OH-6A PHASE-II QUIET HELICOPTER PROGRAM, USAAMRDL Technical Report 72-29, Eustis Directorate, U. S. Army Air Mobility Research and Development Laboratory, Fort Eustis, Virginia (in publication).
6. Lighthill, M.J., SOUND GENERATED AERODYNAMICALLY, Royal Aircraft Establishment (Farnborough) Technical Memorandum No.: Dir. 8, November, 1961, AD 275075.
7. Gessow, A., Myers, G.C., Jr., AERODYNAMICS OF THE HELICOPTER, The MacMillan Company, New York, 1952.
8. Sadler, S.G., DEVELOPMENT AND APPLICATION OF A METHOD FOR PREDICTING ROTOR FREE WAKE POSITIONS AND RESULTING ROTOR BLADE AIR LOADS, VOLUME I - MODEL AND RESULTS, NASA CR-1911, National Aeronautics and Space Administration, Washington, D.C., December 1971.
9. Johnson, H. Kevin, Katz, Walter M., Moore, Gay E., DOCUMENTATION OF THE HELICOPTER NOISE PREDICTION PROGRAM, RASA Report 72-07, available upon request from the Eustis Directorate of the U. S. Army Air Mobility Research and Development Laboratory, Fort Eustis, Virginia.
10. Sternfeld, Spencer, R.H., Schairer, J.O., AN INVESTIGATION OF NOISE GENERATION ON A HOVERING ROTOR, Report D210-10229-1, U. S. Army Research Office - Durham, January 1971.

11. Evans, T.D., Nettles, W.E., FLIGHT TEST NOISE MEASUREMENTS OF A UH-1B HELICOPTER, Paper presented at the AHS/UTA Joint Symposium on Environmental Effects on VTOL Designs at Arlington, Texas, November 1970.